APRIL 2024

Ph.D. in Civil Engineering

RAAD A. NASER ALAMERI

REPUBLIC OF TÜRKİYE

GAZİANTEP UNIVERSITY

GRADUATE SCHOOL OF NATURAL & APPLIED SCIENCES

IMPACT PERFORMANCE OF ENGINEERED CEMENTITIOUS COMPOSITES AT AMBIENT AND HIGH TEMPERATURES

Ph.D. THESIS

IN

CIVIL ENGINEERING

BY

RAAD A. NASER ALAMERI

APRIL 2024

IMPACT PERFORMANCE OF ENGINEERED CEMENTITIOUS COMPOSITES AT AMBIENT AND HIGH TEMPERATURES

Ph.D. Thesis

in

Civil Engineering

Gaziantep University

Supervisor

Prof. Dr. Mustafa ÖZAKÇA

Co-Supervisor

Prof. Dr. Sallal Rashid ABID

By

Raad A. Naser ALAMERI

April 2024

I hereby declare that all information in this document has been obtained and presented in accordance with academic rules and ethical conduct. I also declare that, as required by these rules and conduct, I have fully cited and referenced all material and results that are not original to this work.

Raad A.Nasir ALAMERI

ABSTRACT

IMPACT PERFORMANCE OF ENGINEERED CEMENTITIOUS COMPOSITES AT AMBIENT AND HIGH TEMPERATURES

ALAMERI, Raad A. Nasir
Ph.D. in Civil Engineering
Supervisor: Prof. Dr. Mustafa ÖZAKÇA
Co-Supervisor: Prof. Dr. Sallal Rashid ABID
April 2024
165 pages

Aiming to evaluate the material and structural impact behavior of low-cost Engineered Cementitious Composites (ECC) after exposure to high temperatures, a two-stage experimental work was conducted on Polypropylene (PP)-based ECC and Normal Concrete (NC) specimens. The first stage incorporated of small cylindrical (disk) specimens, besides cubes and prisms were cast to evaluate the compressive and flexural strength of mixtures. After the cured for 28 days its subjected to six high-temperature levels from 100 to 600°C. and unheated group as reference. The second stage incorporated square reinforced ECC and NC plates to conduct instrumented repeated impact tests. The specimens were divided into three groups of 5 plates each, depending on the end conditions; clamped, two-end restricted, and three-end restricted cases. From each group, two unheated specimens as references, while three specimens were heated to 200, 400, and 600 °C. The impact test was conducted by applying a constant drop weight of 33 kg from a constant height of 500 mm repeatedly. For each impact blow, the impact force, acceleration, and central deflection were recorded with time. The results showed that before heating, ECC retained more than 4 times the impact strength and 6 times of impact ductility of NC. The results also showed that exposure to 100 °C has a minimal effect on both cracking (N_{cr}) and failure (N_f) impact numbers of NC, while exposure to 200 °C decreased the impact strength by a large amount. also, ECC specimens exposed to 100 °C retained higher impact strength compared to unheated ones, while heating to 200 °C barely affected the impact strength of ECC specimens. also, the failure impact strength of both NC and ECC decreased by more than 80% after exposure to 300 °C, while it almost diminished when subjected to 400 °C and higher temperatures. The results showed that ECC plates retained 250 to 425% higher impact strength compared to corresponding NC plates. However, the percentage strength decreases of 50 to 90% and 79 to 97% were recorded for the NC and ECC plates, respectively, after exposure to a temperature range of 100 to 600 °C.

Keywords: Repeated impact; ACI 544-2R; High temperatures; Fire; ECC.

ÖZET

MÜHENDİSLİKLE YAPILMIŞ ÇİMENTO ESASLI KOMPOZİTLERİN ORTAM VE YÜKSEK SICAKLIKLARDA DARBE PERFORMANSI

ALAMERI, Raad A. Nasir
Doktora Tezi, İnşaat Mühendisliği
Danışmanı: Prof. Dr. Mustafa ÖZAKÇA
İkinci Danışman: Prof. Dr. Sallal Rashid ABID
Nisan 2024
165 Sayfa

Düşük maliyetli Çimento Esaslı Kompozitlerin (ECC) yüksek sıcaklıklara maruz kaldıktan sonra malzeme ve yapısal darbe davranışlarını değerlendirmeyi amaçlayan Polipropilen (PP) bazlı ECC ve Normal Beton (NC) numuneler üzerinde iki aşamalı bir deneysel çalışma gerçekleştirildi. İlk aşamada, ACI 544-2R'ye göre tekrarlanan darbe testlerinin gerçekleştirilmesi için küçük silindirik (disk) numunelerin dökümü ve testi yapıldı; ayrıca karışımların basınç ve bükülme mukavemetini değerlendirmek için küpler ve prizmalar döküldü. 28 gün kürlendikten sonra 100'den 600○C'ye kadar altı yüksek sıcaklık seviyesine maruz bırakılır. ve referans olarak ısıtılmamış grup. İkinci aşama, aletli tekrarlanan darbe testlerini gerçekleştirmek için kare takviyeli ECC ve NC plakaların dökümünü ve ısıtılmasını içeriyordu. Numuneler son koşullara bağlı olarak her biri 5 plakadan oluşan üç gruba ayrıldı; kelepçeli, iki ucu kısıtlı ve üç ucu kısıtlı durumlar. Her gruptan iki örnek ısıtılmadan referans olarak bırakılırken, üç örnek 200, 400 ve 600 ○C'ye ısıtıldı. Ayrıca hem NC hem de ECC'nin kırılma darbe mukavemeti, 300 ○C'ye maruz kaldıktan sonra %80'den fazla azalırken, 400 ○C ve daha yüksek sıcaklıklara maruz kaldığında neredeyse azaldı. Yapısal sonuçlar, ECC plakalarının karşılık gelen NC plakalara kıyasla %250 ila %425 daha yüksek darbe dayanımını koruduğunu gösterdi. Bununla birlikte, ECC plakaları, karşılık gelen NC plakalara kıyasla yüksek sıcaklığa maruz kaldıktan sonra daha şiddetli bir bozulma sergiledi; burada bir sıcaklığa maruz kaldıktan sonra NC ve ECC plakaları için sırasıyla %50 ila %90 ve %79 ila %79 ila %79 ila %97'lik mukavemet düşüşleri kaydedildi. 100 ila 600 ○C aralığı.

Anahtar Kelimeler: Tekrarlanan etki; ACI 544-2R; Yüksek sıcaklıklar; Ateş; ECC.

To My Mother and father

A strong and gentle soul they taught me to trust in Allah and believe in hard work and for supporting and encouraging me to believe in myself.

ACKNOWLEDGEMENTS

Praise and glory be to Allah who guided me in every step to finish my thesis project. My deep gratitude goes to my supervisor Prof. Dr. Mustafa ÖZAKÇA who gave me the golden opportunity to do this wonderful project which also helped me in doing a lot of research and I came to know about so many new things.

Additionally, I would like to thank both Prof. Dr. Sallal Rashed Abid for his help and support for me.

My final thanks go to my family, my wife and friends who helped me a lot and support me in finalizing this project within the limited time frame My thanks for the Dr. Hayder ALI.

TABLE OF CONTENTS

Page

LIST OF TABLES

Page

LIST OF FIGURES

Page

LIST OF SYMBOLS

$(f_{ct,fl})$	Flexural strength of concrete
$\bar{R}$	The Mean of Failure Impact Number
E_C	Modulus of elasticity or concrete
P_{flex}	Flexural Capacity
T_0	corresponds to the room temperature
V_f	Fiber volume fraction
W_l	Weight Loss
a/d	Shear span over effective depth
f'_c	cylinders compressive strength
f_{st}	Splitting tensile strength for concrete
n_{cr}	Number of Cracks
n_f	Number of Failures
b	Beam width
c/c	Center to Center of Rebar
EAC	Energy Absorption Capacity
L	Beam length
l	Length of Cylinder
R	The failure impact number
R_x	The reliability level

Sf	Silica Fume
SP	SuperPlasticizer
t	corresponds to time in minutes
t	Thickness of wall of beam
α	Shape Parameter
β	Scale Parameter
δ	Displacement
d	Effective depth
ρ	Reinforcement Ratio

LIST OF ABBREVIATIONS

A	Area
ACI	American Concrete Institute
COV	Coefficient of Variation
Dc	Diameter of Cylinder
ECC	Engineered Cementitious Composites
EPFM	Energy Pattern Factor Method
FR	Fiber Reinforcement
FRC	Fiber Reinforced Concrete
LVDT	Linear Variable Displacement Transducer
MOM	Method of Moments
MSDM	Mean Standard Deviation Method
PP	Polypropylene

CHAPTER ONE

INTRODUCTION

1.1 General

In the past years, the exposure of concrete or steel structures to suddenly high-velocity accident such as earthquakes, industrial accidents, terrorist attacks, blast waves, and other similar occurrences has become increasingly important. These types of incidents, which are characterized by high loading rates, are very frequently accompanied by the occurrence and spread of a fire, which exposes structures to highly difficult operating circumstances. There could be a lot of damage done to materials and structures when the extreme thermodynamic loads are combined. This could happen very quickly, and the materials and structures could break down right away.

It is possible for any structural facility, regardless of its purpose or kind of occupancy, to be exposed to undesirable, severe, or accidental loads, regardless of its design or construction. The majority of contemporary reinforced concrete buildings are built to handle not just the standard design gravity stresses, but also lateral loads such as wind and earthquakes. However, taking into account the possibility of unintentional loading during the design process is not a standard method mandated by building design rules since it would increase the overall construction cost.

Fires and impact loads are two of the most common forms of unintended loads that may occur. The quick rise in temperature caused by the burning of furniture, nonstructural materials, and electrical wiring may cause a significant reduction in the structural capability of slabs, beams, and columns, especially in older buildings. On the other hand, unexpected impact loads can cause a lot of concentrated damage that could weaken the structural integrity of a building or other structure. When a building is subjected to repeated accidental impacts, it is subjected to a type of unfavorable load that most structures are not designed to withstand. It is essential to evaluate and comprehend the behavior of the structural material.

It is essential to evaluate and comprehend the behavior of the structural material that is being used in order to reduce the impact of such incidents, the behavior of reinforced concrete structures when subjected to high temperatures and subsequent dynamic stress continues to be extensively researched. In recent years, a large number of researchers have investigated the dynamic and thermal behavior of concrete in various studies. Several studies on concrete loaded under a relatively wide range of strain loading rates at room temperature can be found in the literature, as can studies on thermal deterioration or the effects of temperature changes on the performance of structural parts made of concrete. But when the two issues are considered in the same sentence, there is hardly any investigation.

Following an investigation of a number of terroristic disasters that have happened in recent years, The relationship between fire situations and impact has been shown to be crucial in identifying the actual damage entity and the way in which the building collapsed. Based on the research conducted by Bažant and Zhou (2002) regarding the World Trade Center attack in New York, as illustrated in Figure 1.1, it became evident that the structural failure was not exclusively attributable to the aircraft's impact; rather, it resulted from the confluence of the impact and the subsequent fire outbreak induced by the fuel's ignition dispersed across the impact zone.

It is essential for the design and construction of concrete structures to have a solid understanding of the influence that rate dependency has on the structural response, resistance, and failure mechanism of concrete structures when they are subjected to dynamic loading conditions.

1.2 Problem Statement and Motivation

When concrete is exposed to fire, it is well known that it exhibits considerable changes in its physical and mechanical characteristics. Concrete strength, porosity, and heating rates are all variables that influence the entity of the variation. Under certain circumstances, spalling phenomena such as cover explosions and the ejection of large and tiny fragments from the concrete surface may occur.

Figure 1.1. The World Trade Center disaster in New York City, depicting the collision of the second plane.

Extreme conditions such as vehicle collisions with columns (dynamic high strain rate) and vehicle explosions are frequently coupled together. In a similar vein, a fire scenario might arise after terrorist attacks, which have become all too frequent in recent years. For instance, a blast explosion or a missile hit can both result in the development of a fire scenario.

When looking at accidents in industrial processes, it is possible to see how important the combination of these two impacts is to the outcome (Khan, & Abbasi, 1998). Specifically, with regard to chemical process industries, the danger of a multi-accident occurrence, often known as "domino-effects," is quite significant and must be taken into consideration throughout the building safety review process. In these circumstances, the spread of fire caused by the uncontrolled oxidation of chemicals has the potential to result in the explosion of surrounding units. Shock or blast waves are formed as a result of the quick and severe release of energy, and the walls of pipelines or containers are shattered into fragments, which are then thrown forth like missiles by the explosion.

To determine how terrible the damage is, the damage produced by the pieces impacting the building's structural parts must be compared to other events, such as the length of time exposed in the prior fire scenario.

When compared to the identification of the post-fire material properties of other materials, the identification of the material characteristics of concrete structures after a fire result in a greater degree of difficulty. Due to the fact that the basic components of concrete, namely cement paste, aggregates, and pore water, undergo a variety of different kinds of physical and chemical changes when they are subjected to high temperatures, the behavior of concrete at high temperatures is known to be very difficult. In addition, the heterogeneous nature of the concrete causes separate thermal expansions and shrinkages between the aggregates and the cement paste, which might lead to cracking under certain conditions.

All of these events are responsible for the significant degradation of concrete, which can be readily traced by comparing the mechanical characteristics of the concrete with the rise in temperature exposure over time. The evolution of concrete degradation and the buildup of thermal deformations are both controlled by a large number of other elements as well, among other things, the amount of moisture that is lost, the rates at which the structure is heated and cooled, the amount of time that it is exposed to the structure, the highest temperature that can be reached, and the potential of an externally applied load.

1.3 Low Velocity Repeated Impact Load

When an accident occurs, one of the things that most typical dwellings and commercial buildings are not built to sustain is the force of the impact. The majority of the design codes that are now available do not contain protections for this sort of unintentional load. The impact load might be caused by the dropping of masses from higher levels or by the collision of moving vehicles with each other. Explosive blasts that happen in war zones or because of terrorist activities are two of the main causes of this unpleasant burden.

In the case of brittle materials such as concrete, impact forces expose the material to short-term dynamic loads that cause the material to experience unexpected and

unwanted stresses. Such types of loads need improved microstructural performance in order to be efficiently absorbed.

Most buildings are not designed to withstand this type of unfavorable load, which is the source of the repeated accidental impact that happens in most buildings. In the short term, impact loads are a type of dynamic load that causes stress in the material that is being looked at. Because they expose the material to more stresses, impact loads are more effective on brittle materials like concrete. It is possible to sustain repeated impacts as a result of the accidental falling of building materials during the construction phase, or falling other objects during the life of building from higher stories (Nili & Afroughsabet, 2010a; Nili & Afroughsabet, 2010b; Wang & Chouw, 2017; Abid et al., 2021a)

Furthermore, according to research by Wardhana & Hadipriono, (2003) around 3% of 503 bridges in the United States broke due to car collisions during an 11-year period from 1989 to 2000. Figure 1.2 shows two instances of bridge pier and superstructure collapses. Extensive research has been conducted in the academic literature to investigate the impact of various loading-related and structural parameters on the force of the automobile collision as well as the structural responses of the damaged pier.

Figure 1.2. Failure of the bridge column as a result of a collision with a truck.

In parking garages, the collision of cars can also cause repeated impacts on columns and walls, which can cause structural damage. Other examples include repeated projectile hits or explosive shrapnel in conflict-affected areas (Jabir et al., 2020; Salaimanimagudam et al., 2020). In order to figure out how repeated impacts affect

the structure's microstructure and residual performance, it's important to know how cracking and fracture behavior under these types of loads will affect them.

ACI 544.2 R-89 (ACI 544.2 R-89, 1999) standard repeated drop weight impact test can be used to conduct a preliminary evaluation of material behavior under repeated impacts. This test is considered to be the most straightforward and least expensive impact test available for evaluating the impact performance of concrete (Haridharan et al., 2020; Murali et al., 2020). Several recent researchers have used this test to see how well different types of concrete mixtures can withstand being hit, and the results have been good.

Concrete is a kind of cementitious material which is composed mainly of Portland cement and aggregate that are mixed with water to create a construction solution It is moderately affordable in terms of price and has sufficient compressive strength (f_c') for the task (Babalola et al., 2021; Gagg, 2014; Imbabi et al., 2012; Sharma et al., 2017).

Despite significant advancements in the field of material science, as well as the development of many evolutionary modern types of concrete that possess significantly superior strength and ductility characteristics by incorporating new fiber-reinforced cementitious composites, normal weight, normal strength concrete remains the industry standard for the time being. Concrete based on Portland cement is still the most widely used type of reinforced concrete structure (Behera et al., 2014; Tufail et al., 2017).

Although several simplified ways of predicting the reactions of reinforced concrete buildings under impact loads exist in current design codes, The brittle damage behaviors of concrete buildings under impulsive impact loads are not something that they are able to foresee before they occur.

Concrete structures are susceptible to experiencing localized failure modes and damage when subjected to high-rate impact loads. These damages and failure modes include brittle and punching shear failure, (Bangash & Bangash, 2005; Chen et al., 2015) or overall failure modes as depicted in Figure. 1.3. palling Scabbing Perforation Punching Overall response.

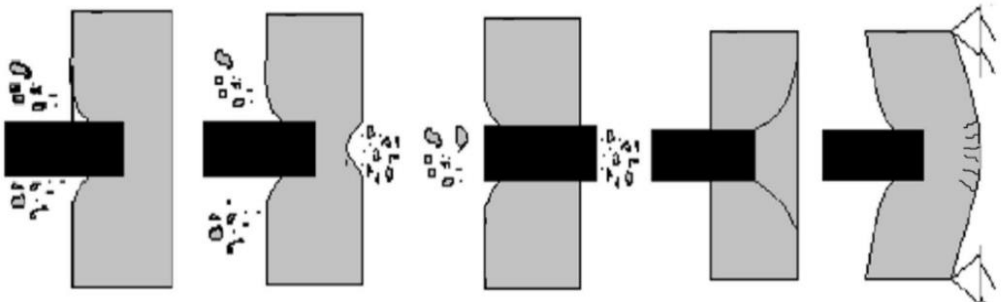

Figure 1.3. Typical failure modes of concrete structures under different impact loads.

1.4 Repeated Drop-Weight Impact Instrument Test

In order to evaluate the impact response of materials and structures experimentally, a variety of different tests are available, one of which is the impact test (also known as the drop-weight test). There were two approaches to drop-weight tests in ACI 544.2 R-89 (ACI 544.2R-89, 1999), both of which were successful. The instrumented drop-weight test is used to determine how structural members respond when they are struck by a heavy object. This is the most common method of accomplishing this in general.

For this reason, this test is only for reinforced beam and slab elements, and it comes with a lot of costs in terms of sensor instruments and data acquisition hardware. A simpler test, the alternative drop-weight impact test, can be performed on small specimens and does not require any special instrumentation or sophisticated measurement systems. It can be performed on any size specimen.

This test requires that a drop weight of 4.54 kg be dropped on the test specimen from a height of 457 mm be dropped on the specimen repeatedly until a surface crack is visible on the specimen, after which the repeated impacts must be resumed until the specimen fails as a result of fracture failure.

Impact logs keep track of how many times the first crack and failure occur. The cracking impact number and the failure impact number, respectively, are the number of impacts at which the crack and failure occur for the first time. As a qualitative evaluation technique, the test is generally regarded as one that compares the effects of two different variables. Different concrete mixtures have varying degrees of resistance to cracking and failure based on their ability to absorb higher or lower cracking and

failure impact numbers, depending on the concrete mixture in question. The standard test specimen design is based on a cylindrical (disk) test specimen with dimensions of approximately 150 mm in diameter and 64 mm in thickness, and a thickness of approximately 64 mm. Under normal circumstances, the drop weight is manually raised to the specified drop height and then released, with the steel ball resting in the center of the specimen's top surface, allowing it to be freely dropped on the specimen's top surface by gravity, as described in the standard test. Following the steel ball acts as a load distribution point and is held in place by a special framing system that also serves to hold the concrete disk specimen in place (see Figure 1.4).

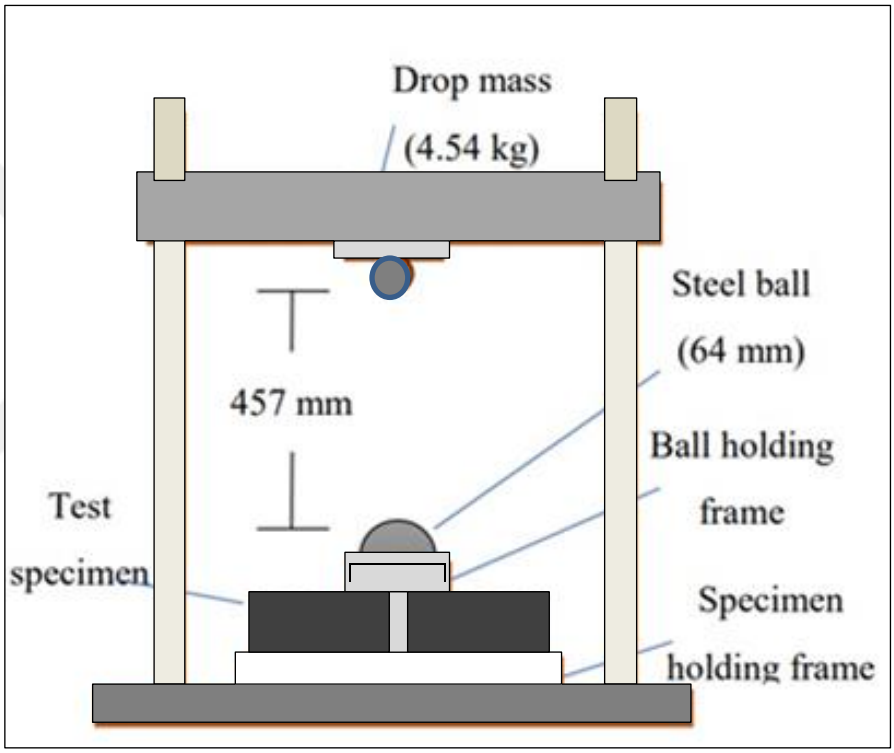

Figure 1.4. The drop-weight impact test.

The manual operation, on the other hand, has been discovered to require a significant amount of effort and time, particularly because at least 6 replication specimens are required to assess the test records, as previously stated, in order to account for the wide dispersion in the results of this particular test.

There are several types of tests that are intended to simulate the impact loading of concrete and other materials. The drop-mass impact test and the Charpy pendulum test (Thomas & Sorensen, 2018) are the most famous and widely used test techniques,

while other tests that simulate the higher speed impact like projectile and explosive impact tests are considered costly and sophisticated ones.

1.5 Concrete and Fire Resistance

As compared to other (unprotected) construction materials, concrete has a variety of characteristics in terms of structural design and remarkable fire activity, as shown in Figure 1.5 In this way, it is important to note that concrete has two main reasons for its good fire performance: the first is because of the material itself, and the second is because of how well it works with the rest of the structure. Because concrete is noncombustible and has a modest temperature increase rate throughout its cross section, it may be used in most structural systems without extra fire protection.

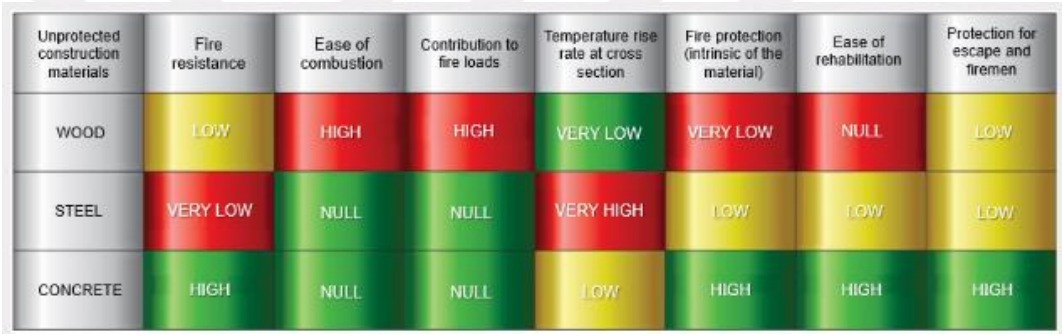

Unprotected construction materials	Fire resistance	Ease of combustion	Contribution to fire loads	Temperature rise rate at cross section	Fire protection (intrinsic of the material)	Ease of rehabilitation	Protection for escape and firemen
WOOD	LOW	HIGH	HIGH	VERY LOW	VERY LOW	NULL	LOW
STEEL	VERY LOW	NULL	NULL	VERY HIGH	LOW	LOW	LOW
CONCRETE	HIGH	NULL	NULL	LOW	HIGH	HIGH	HIGH

Figure 1.5. The performance of unprotected building materials under fire (Jacobs, 2007).

Structures may not undergo a total breakdown during a fire, following that, it may be possible to repair the building safely to make it serviceable again. For this purpose, it is needed to solve the post-fire residual resistance of concrete. Furthermore, today's urban fire control technologies have the capacity to extinguish the fire swiftly. Also, the coating used to shield structural parts against fire is increasingly becoming a standard in commercial applications. In these conditions, the temperatures do not approach the necessary levels to trigger the structural breakdown. Therefore, such buildings might endure the extremely damaging impact of fire, as they do not undergo long-term fire exposure.

Since the widespread use of Portland cement manufacturing, ordinary normal strength concrete has proven to be an excellent construction material. However, as a result of

advancements in building materials technology, new concrete varieties with improved features have been introduced. The necessity for cementitious materials that can absorb large amounts of plastic energy before failing was the impetus for the development and introduction of ECC materials. ECC is a kind of flow-able concrete that has excellent fresh qualities as well as improved plastic deformation resistance when it is freshly poured.

Fire accidents continue to occur despite developments in the construction industry to avoid such cases. Therefore, studies that clarify structural and structural member performance under fire conditions are still required. Brushlinsky, et al., (2018) were reported that in the USA, 494,000 structural fires were reported during 2014–2015, while 154,700 fires were reported in England, 28,200 of which were accidental fires. Therefore, these records show up the continuous need of research works on the performance of structures, structural materials and structural members during fire and their residual performance after fire.

Accidental fires can occur in concrete structures, as well as in other types of structures, at any time. These fires can be caused by electrical problems or by people occupying the structure in an inconvenient location. Fires can reach temperatures of up to 1000 °C in a very short period of time if there is furniture present. Every year, tens of thousands of fires are reported in countries such as the United States and the United Kingdom, with structural fires accounting for 40% of all reported fires (Buchanan & Abu, 2017).

Despite the fact that concrete is considered to be a fire-resistant material, exposure to high temperatures, particularly with a steep temperature increase, would cause the concrete structural members to deteriorate significantly (Guo, et al., 2014). When paired with mechanical characteristics, they are crucial for gaining an understanding of the nature of the damage in terms of the strain and deformation of the structural parts. (Kodur, 2014).

On the microstructural scale, such gradients would cause internal thermal stresses to be generated, which would result in rapid material degradation (Alimrani, & Balazs, 2020; Drzymała, et al., 2017). Due to non-uniform thermal gradients, non-uniform thermal movements (expansion) of the different material parts, and the chemical

decomposition of calcium hydroxide above 400 °C the effective degradation of the strength would occur, leading to failure (Chu, et al., 2016; Rafiei, et al., 2021; Deng, et al., 2020).

Researchers have used three types of fire test procedures to simulate the reduction in strength in a material due to high temperature exposure; two of these procedures simulate the conditions of concrete strength during fire exposure for compression and flexural members, respectively. The third procedure simulates the reduction in strength in a material due to high-temperature exposure. This setup simulates the performance of compression members such as columns or compression parts of beams when they are stressed by 20% to 40% of their strength (Phan & Carino, 2003; Phan & Carino, 1998; Husem, 2006). The first of these tests, the stress fire test, is the first of these tests.

It is performed in this test after the specimens have been preloaded to a constant stress level and heated to the desired level of temperature, at which point the temperature is maintained constant to ensure that the material has an approximately zero thermal gradient (temperature saturation to the steady state).

Previous studies by Phan & Carino (1998) revealed that when specimens are cooled in water (as in the case of water distinguishing a fire), the strength of the specimens deteriorates at a faster rate than when they are cooled under convectional cooling. In the case of dehydrated calcium silicate that has been exposed to temperatures greater than 400 °C, the volume changes that result from rehydration (with cooling water) can have a destructive effect on the microstructure of the concrete (Husem, 2006).

Several research studies on the evaluation of concrete impact strength after high temperature exposure have been published in the literature, the majority of which investigate high-strain rate impact tests and blast tests (Chen, et al., 2015; Zhai, et al., 2016; Zhai, et al., 2017; and Mirmomeni, et al., 2017; Kakogiannis, et al., 2013), while only a few studies have been published on low-velocity impact tests on reinforced concrete members (Jin, et al., 2021). The majority of these studies (Pan, et al., 2016 and Yu, et al., 2017; Jin, et al., 2019) focused on developing numerical analyses to evaluate the dual effects of high temperature and high strain rate impacts on reinforced concrete and composite structural members.

A combination of fire exposure and low-velocity repeated impacts is likely in many structures, including parking garages, but the authors were unable to locate sufficient literature studies that attempted to investigate the post-fire repeated impact performance of concrete in this situation. Mehdipour, et al., (2020) looked into the residual mechanical properties of concrete that had recycled rubber as the coarse aggregate replacement, metakaolin as a partial replacement for Portland cement, and steel fibers as the reinforcement.

The ACI 544.2 R-89. (1999) test was used to evaluate the residual repeated impact strength after exposure to temperatures of 150, 300, 450, and 600 °C. The authors found that the residual repeated impact strength was the strongest of the mechanical properties investigated. The results of the tests revealed that high temperatures could have a significant impact on residual cracking and failure impact numbers, with only one impact being sufficient to cause cracking in specimens heated to 600 °C. As a result, it was said that for heated fibrous specimens, multi-surface cracking was seen instead of the circular fracture that was seen for unheated fibrous specimens.

This study investigated the impact resistance of NC to low-velocity repeated impacts after being exposed to high temperatures caused by accidental fires in the course of its investigation. As previously discussed in the preceding sections, such a scenario is possible throughout the service life of concrete structures, despite the fact that the number of studies on the subject is extremely limited. For this reason, a research project was started. The first step was to study the most common concrete type used in reinforced concrete structures, which is normal-weight, normal-strength concrete, which is the first step in the process.

1.6 Historical Background

Despite the fact that the fire extended to many stories and raged for 26 hours, the building was able to stay standing, as seen in Figure 1.6 The only section of the structure that did not collapse was the steel perimeter columns above the 20th level, which sustained the floors underneath them. However, it is important not to take the fire resistance of concrete buildings for granted. A suitable structural fire design is required, but concrete remains a complicated material composed of various elements that respond in a variety of ways when exposed to high temperatures. Multiple

physicochemical reactions take place in the concrete, leading to a reduction in the strength and stiffness of the structure.

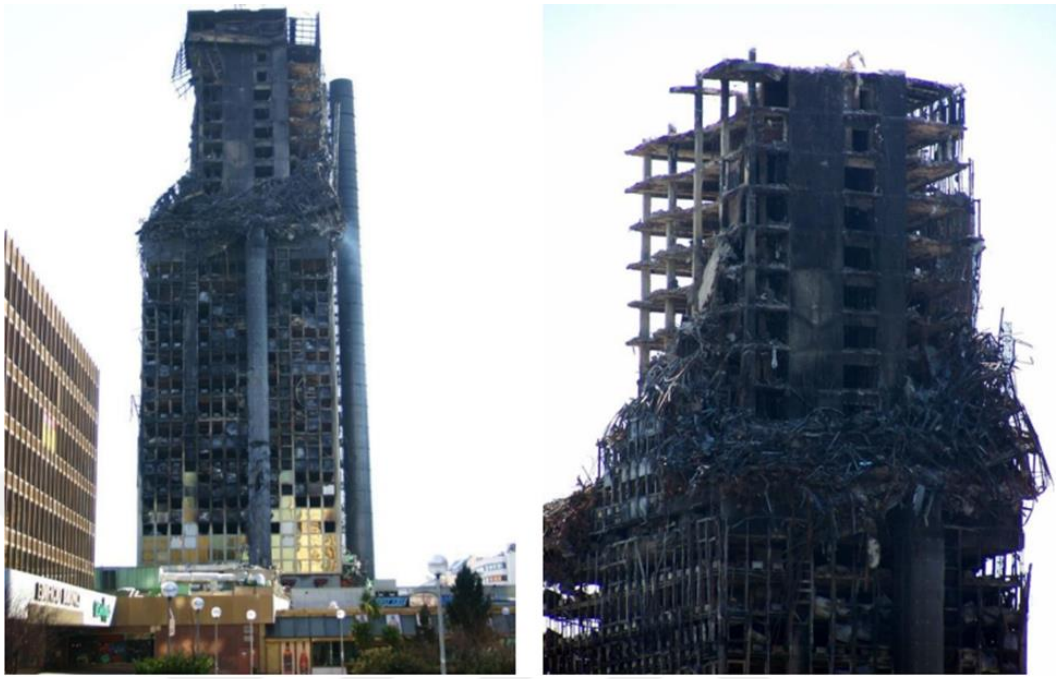

Figure 1.6. The Windsor Tower in Madrid after a 26-hour fire in 2005 (Ghali, et al., 2015).

1.7 Polypropylene (PP)

PP fibers as shown in Figure 1.7 are a kind of polymer fiber defined by the CEN European Standard EN 14889-2 (2006) as straight or distorted pieces of extruded, orientated, and cut polymer material. CEN EN 14889-2 (2006) differentiates between two forms of PP fibers: microfibers and macro -fibers. Microfibers are smaller than macro- fibers. Primarily, they vary in length, but more significantly, they differ in the role that they serve in the concrete, which is described below.

Macro-fibers are also referred to as structural fibers since they have the ability to replace conventional reinforcement in the form of steel bars while also transferring loads operating on the structural members. As a result, the time required to fabricate steel reinforcement, as well as the associated investment costs, are reduced. In most cases, the length of these insects is between 30- and 50-mm. Microfibers, on the other hand, are less than 30 mm in length and do not perform the load-bearing role.

Their primary function is to prevent plastic shrinkage from occurring in the concrete and to restrict the production of fractures in the concrete. As a consequence, they improve the durability of the element and extend its useful life as a result. In certain situations, Micro PP fiber may be used as an alternative to crack control meshes.

(a) (b)

Figure 1.7. PP (a) microfibers and (b) macro-fibers.

1.8 Aim of Study

The suggested research was created to bridge a knowledge gap in this field by examining the influence of the performance of ECC on the performance of other material.

In order to better understand how well this product performs both at ambient temperatures and after being exposed to fire, ACI 544.2R-89. (1999) is intended to be the primary testing technique for the repeated drop-mass impact tests, with additional tests such as compressive strength (f_c'), tensile strength, modulus of rupture, structural performance, and fracture tests also planned to be carried out as part of the experimental program for this research. The preparation and testing of many ECC mixes will be done to see how they react to fires and how well they can withstand being hit by objects that are hot, also the experimental investigation in this research included the static thermos-dynamic (impact) structural behavior of reinforced concrete slab

1.9 The Scope and Objectives of The Study

Specifically, the goal of this research is to investigate the static and dynamic (impact) behavior of concrete following temperature exposure, as well as the changes in material characteristics and failure mechanisms, from an experimental standpoint.

The thermodynamic behavior of reinforced concrete structures (slabs) is also covered in this study. The purpose of this study is to validate a powerful instrument that can be used to analyze the impact-induced structural behavior of reinforced concrete surfaces in chilly and heated environments.

Many experimental tests have been conducted on plain and ECC concrete pieces, as well as reinforced concrete slabs, among other things. The fact that there are so few trials accessible in the literature that correspond to the combined thermal and dynamic load is something that should be brought to your attention as well. This is especially true in the case of reinforced concrete buildings.

It is possible to describe the primary aims of the study provided here as follows:

1. Using an experimental approach, evaluate the effects of combined thermal and dynamic stresses on concrete and reinforced concrete (slabs). This should be done from the perspective of an experiment.
2. It is important to investigate the relevance of taking into account the effects of temperature effect on concrete when assessing the genuine structural capacity of structures.
3. Investigate the sensitivity of the concrete under dynamic loads at various degrees of previous fire exposure in an experimental setting.
4. Experimental study the response of the reinforced concrete structural system to impact loads in the presence of residual and hot conditions.

The ACI 544.2 R-89. (1999) is planned to be the main testing technique to perform the repeated drop-mass impact tests, while other tests such as the compressive strength (f_c'), tensile strength, modulus of rupture, structural performance and fracture tests are also intended to be conducted in the experimental program of this study. ECC mixture are to be prepared and tested to evaluate their post-fire mechanical response, and their impact resistance both before and after exposure to high temperatures.

To better evaluate the residual structural response after accidental impact and to assess the resistance of the developed impact absorbance materials, the materials or the structural members should be subjected to impact simulation tests.

On the other hand, the simplified repeated drop-weight test recommended by ACI 544.2 R-89. (1999) can be considered as a practical and cost-effective impact test. This test can simply be used in the laboratory or in the field to compare the impact resistance of different concrete mixtures or different materials. The ACI 544.2R-89. (1999) repeated impact is a simple mechanical test that requires no sophisticated sensors or measurements.

1.10Thesis Layout

Current research is provided in seven chapters, the first of which is titled "Introduction" The remaining chapters are as follows:

Chapter 2 looks at the basics of low-velocity impact load and the effect of fire on ECC concrete structures. It also gives a brief history of previous research that is relevant to this study.

Chapter 3 provides a summary of the experimental work specifics as well as the construction materials that were used.

In Chapter 4, the outcomes of the experimental study are presented and discussed of Material-Scale Tests.

In chapter 5, the results and discussion of plate specimens and the author sums up the findings of this work.

Chapter 6, the Statistical Evaluation of Test Results.

Finally, Chapter 7 conclusion and gives some ideas for future researches.

CHAPTER TWO

LITERATURE REVIEW IMPACT

2.1 General

When a building is subjected to repeated accidental impacts, it is subjected to a type of unfavorable load that most structures are not designed to withstand. The use of concrete members reinforced with fibers has been steadily increasing in the construction of new structural buildings, and the advantages of using fibers in concrete mixtures for enhancing properties of NC such as compressive strength (f_c'), flexural strength (modulus of rupture) and impact load resistance have been demonstrated until after the building has been exposed to fire. It is important to note that one of the advantages of concrete is that it has excellent heat resistance without the need for any additional materials.

To assess the impact strength of concrete, the ACI 544.2 R-89 (1999) drop hammer impact test may be employed. Using this basic test approach, a lot of contemporary research investigations are able to collect data on a variety of variables. This test does not require the use of sophisticated sensors or data-collection equipment, making it straightforward to conduct. When this test is done, the results can be very volatile because of a wide range of things, like:

Crack initiation is detected with the use of a visual examination technique. Some of the recorded impact counts may be off because of the wrong reasons given at or around the time of the first break or failure.

In the event that a single point of impact is reached on the concrete's top surface, it may be immediately localized on a toughened element, including fibers and coarse aggregate, or it can be directly localized on the soft interlayer of the cement matrix. A hard thing to do is to lift, hold, and lower the drop mass from a certain height on a regular basis.

For the reasons previously stated, it is commonly accepted that a statistical technique adequate for assessing the variability in experimental test results must be used. In order to reduce the influence of the factors listed above, a minimum of six specimens has been recommended in previous research, including this one.

In recent decades, researchers have focused their attention on determining the impact resistance of concrete, especially Fiber Reinforced Concrete (FRC), due to the widespread usage of this material in both the civil and military industries. ACI 544.2 R-89, (1999) tests the repetitive impact loading of concrete disc specimens supported on a rigid steel plate. The impact is imparted via a steel ball situated in the center of the top surface, which is located in the center of the top surface. This test has previously been used in several studies to evaluate the reactions of various concrete types reinforced with steel fibers (Ismail & Hassan, 2017; Ding, et al., 2017; Abid, et al., 2020a) or other types of synthetic or natural fibers (Badr, et al., 2006; Nili & Afroughsabet 2010b; Zhu, et al., 2009).

Some other research, on the other hand, employed a similar approach on beam specimens that were supported by just two basic supports. As a result, it is necessary to apply repetitive three-point flexural impact loading (Rao, et al., 2011).

To comply with the requirements of ACI 544-2 R-89 (1999), a drop-weight of about 4.5 kg should be able to drop freely from a drop-height of roughly 450 mm on a test specimen. In accordance with ACI 544-2R standards, the test specimen is a disk with an estimated diameter of 150 mm and an approximate thickness of 64 mm, respectively. Some prior studies sought to explore the effect of drop-weight or drop-height on the impact resistance of fibrous concrete, but their efforts were ultimately unsuccessful.

Several conclusions may be drawn from the most recent literature review, which was completed at this point in the present study, including the following:

1. The amount of research available on the repeated impact performance of ECC is quite low, particularly for those integrating PP fibers.
2. In general, only a few studies in the literature have attempted to evaluate the impact performance of materials after being exposed to fire using the low-velocity impact test.

3. For the dynamic and thermal structural behavior, there is no more studies focused on the impact residual resistance of reinforced and ECC -PP plates after exposure to temperatures as in the case of fire.

When it comes to material components, ECC uses elements that are comparable to those used in FRC. Several typical chemical additives are used in the mix, as well as water, cement, sand, and fiber. Coarse aggregates are not employed because they have a negative impact on the ductile behavior of the composite, which is unique to it. A typical composition has a water-to-cement ratio of 0.5 or less, as well as a sand-to-cement ratio of 0.5 or less. In contrast to certain high-performance FRCs, ECC does not need a great quantity of fiber to achieve its performance.

Despite the fact that the composite is intended for structural purposes, a discontinuous fiber content of 2 % or less by volume is frequently considered appropriate. Because of the minimal quantity of fibers in ECC and the fact that it is diced, the mixing procedure is quite similar to that used in the production of conventional concrete. Another advantage of ECC is that, by purposefully controlling the quantity of fibers used, several private studies have concluded that it is economically feasible in particular structural applications. When it comes to ECC, a variety of fiber types may be employed; nevertheless, the detailed composition must adhere to specific constraints dictated by micromechanics concerns. (Kanda and Li, 1998; Li, 2019).

2.2 Concrete at High Temperature

The capacity of a building or structural element may be characterized in terms of fire resistance, which is defined as the duration during which the structural component maintains its structural integrity and stability while being exposed to a source of fire. However, this notion may be applied not only to the overall structure but it can also be applied to the qualities of a single material, which in turn affects the performance of the element to which it belongs. As a result, to understand how the structure responds when subjected to high temperatures, it is necessary to first understand the behavior of concrete when exposed to high temperatures. One of the worst things that can happen to concrete is when it is exposed to fire. This causes the concrete to lose its resistance and stiffness, which causes a big change in how the concrete behaves.

2.2.1 Fire scenarios

It is required to illustrate real-world fire activity in a schematic manner to examine the effects of heat exposure and evaluate the structural resistance. To account for this, the temperature-time curves are used. For design purposes, fire curves are always stated as temperature-time ($T-t$) curves, and the majority of them are derived from Eureka tests, ISO curves Euro code curves, hydrocarbon curves, and Rijkswaterstaat curves, among other sources (ISO 834-1, 1999; EN 1991-1-2:2002; Wald, et al., 2009), They distinguish themselves from one another based on the idea of fire severity, which may be interpreted as a measure of the intensity of a fire's exposure.

Because they show how different fire scenarios might play out, each curve has a different slope, maximum temperature, and time of heating as given in Figure 2.1. This is because they show how the temperature of the gas that the structure is exposed to changes as a function of the fire load (fuel) type and quantity. In general, standard temperature-time curves can be divided into three categories based on their primary application domains such as buildings, offshore/petrochemical, and tunnels. (Khoury, 2000).

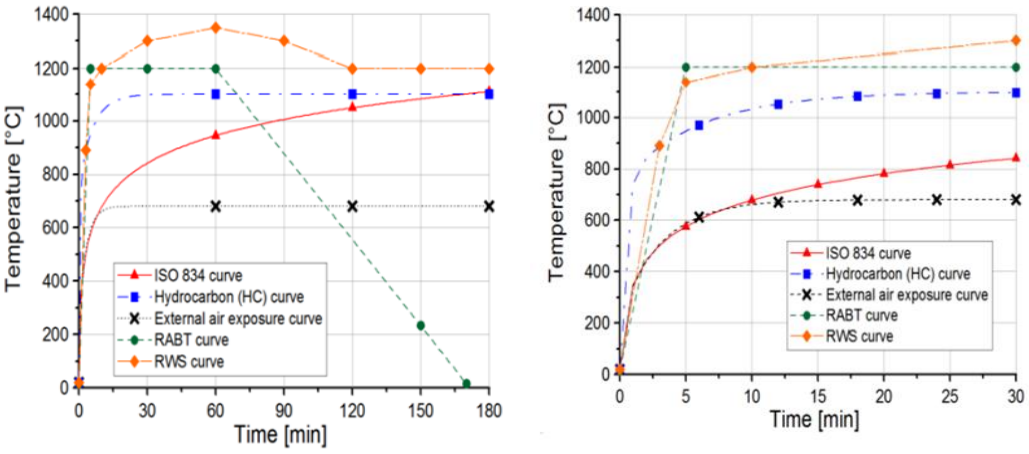

Figure 2.1. Standard temperature-fire curves: (a) global, (b) initial temperature rise (first 30 minutes).

2.2.2 ISO 834

Among structural engineers, the ISO 834 curve (ISO 834-1, 1999) is the one most often seen while designing and assessing structural parts and structures. It is sometimes

referred to as the "cellulosic curve" since the primary fire source is thought to be paper, wood, cloth, and other similar materials. The first slope is quite steep, with temperatures rising from 20 to 671°C in the first ten minutes. The temperature reaches 945 °C after one hour. The temperature-time increase $T\ (t)$ (in degrees Celsius) may be expressed mathematically by the following equation:

$$T(\ t) = \ T_0 + \ 345log10\ (8t + \ 1) \qquad (2.1)$$

where T_0 corresponds to the room temperature, generally assumed equal to 20 °C and t, corresponds to time in minutes.

2.2.3 The curve of hydrocarbons

The hydrocarbon curve is a temperature-time form that was used in this specific circumstance as an alternative. As a result of the diverse sources of fuel used in the offshore and petrochemical sectors, the maximum temperature reached during a fire in these industries is much greater. In these circumstances, gasoline, natural gas, and chemicals are used in the combustion process, and the temperature rises considerably more quickly than in the case of cellulosic material burning, reaching about 1100 °C in the first 10 minutes. According to the following equation, the temperature trend of the hydrocarbon fire curve is defined as:

$$T(t) = T_0 + 1080(1 - 0.325e^{-167t} - 0.675e^{-2.5t}) \qquad (2.2)$$

2.2.4 Fire curves on the outside

In addition to the ISO 834 and the hydrocarbon curves, the Euro code 1 also includes a description of the exterior fire curve. This curve, which represents the behavior of structural components in a façade that is separate from the main structure, has the following description:

$$T(t) = T_0 + 660(1 - 0.687e^{-0,32t} - 0,313e^{-3,8t}) \qquad (2.3)$$

2.2.5 Rijkswaterstaat (RWS) curve is a radial weighting curve

It has been discovered through the investigation of several catastrophes that tunnel fires display far more severe fire situations than those represented by the standardized

curves. As a result, the Netherlands has developed a new fire curve for use in the assessment of tunnel-protecting materials as a result of this development. The temperature increases quite fast in this curve, hitting 1200 °C in the first 10 minutes and then continuing to grow until it reaches 1350 °C (the melting point of concrete). High temperatures are maintained at these levels for 120 minutes, mimicking a fire load of 300 MW that might last up to 120 minutes (a 50 m^3 fuel, petrol, or oil tanker fire). The most significant difference between the Rijkswaterstaat (RWS) and the hydrocarbon curve is that the latter depicts the temperatures that would be anticipated from a fire that occurs in a somewhat open region, where dissipation of heat would occur, but the former does not. The RWS curve is based on the assumption that the temperature field develops in a confined space (tunnels) where heat dissipation is restricted, resulting in the structure being exposed to greater temperatures.

2.2.6 The RABT curve

This curve is a kind of curve that is used to represent something. This curve was created following a series of program tests in Germany, and it is known as the RABT curve (Haack, 1998). When compared to the RWS curve, it depicts a less severe tunnel fire scenario than the former. There is a quick temperature rise. It reaches 1200 °C (the melting point of some aggregates) in less than an hour, then stays there for about an hour before dropping to room temperature (the cooling branch).

2.3 Chemo-Physical Reactions During High-Temperature Exposure

Concrete is a composite heterogeneous substance made up of aggregates, cement, and water that are mixed together. The complicated behavior of concrete and reinforced concrete buildings when exposed to fire or high temperatures is due to the variances in the mechanical and physical qualities of the component materials used in the combination. Furthermore, changes in the material characteristics are not only produced by physical changes but also by chemical reactions occurring at the level of each individual concrete component, resulting in a cascade of changes. The chemical reaction reactions that take place in the cement paste have a direct impact on the strength of the finished concrete.

It is made up of a blend of calcareous and clay components that include lime and silica, which are reduced in size to microparticles throughout the production process. It is possible to get tricalcium silicate (Ca_3O_5Si or C_3S) and dicalcium silicate (Ca_2SiO_4 C_2S) at the conclusion of the procedure. During the hydration process, the calcium silicate hydrate gel (CSH) forms between the cement particles.

This gel is made up of calcium hydroxide crystals $Ca(OH)_2$. Changing the proportion/type of concrete ingredients, as well as the water-cement ratio (w/c), will have an impact on the final global mechanical characteristics of the concrete, as well as the influence of temperature exposure.

2.4 Concrete's Thermal Expansion

In the same way that many other construction materials do when subject to high temperatures, concrete, and reinforced concrete show thermal expansion when exposed to high temperatures. When the above-mentioned chemo-physical processes (loss of evaporable water in the cement paste and aggregates, reduction of chemically-combined water in the hydration products, transformation of siliceous aggregates, dissociation of calcium hydroxide, and de-carbonation of calcareous aggregates) are combined, micro-strain, micro-cracking, and deterioration of the entire concrete microscopic structure result.

For example, a significant percentage of the concrete strength deterioration may be traced back to the difference in volume expansion between aggregates and cement paste, which can be measured directly. Hardened cement paste expands with a maximum dilatation of 0.2 % when heated to 150 °C; when heated to 300 °C, the hardened cement paste begins to shrink , and when heated to 800 °C, the hardened cement pastes contracts with a maximum contraction of 1.6–2.2% (see Figure 2.2). However, when concrete is exposed to high temperatures, the aggregates used in the mix usually expand, with an average Coefficient of Thermal Expansion (CTE) of 5.5 x 10-6 $°C^{-1}$ at normal temperature (Bažant& Kaplan, 1996). This means that the aggregates used in the mix usually expand.

The solidified cement paste initially expands and then contracts when heated, while the aggregate continues to expand at a constant rate. In the bond (contact) zone,

differential stresses are formed as a result of the thermal incompatibility between the two concrete ingredients, resulting in the formation of microcracks. Typically, in a typical concrete mixture, the expansion of the aggregates is greater than the contraction of the cement paste, and the aggregates' combined expansion results in the expansion of the concrete as a whole. There are exceptions to this rule, though. For example, lightweight concrete that is made with pumice particles may shrink when heated to around 300 °C (Bažant & Prat, 1988).

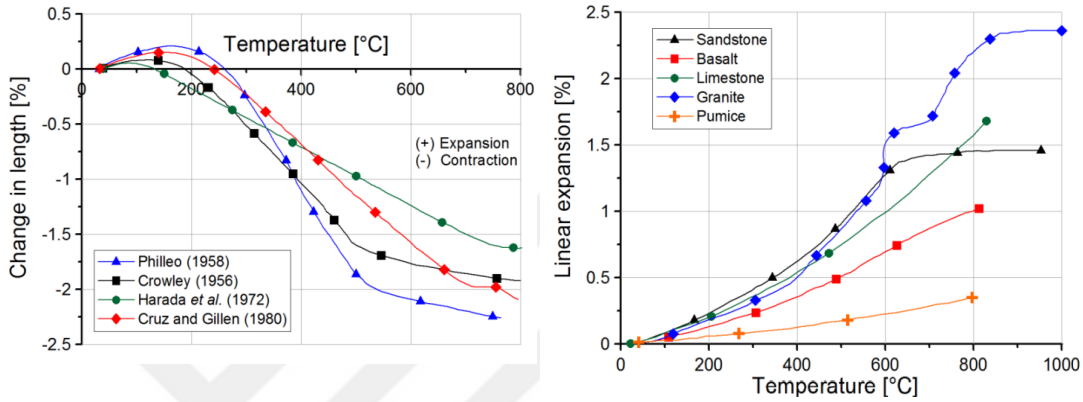

(a) (b)

Figure 2.2. Length change of Portland cement paste specimens; (b) linear thermal expansion of various rocks adapted from (Bažant& Kaplan, 1996).

2.5 Cracking and Spalling of Concrete

During the heating of concrete, the internal water distribution changes, resulting in a large rise in the pore pressure of the concrete. In particular, in certain circumstances, the rise in internal pore pressure, along with temperature-generated stresses, results in the breaking off of concrete chunks from the surface of the structural element in question (spalling). The phenomena may be violent or nonviolent depending on a variety of elements such as the heating rate, the shape and size of the pores, the temperature achieved, the geometry, and so on and so forth. Generally speaking, the phenomena of spalling may be separated into four categories.

These include aggregate spalling, explosive spalling of the concrete cover, surface spalling, and corner/sloughing off spalling. It is common for the first three phenomena to occur during the first 20-30 minutes of fire exposure, whereas the last happens between 30- and 60-minutes following fire exposure. These two occurrences, which

are the most severe of the preceding ones (explosion and surface spalling), are both impacted by the heating rate (20–30 °C/min). When exposed to high temperatures, NC and high-performance concrete respond in very different ways to one another. Because HPC is produced by lowering the water/cement ratio (resulting in low permeability) or by utilizing silica-fume (resulting in thick concrete with reduced permeability), the likelihood of spalling is much greater than that of NC (Bosnjak, 2014). The issue of spalling is very complicated, and it has not yet been completely understood as a result. There is a plethora of hypotheses to explain it in the literature. Furthermore, three hypotheses based on three separate probable spalling processes have been developed: pore-pressure spalling, thermal stress spalling, and a combination of pore-pressure and thermal stress spalling.

2.6 Behavior of the Different Concrete Types After Fire

The fire behavior of concrete and reinforced concrete is significantly impacted by the properties of the elements that make up the structure: concrete and steel. It is critical for both materials to study and comprehend how their mechanical, thermal, and deformation characteristics interact with one another as well as with the external environmental conditions they are exposed to. While the mechanical characteristics of the material are affected by temperature, the thermal properties of the material are directly associated with the extent of heat transfer through the structural section. In addition, the deformation characteristics of the material must also be taken into consideration.

Every year, a large number of fire incidents are recorded, with almost half a million unintentional fires documented in the United States between 2013 and 2014, and more than 150,000 fire accidents reported in the United Kingdom during the same time (Arna'ot, et al., 2017). Forty percent of these incidents were determined to be structural fires. Fire incidents were reported in 39 nations between 1993 and 2016, with more than a million fatalities occurring over that time period (Brushlinsky, et al., 2018).

The most important issue to ask after a structural fire is whether the concrete structure can be re-occupied as is, whether it has to be repaired before being re-occupied, or if it needs to be destroyed (Albrektsson, et al., 2011). In making this type of a decision, the accuracy with which residual qualities of concrete are estimated, particularly the

mechanical strength required to bear the design loads, is critical. The physical and chemical reactions that occur inside the microstructure of concrete are mostly determined by the temperature that is achieved and the length of time that the concrete is exposed to fire. However, the composition of the mixture, its porosity, and the thermal characteristics of the aggregate are all important elements in determining the thermal resistance of concrete buildings (Guo, et al., 2014; Tufailet, et al., 2017; Babalola, et al., 2021; Rafiei, et al., 2021), as well as the amount of water in the mixture. Due to the heterogeneous nature of concrete, it undergoes several chemical and physical changes as the temperature rises (Drzymala, et al., 2017).

They are essential, in conjunction with mechanical qualities, for identifying the entity of the damage in terms of strain and deformation of the structural components and for determining the extent of the damage (Kodur, 2014). Because of the phenomena of moisture migration that happens during fire exposure, analyzing the behavior of concrete when subjected to thermal stress is much more challenging than analyzing the behavior of other materials. As a result, the concrete response for different types and strengths of concrete could be very different based on this parameter's value.

The influence of high temperatures on the residual mechanical characteristics of concrete after fire exposure, as well as the post-fire structural assessment of buildings (Sultan & Alyaseri, 2020; Husem, 2006), have been the subjects of much study. The percentage residual strength of concrete is controlled by the changes in the microstructure of the concrete as a result of exposure to various temperatures.

2.6.1 The thermal characteristics change of concrete at high temperatures

The temperature distribution and the rate of heat transmission through a concrete structure's members are determined and affected by the thermal characteristics of the concrete type used in the construction of the structure. The basic thermal characteristics of concrete are defined as follows: thermal conductivity, specific heat capacity, and thermal diffusivity. This is important when you want to figure out how fire-resistant a reinforced concrete structure is (thermal analysis) or figure out how hot it is (Bischoff & Perry, 1991)

The following activities are dependent not just on the kind of cement used but also on the type of aggregate used (Phan & Carino, 1998; Netinger, et al., 2011; Deng, et al., 2020; and Phan &Carino, 2003). Because of the differences in thermal actions between the cement matrix and the aggregate, which are caused by the different thermal properties of the two materials, the bond between the two is broken at higher temperatures, further weakening the concrete structure and degrading its residual strength (Al-Owaisy, 2006; Sultan & Alyaseri, 2020; and Cheng, et al., 2004).

2.6.2 High-temperature mechanical properties of concrete

The physical and chemical changes that occur in concrete when exposed to high temperatures have a substantial impact on its mechanical qualities. When evaluating the mechanical characteristics of heated specimens, it is critical to differentiate between the hot and cold states of the specimens. Concrete specimens are heated to a certain temperature and allowed to thermally stabilize at that temperature for a specified time period before being evaluated in hot conditions to determine their mechanical characteristics. Instead, the specimens are heated to the desired temperature and then cooled to room temperature before being analyzed. The mechanical qualities of the second scenario are referred to as "residual concrete properties" in this situation.

Temperature changes have an impact on the strength of the concrete. The initial physical action of fire happens at a temperature of around 80 to 120 °C when the free water contained inside the concrete evaporates (Abrams,1971). This action has only a modest impact on concrete deterioration, but the subsequent action, which typically happens at temperatures greater than 300 °C but lower than 450 °C, constitutes the beginning of the major material degradation process. The dehydration of the C-S-H gel from the hydrated cement matrix is the mechanism by which this occurs (Düğenci, et al 2015; Abbas et al., 2021; Chu, et al., 2016).

Pour water vaporization above 100 °C has been reported to have a mostly positive effect on the compressive strength (f_c') (Al-Qwaisy, 2007; Toric, et al., 2013; Alimrani & Balazs 2020), whereas the serious strength reduction begins above 300–400 °C, where the chemical decomposition of calcium silicate hydroxide severely degrades the

material's microstructure. has been reported to have a mostly negative effect on the compressive strength.

Mechanical properties of materials that were exposed to 500 °C, such as flexural strength, shear strength, and modulus of elasticity, all suffered a lot of damage (Husem, 2006 and Al-Owaisy, 2007; Toric, et al., 2013; and Alimrani & Balazs, 2020.

Despite technological advancements in fire control systems, trusted fire records reported hundreds of unintentional structure fires every year all over the world (Netinger, et al., 2011). Because of the constant advancements in building materials technology, new studies in this area are continually needed to assist engineers in making judgments regarding the likely post-fire occupancy of fire-exposed structures (Roufael, et al., 2021; Deng, et al., 2020).

2.7 The Link Between Stress and Strain

The link between concrete stress and strain is essential for predicting the behavior of concrete constructions. A reduction in the initial slope of the elastic branch (elasticity modulus) and the maximum stress (strength) is observed for specimens heated without load, as previously discussed by many authors (Diederichs & Schneider, 1981; Khoury, 1999; Schneider, et al., 1982; Khoury, 2006), as the temperature increases. It looks like the same things happen when concrete specimens are heated when they're under a lot of pressure (see Figure 2.3).

2.8 Concrete Loaded at High-Rate Load

In most cases, ordinary structures are constructed based on conventional static actions prescribed by design standards. However, in recent years, the role of dynamic actions in structural design has grown significantly.

Concrete and reinforced concrete structures may be subjected to a variety of quasi-static and dynamic operations during their lives. Typical dynamic loads can be observed in the following situations: earthquake, projectile or aircraft impact, blast wave propagation, vehicle or ship collision with buildings, bridges, or offshore infrastructure, impact, missile, and so on (Daudeville & Malécot, 2011). Dynamic loads can also be observed in the following situations: As a result of the rapid

advancement of computer technology, it is now feasible in engineering practice to conduct numerical studies that can accurately model complicated structural issues such as impact and blast loads.

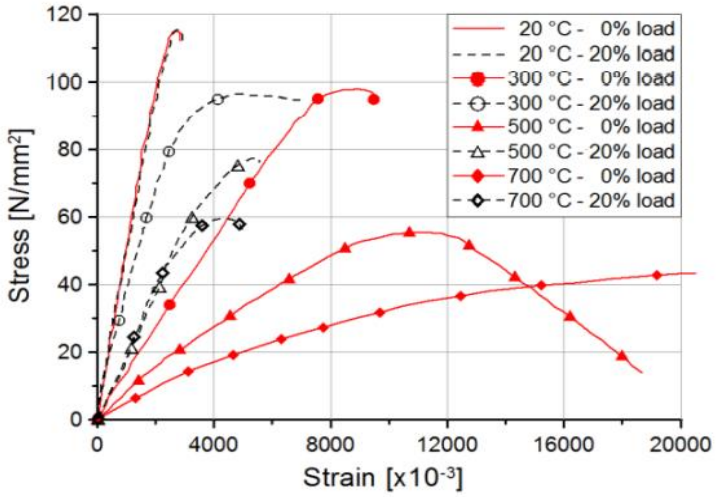

Figure 2.3. Stress-strain curves for different testing (compression) temperature levels; comparison between unloaded (0% applied load) and loaded (20% applied load) tests for Ultra High Strength concrete specimens containing steel fibers (Khoury, 1999).

As a result, numerical simulations can be used to identify the entity's structural damage or loading capacity in advance, allowing for the implementation of safety checks, assessments, and design rules that can ensure structural integrity and user protection even in the presence of extreme loading conditions. For both static and dynamic loading, it is important to use a numerical model that can account for realistic material response under complex loading situations. This is important so that you can predict the structural behavior under complex loading conditions.

2.9 Dynamic Behavior of Concrete After High Temperatures Exposure

The behavior of concrete and reinforced concrete structures subjected to high temperatures and dynamic circumstances has been studied in the preceding paragraphs. Depending on the circumstances, buildings might be vulnerable to the simultaneous action of fire and impact, as in the event of industrial chemical explosions or terrorist attacks, among other things. Because of the damage caused by

the fire exposure, the concrete's impact resistance is significantly reduced under these circumstances.

More importantly, as compared to concrete at room temperature, the structural response to the strain-rate effect is much different (Huo, et al., 2013). For this reason, to gain a better understanding of concrete's mechanical properties and global structural behavior under a variety of conditions, it is necessary to investigate not only the static but also the dynamic behavior (effect of strain rate) of concrete that has previously been exposed to elevated temperatures. Much research on the behavior of concrete and reinforced concrete structures under dynamic loading after exposure to high temperatures has been published, indicating that engineering knowledge when these two issues are coupled is quite restricted and needs to be improved.

2.10Impact Force

There are a variety of events that may be seen when two bodies collide with each other, depending on the original features of the impacting bodies. The exchanged impact forces change when there are changes in the material characteristics, the initial impact velocity, and the type of structure that was damaged, as well as the entity, the extent, and the severity of the damage that was done.

As a result, depending on whether the element deformability is low or high in comparison to the target deformability, impacting bodies may be categorized as either "hard" or "soft" (Kennedy, 1976). The impact produced by a collision between two bodies is analyzed in the issue under consideration: one body is at rest, while the other is striking with an initial velocity. The system may be seen as an impact between two masses, m_1, and m_2, which can be examined mathematically. In addition, the stiffness of the system is described by two separate variables, k_1 and k_2, which are independent of one another. There is one stiffness, k_1, that is put between the two masses. The other stiffness, k_2, is used to describe the structure's deformation and resistance force as shown in Figure 2.4.

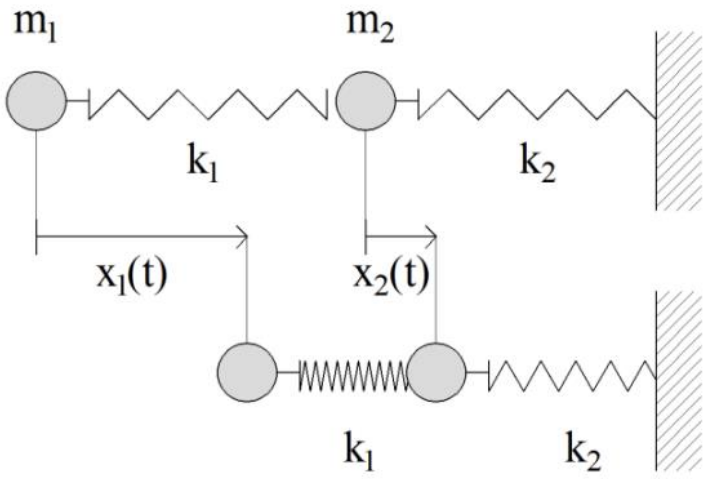

Figure 2.4. Simplified mechanical model for the impact problem proposed by Eibl (1987).

On the other hand, certain components of some structures are exposed to repeated unintentional impact loads, such as the impact of falling items or the lateral collision of moving vehicles, which are examples of forms of repeated accidental impact loads (Nili & Afroughsabet, 2010b). Aside from offshore construction, where the waves of ocean water expose these structures to repeated hydraulic impacts, other instances of repeated impacts include bridges and tunnels. If you have a hydraulic structure, such as a stilling basin, the water serves as an impacting force on the runway downstream of the structure (Salaimanimagudam, et al., 2020; and Wang & Chouw, 2017).

Other instances of repeated impacts are the forces exerted by aircraft wheels on airport runways (Abid, et al., 2020b), which are exposed to repeated collisions. Various approaches may be used to determine the impact strength of concrete. In ACI 544-2R (1999), the repeated impact test was added. It is the simplest impact test and the only one that can be used to simulate repeated impact.

Accidental non-design loads include the impacts of falling masses on beams and slabs, as well as the collision of driving autos with columns and walls, which are all examples of non-design loads. Such loads may create severe localized damage that can compromise the structural integrity of the member or cause a portion of the structure to fail. When these effects are repeated over and over again, the consequences grow more severe.

As an illustration, consider parking garage columns that are subjected to daily high traffic with the possibility of repeated impacts by moving vehicles (Abid, S.R. et al., 2020b), which are prone to repeated impacts by moving vehicles. Another example of repeated impacts is the tire impact of an aircraft landing on an airport runway, which occurs when the aircraft tires hit the runway (Salaimanimagudam, et al., 2020). The water velocity reducing elements in hydraulic structures, such as chute blocks in stilling basins, are subjected to repeated impacts from high-velocity water and debris carried by the water (Ayoob & Abid, 2020). For many decades, the performance of concrete materials and structural members under the influence of impact loads was the primary focus of scientific investigation.

Depending on the velocity of the impactor and the direction of the impactor, a variety of testing methodologies are available to analyze the various impacting loads that may be applied. Experiments involving high strain rates, such as the projectile testing technique, may be used to assess the performance of a structural part when it is subjected to any kind of projectile in combat situations, conflict zones, or terrorist strikes (Kim, et al., 2018; Feng, et al., 2019).

2.10.1 Fiber's History.

The modern era of fiber-reinforced concrete research and development began more than 50 years ago. The first scientific study on FRC were published by Romualdi and Batson (1963) and Romualdi and Mandel (1964). In fact, A. Bernard received the first patent in the USA California in 1874 for a dispersed reinforced concrete element containing steel fibers. Bernard's patent demonstrated that the strength of concrete was increased by the addition of irregular steel scraps (Singh, 2016). Today, there are many types of fibers that are employed as reinforcement Table 2.1. According to ACI 544, there are four types of FRC depending on the fiber material used. These are;

- Type I is steel FRC (include carbon steel, stainless steel and/or alloy steel fibers)
- Type II is glass FRC (contains Alkali Resistant Glass Fiber which is glass fiber that has been treated with zirconium oxide to help it withstand alkalinity.)
- Type III is synthetic FRC (include carbon, nylon, PP, polyvinyl alcohol, polyethylene and/or polyacrylonitrile fibers)

- Type IV is natural FRC (include plant, animal, and/or mineral fibers)

Researchers are continually exploring current fiber applications and seeking new ways to improve the properties of building materials (Katzer, 2006; Hait, et al., 2024).

Table 2.1. Types of fibers widely used in concrete and their properties.

Fiber types	Relative density (g/cm^3)	Tensile strength (MPa)	Modulus of elasticity (GPa)	Diameter (μm)	Ultimate elongation (%)	Operating temperature (℃)
Steel	7.8	400~2100	154~200	300~800	3.0~4.0	<600
Basalt	3.0	3000~5000	80~110	10~15	3.1	<700
Glass	2.7	14~2800	70~90	8	2~3.5	<300
Carbon	1.76	2450~3150	205	7~8	1	<500
Polyvinyl alcohol	1.2	1600~2500	40~80	39	6	<200~400
Polyacrylonitrile	1.18	>600	>10	12~21	>15	<300
Polyethylene	0.96	2850	73.9	35	10	<200~400
Nylon	1.16	900~960	4 ~ 6	30	18~20	<250
PP	0.91	400~650	5 ~ 8	43	18	<400

2.10.2 Fiber reinforced concrete (FRC)

The ACI 544 and ACI 318 codes and other (ACI, 2018; ACI 318, 2014; AFGC-SETRA, 2002; für Stahlbeton, 2007; CNR-DT 204, 2006). often demonstrate solutions that have a significant influence on the services provided by the facility, such as mechanical and electrical work, as well as drop panels that need extensive slab formwork customization, among other things (Jarallah, 2016).

Stress condensation at the tips of flexural and shear cracks is reduced, and the spread of the cracks is controlled by the inclusion of fibers. Additionally, the inclusion of fibers not only changed the shape of the punching failure surface on the tension side,

but also gradually moved the failure surface away from the column face (Swamy, et al., 1979). When 1% fiber volume is added to the structure and it is put into service, the deflections are reduced by about 30%, and the strain compressive of concrete and the rotation are reduced by about 40–50%. Improved crack control was also observed, with a 21% increase in crack load recorded as a result of the inclusion of steel fibers (McHarg, et. al., 2000).

In recent years, researchers have looked at the impact performance of concrete with PP fibers (Badr & Ashour, 2005; Badr, et al., 2006; and Rahmani, et al., 2012; Myers & Tinsley, 2013), micro-steel fibers (Abid, et al., 2020a), steel fibers (Ismail &Hassan, 2017; and Abid, et al., 2021b; and Nili & Afroughsabet, 2020b), glass fibers (Murali, et al., 2021b), carbon fibers (Haridharan, et al., 2020), natural fibers (Ramakrishnan, et al., 2021), and hybrid fibers (Feng, et al., 2019; Maalej, et al., 2005). Recent studies have looked at the effects of fiber type, fiber dose, fiber distribution, and intermediate fiber meshes on enhancing the impact resistance of preplaced aggregate concrete with single, double, and triple layers and the results have been promising (Arna'ot, et al., 2017a; Babalola, et al., 2021; Phan & Carino, 1998; Phan & Carino, 2003; Cheng, et al., 2004; Al-Owaisy, 2006).

2.10.3 Polypropylene (PP) fiber used

PP gained commercial popularity including the construction industry after Italian chemist Natta and his colleagues (1954) succeeded in converting PP into an isotactic polymer. because it is thin and light, environmentally friendly, has a good performance/cost index, high flexibility, low corrosiveness, and has a low impact on public health (Anto & Bhuvaneshwari, 2022). The widespread use of PP fibers in concrete started after the late 1970s (Balaguru, 1992). When the United States Corps of Engineers needed to create explosion-proof structures, PP fibers were recommended as an additive to cement for the construction of the buildings. This included the incorporation of numerous natural and man-made colors into the cement and mortar (Hao, et al., 2016).

PP is a polymer formed from pure monomeric C_3H_6 hydrocarbons, such as paraffin wax, and is used in the production of plastics. In addition to its low price, easy to process, excellent chemical resistance, and translucent to opaque properties, PP is

hydrophobic and inert as well as resistant to plastic shrinkage cracking and very stable in the alkaline environment of concrete. However, it has disadvantages such as rather low physical properties (e.g. low modulus of elasticity) and fairly low heat resistance (i.e. poor fire resistance, sensitivity to sunlight) (Latifi, et al., 2022).

2.10.4 Engineering cementitious composite (ECC)

ECC stands for Engineering Cementitious Composites, which is what the original creators used to show how the micromechanics principles that underpin the development of this material is shown in its the name (Li, 1998). ECCs have since been employed in a variety of applications (Li, et al., 1998a, 1998b, 2007, 2019). Since then, multiple experiments have been carried out in order to introduce various ECC combinations with varying fiber kinds and concentrations. There is a wealth of information available in the literature on the various mechanical features of ECCs.

When it comes to physical components, ECC employs components that are comparable to those used in FRC. It is made up of water, cement, sand, fiber, and a few typical chemical additives as well. Avoid using coarse aggregates since they have a detrimental impact on the ductile behavior of the composite, which is what makes it special. The standard composition employs a weight-to-cement ratio of w/c, with a sand-to-cement ratio of 0.5 or below. In contrast to other high-performance FRCs, ECC does not rely on a vast quantity of fiber.

However, because the compound is intended for structural purposes, using 2% or less of the volume of non-contact fiber in a given application is usually sufficient. In part because of the minimal quantity of fiber utilized and the fact that they are all unique, the ECC mixing technique is quite similar to the one used in conventional concrete mixing. A number of feasibility studies have also shown that ECC is economically feasible in particular structural applications by carefully restricting the quantity of fiber used. Different kinds of fiber can be used in the ECC, but the exact construction must follow a set of rules that are based on micro-mechanical concerns in order to work properly (Kanda & Li, 1999).

A study conducted using ECC reinforcement systems revealed that the out-of-plain resistance of building walls was greatly enhanced when subjected to semi-static stress.

In particular, the ultimate load capacity and maximum deflection of the masonry wall rose by a factor of 6.5 and 22, respectively, and by a factor of 4.2 and 15.9, respectively. The steel mesh inside the ECC strengthening layer increases the ultimate load capacity of the samples from 17% to 74%, depending on the sample. In addition, the capacity of ECC to cause strain hardening and the development of many micro-cracks was shown in the masonry application (Maalej, et al., 2005).

ECCs are a type of high-performance self-compacting concrete that exhibits extraordinary ductility with strain hardening and multiple cracking under tensile and flexural stresses when compared to conventional concrete with similar strength and fiber content (Prasad & Murali, 2021; Ramakrishnan, et al., 2019).

The high velocity impact resistance of this hybrid-fiber ECC has been investigated experimentally, which indicates that it has a high capacity to absorb energy as well as the ability to resist multiple effects with small fragmentation. Remove the portion and size of the small hole on the shock surface that has been studied experimentally. Maalej et al. (2005) found that ECC is a good material for building structures that can withstand explosions because it is impact and design resistant.

In order to better address the functional requirements of impact and blast resistant constructions, a hybrid-fiber ECC with the proper volume ratio of high and low modulus fibers has been created. In this form of hybrid fiber, which has been found to provide an ideal balance between ultimate strength and strain capacity, 0.5percent steel and 1.5 percent polyethylene fiber are used in this form of hybrid fiber. (Zhang et al., 2004.

The capacity of ECC to minimize stress and the transfer of damage in the joints to the interior of the shear slabs is responsible for the improvement in structural strength and ductility found in ECC slabs. ECC slabs have higher ductility and greater ductility than conventional slabs. The shear stress test, which is often used to demonstrate the prevention of local fractures in the joint, also demonstrated this (Kanda & Li, 1998).

In addition to the common qualities of high tensile softness and many fine cracks, ECC represents a family of materials with a variety of diverse uses and properties. The unification of self ECC (for example, ECC M45 and its variations) is being planned

extensively on the construction site. For ECC-M45, the proportions of the ECC mix design by weight is given by Kong et al., (2003).

Modifications to the standard mix were implemented in several different building projects. Japan is the only country that produces a complete range of ECC products (Kunieda and Rokugo, 2006).

After steel yields, it is possible to estimate the shear capacity of an ECC beam by a linear superposition of the contributions made by the ECC material as well as the shear and axial steel reinforcements. This is possible since both materials flex in a compatible manner even after steel yields. It was thought that this technique would be relatively accurate and cautious (Rokugo, et al., 2007) .

The initial moisture loss from the free pore water evaporation (forming larger pores and capillary pores) and the hydration of the free fly ash that was not hydrated during the curing period were the reasons given by Bhat et al. (2014) for the increase in the tensile strength of PVA-ECC after exposure to 100 °C.

2.11Repeated Impact Strength of ECC

The ACI 544-2R repeated impact tests are used in this study to depict the impact strength as the retained numbers of impact blows in the cracking and failure stages.

Several major studies have been undertaken in recent years to assess the repeated impact strength of various concrete kinds using this testing approach, with the results being published in peer-reviewed journals. Self-compacting concrete was explored by Mastali & Dalvand (2018) to determine the influence of the length and dose of recycled carbon fiber reinforced polymer on the repeated impact performance of self-compacting concrete. Ismail & Hassan, (2017) performed experimental experiments utilizing the ACI 544-2R protocol to assess the impact resistance of self-compacting concrete mixes that included varying amounts of steel fibers and crumb rubber.

According to the test findings, the impact numbers rose by up to 30% and the impact ductility improved, while the integration of 1% steel fibers greatly improved the retained impact numbers by more than 400 percent, according to the test findings. Mahakavi & Chithra, (2019) studied the mono and dual effects of hooked-end and

crimped steel fibers on the ACI 544-2R impact resistance of self-compacting concrete, and they found that when the two fiber types were hybridized, there was a considerable improvement in impact resistance. According to Jabir et al., (2020) the impact resistance of ultra-high-performance concrete may be improved by using single and hybrid micro steel fibers and PP fibers in various combinations. Abid et al., (2021b) performed repeated impact tests on self-compacting concrete with micro steel fibers levels of 0.5, 0.75, and 1.0 percent in accordance with ACI 544-2R and flexural (Abid et al., 2020a) standards. The findings showed that adding 1.0 percent of steel fibers could enhance the impact resistance by more than 800 percent when compared to the reference plain specimens, while another study (Abid, et al., 2021a) found that adding 1.0 percent of steel fibers could raise the impact resistance by around 1200 percent. Murali and colleagues (2019; 2020; 2021a; 2021b; and 2021c) carried out a series of experimental activities to investigate the repeated impact capabilities of multi-layered fibrous concrete.

The use of intermediate fibrous meshes may improve the material's impact resistance throughout the cracking and failure phases of the process, according to studies on this material (Ramkumar, et al., 2019). Steel fibers, on the other hand, were shown to have made the most significant contribution to the development of impact strength.

Mehdipour and colleagues (2020) conducted mechanical and repetitive impact tests on concrete specimens that had been exposed to temperatures of up to 600 °C. They looked at the effects of replacing a portion of the cement with metakaolin and a portion of the coarse aggregate with crumb rubber. Their findings demonstrated that high temperatures had a detrimental effect on the retained impact counts, with specimens subjected to 600 °C cracking after just one hit. According to Al-Ameri et al. (2021), they investigated the ACI 544-2R repeated impact performance of normal weight-normal strength concrete after it was subjected to extreme temperatures. The findings revealed that the influence of 100 °C on the retained impact numbers was negligible, and that the residual impact strength after heating to 600 °C was less than 4 percent of the initial value. On the other hand, previous researchers (Sahmaran, et al., 2010; Sahmaran, et al., 2011; Çavdar, 2012; Li et al., 2016; Liu et al., 2917; Li et al 2019; Zhihui et al., 2020) have done some investigations into the residual mechanical characteristics of ECC after it has been exposed to high temperatures.

It is clear from the literature review that there are just a few experimental studies on the repeated impact strength of ECCs that have been published in the scientific literature. In a similar vein, there is a significant information gap about the residual impact strength of fibrous concrete after exposure to high temperatures. To the best of the authors' knowledge, no previous research has looked into how ECCs hold up after being exposed to high temperatures.

The purpose of this study was to close this knowledge gap by directing an experimental program to evaluate the cracking and failure repeated impact performances and impact ductility of PP-based ECCs after exposure to high temperatures approaching 600 °C. It is necessary to do this sort of study since both accidental fire and impact loads are predicted to occur over the structure's lifetime. The findings from this study can be used to figure out how structural components made from ECCs would react in the event of an accident like this.

2.12Impact Ductility

Impact Ductility One of the structural physical quantities that are used to define the response of flexural members under loads is ductility, which is a kind of quantitative measurement to define the capacity of the member to sustain plastic deformations (Abbass, et. al., 2020) A similar definition was also used in previous studies to estimate the plastic range of repeated impact that the specimen can withstand before failure. The impact ductility index (D) can thus be defined as the ratio of the failure impact number to the cracking impact number

CHAPTER THREE

EXPERIMENTAL WORK

3.1 General

As preceded in the previous chapters, the main aim of the work presented in this thesis is to fill the knowledge gaps regarding the impact properties of ECC with low-cost PP fibers and to evaluate the deterioration degree of impact resistance after exposure to high temperature as in case of accidental fires.

Therefore, the experimental work is mostly composed of three main elements that define the objectives of the work. These three elements include the definition of the used mixtures and their composing materials, while the heating regimes to high temperatures targets and cooling down to room temperature is the second element. On the other hand, the third main element is the impact tests. For this, this chapter is divided into four sections. The first overviews the experimental program plan exploring the sequence of work starting from material testing and mixing and ending with data collection from impact tests and other secondary tests.

The second part presents the used concrete and ECC mixtures and shows the properties and details of the used materials, mixing, and curing procedures, in addition to the adopted control mechanical tests. The third section of this chapter discloses the step-by-step procedure of the heating and cooling process of the tested specimens. Finally, the details of the material-scale and structural-scale impact tests are reviewed in the fourth section, where the section describes the testing procedure, test machines, specimens' dimensions, and test setups.

3.2 Experimental Program Description

In this section, the program of the experimental work is explained so that the following sections that deal with the details of the experimental work become easy to follow and their aims become clearer. A brief description of the two-stage experimental program of this study is presented herein. The experimental work is composed of two subsequent stages; the first is the material-scale testing, while the second is the structural scale testing.

It is worth mentioning here that using the term "scale" does not necessarily refer to the physical scaling of the test specimen, whereas the term "material scale" refers to all tests of unreinforced (plain) specimens that are designed to investigate the effect of high temperature on the performance of the concrete and ECC material. On the other hand, the term "structural scale" is adopted here as a reference to the reinforced concrete and reinforced-ECC plate specimens, which were subjected to repeated impact loads. It should also be mentioned that two fixed mixtures were used in both stages. The first is a PP-reinforced ECC, while the second is a conventional concrete mixture having approximately a similar design compressive strength. The details of the mixtures and materials used will be explored in the following section.

3.3 Material Scale Testing

The first part includes the casting, heating, and testing of different types of standard mechanical tests of specimens. Cubes with 100 mm side lengths were adopted to evaluate the compressive strength (f_c') of both mixtures before and after exposure to high temperatures. The average of six cubes was considered as the compressive strength (f_c'). On the other hand, the average of six prism specimens was taken to represent the flexural strength (modulus of rupture) of each mixture at each temperature level. The prisms were 100×100×400 mm in dimensions, while the test span was 300 mm.

The third test is the ACI 544-2R repeated impact test, which will be detailed in the following sections. Cylindrical disk specimens with a diameter of 150 mm and a depth of 64 mm were used to conduct this test considering the average of six specimens as the retained strength. Seven temperature levels were considered in this stage, which are the unheated (reference) or room-temperature (approximately 25 °C), 100, 200,

300, 400, 500 and 600°C. The details of the heating and cooling procedure and apparatus will be clarified in the following sections. Figure 3.1 shows a flowchart that describes the sequence and variables of the first-stage test program.

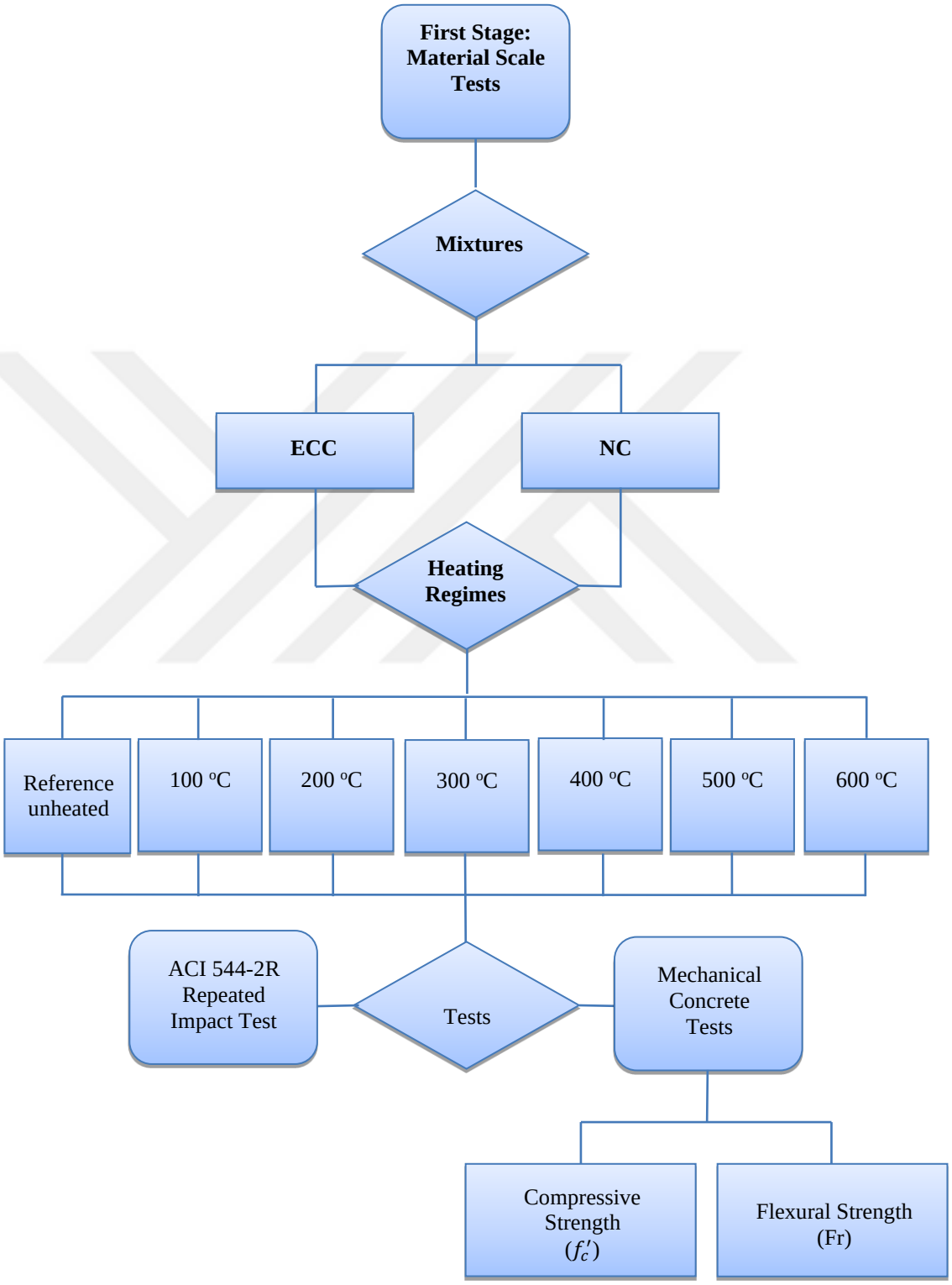

Figure 3.1. Test sequence of the material-scale stage.

3.4 Structural Scale Testing

In the second part of the experimental work, reinforced square palate specimens were subjected to elevated temperatures and tested under repeated impact loads. The instrumented drop-weight test was considered to evaluate the residual impact strength of the test specimens. The test included different measurements of force, deflection, and vibration and considered for different structural boundary conditions. Three boundary conditions were considered to simulate the simple support case, two-opposite sides restricted case, and four-sides restricted case.

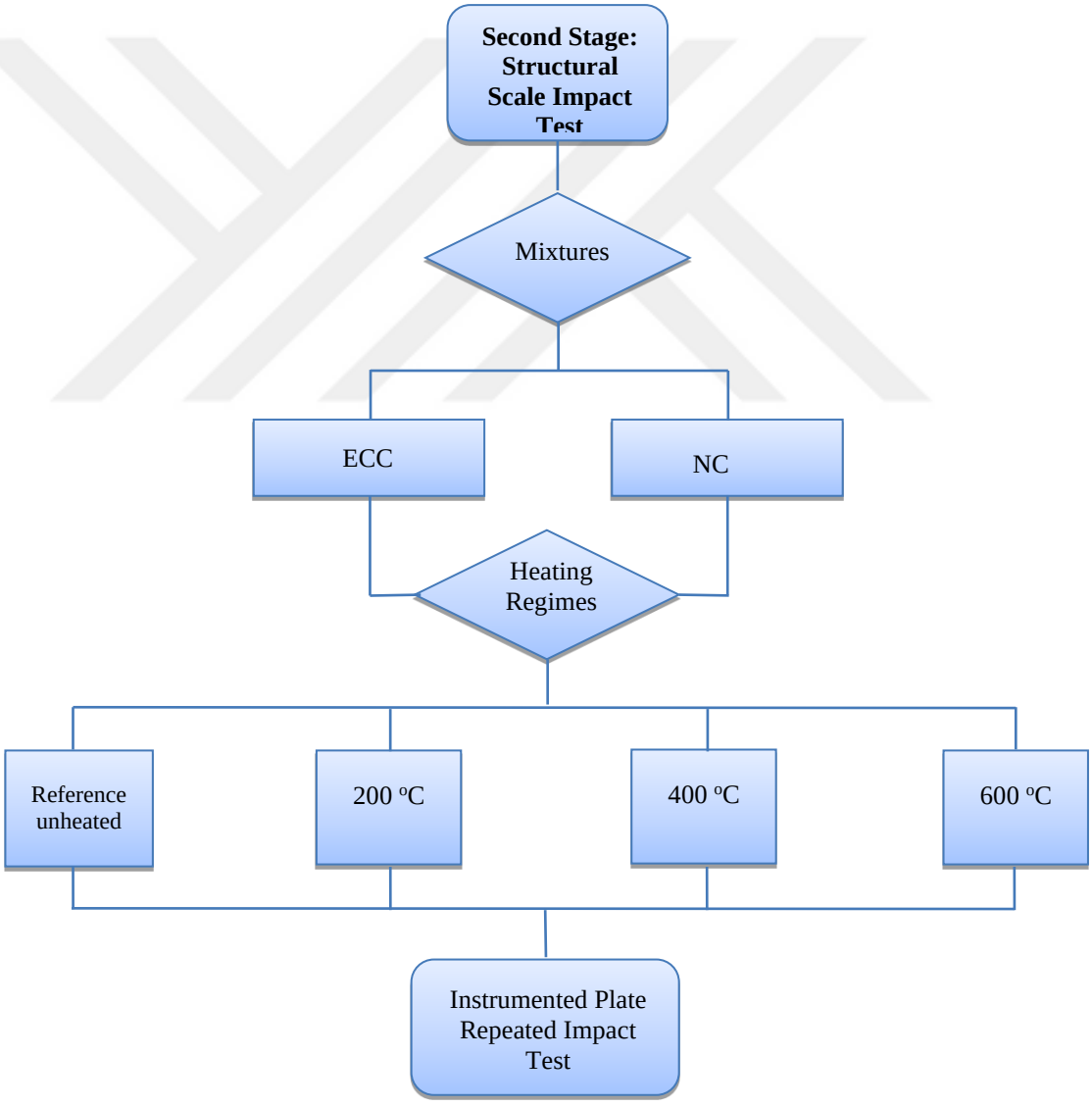

Figure 3.2. Test sequence of the structural-scale stage.

The details of the plate specimens are given in this Chapter. The material-temperature behavior of the first stage tests showed that to understand the thermal behavior of strength, the temperature levels can be reduced to four stages instead of the seven stages. Therefore, in the second stage, the plate specimens were subjected to room temperature (25 °C), and three temperature levels 200, 400, and 600 °C. Figure 3.2 illustrates the program sequence of the second stage.

3.5 Mixtures and Materials

3.5.1 Mixtures

Two fixed mixtures were used to evaluate the post-high temperature exposure strength of ECC. The first is a normal-strength conventional concrete mixture (NC) that has an approximate design strength of 40 MPa, while the second is an ECC mixture. The ECC mixture was adopted following the standard M45 ECC (Li, 2008). However, instead of the typical PVA costly fibers, low-cost PP fibers were used. The aim of the study is to evaluate the residual impact strength of the ECC mixture, while the NC mixture was introduced for comparison purposes. The NC mixtures include the typical gradients of conventional concrete of cement, sand, and gravel in addition to water. The ECC mixture incorporates 1.2 fly-ash/cement ratio, 0.8 silica sand/cement ratio, and 0.27 water/cementitious materials ratio, in addition to 2% volumetric content of PP fibers. Table 3.1 shows the details of both mixtures.

Table 3.1. Mix compositions of the NC and ECC (kg/m^3).

Mixture	Cement	Fly Ash	Sand	Silica Sand	Gravel	Water	SP‡	Fiber
NC	410	NA	787	NA	848	215	NA	NA
ECC	570	684	NA	456	NA	330	4.9	18.2

‡SP: SuperPlasticizer

3.5.2 Materials

3.5.2.1 Cement and fly ash

Locally manufactured Portland cement (Type 42.5) was used in each of the two mixtures. The used cement has the chemical composition and physical properties addressed in Table 3.2. On the other hand, fly ash type F was used as a secondary

cementitious material in the ECC mixture only. The chemical composition and physical properties of the used fly ash are listed in Table 3.2.

Table 3.2. Chemical and physical properties of cement and fly ash.

Content	**Cement** (%)	**Fly Ash** (%)
SiO2	20.08	56.0
Fe2O3	3.6	24.81
Al2O3	4.62	5.3
CaO	61.61	4.8
MgO	2.12	1.48
SO3	2.71	0.36
Loss on ignition (%)	1.38	5.78
Specific surface (m^2/kg)	368	-
Specific gravity	3.15	2.20
Compressive strength 2 days (MPa)	27.4	-
Compressive strength 28 days (MPa)	46.8	-
Fineness (% retain in 45 μm)	0	28.99

3.5.2.2 Fine and coarse aggregates

The fine and coarse aggregates were only used within the NC mixture. Local crushed gravel and river sand from Wasit provision/Iraq were used as coarse and fine aggregates. The maximum aggregate size of the gravel was 10 mm, while the sieve analysis of both fine and coarse aggregates is shown in Figure 3.3.

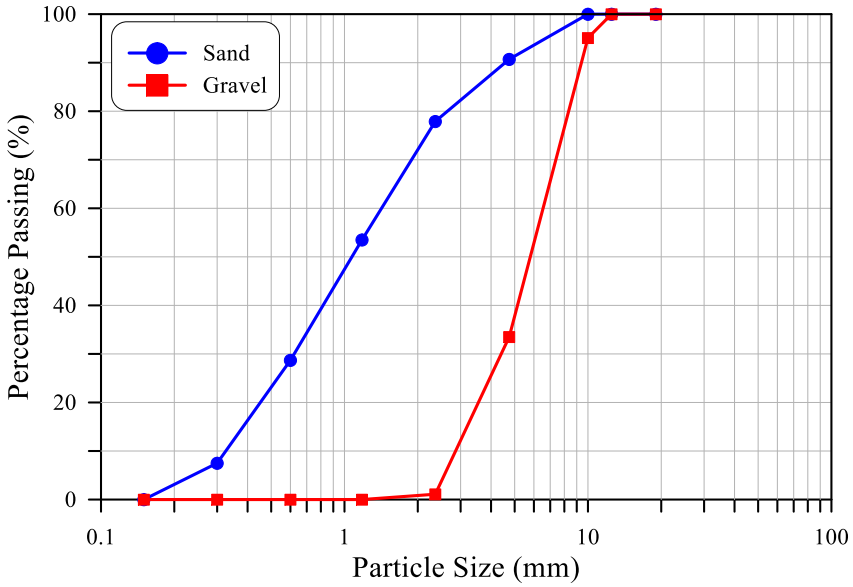

Figure 3.3. Grading of fine and coarse aggregates.

3.5.2.3 Silica sand

As preceded, ECC includes no sand or gravel, where the filler of the mixture is composed of a single type of very fine silica sand with grain size of 80 to 250 micrometer and a bulk density of 1500 kg/m^3. The appearance of the used silica sand is shown in Figure 3.4.

Figure 3.4. Appearance of the used fine silica-sand.

3.5.2.4 Polypropylene (PP) Fibers

PP fibers having the properties shown in Table 3.3 and appearance shown in Figure 3.5 were used with the ECC mixture at a constant volumetric content of 2 %.

Table 3.3. Properties of the used PP fiber.

Property	Density	Length	Diameter	Tensile Strength	Elastic Modulus
Value	910 kg/m^3	12 mm	0.032 mm	400 MPa	4000 MPa

Figure 3.5. Appearance of the used PP fibers.

3.5.2.5 Superplasticizer

For the ECC mixture, a superplasticizer type ViscoCrete 5930-L from Sika® was used to assure the required workability due to the large amount of fine materials. The properties and advantages of the used superplasticizer which is shown in Figure 3.6. can be listed as:

- Strong self-compacting behavior. Therefore, suitable for the production of self-compacting concrete
- Extremely high-water reduction (resulting in high density and strengths).
- Excellent flowability (resulting in highly reduced placing - and compacting efforts)
- Increase high early strengths development.
- Improved shrinkage- and creep behavior.
- Reduced rate of carbonation of the concrete.
- Improved Water permeability.

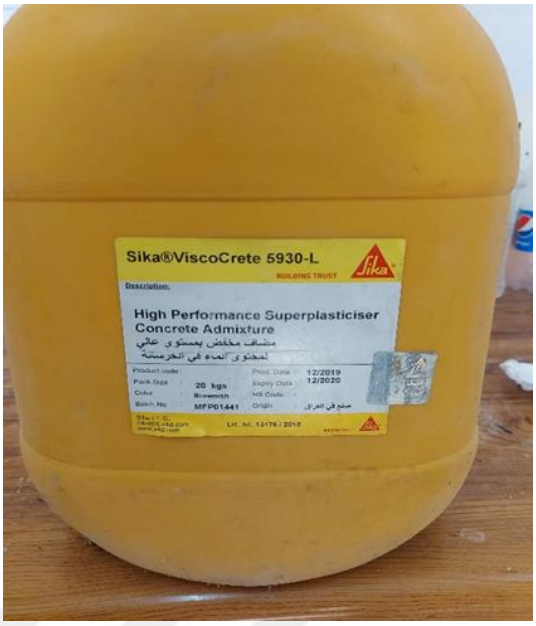

Figure 3.6. The appearance of the used superplasticizer.

3.6 Material-Scale Tests

The main material test within the material-scale tests is the standard ACI 544-2R (ACI 544.2 R-89, 1999) repeated impact procedure. On the other hand, the compressive strength (f_c') is the basic concrete test that must be considered for every concrete or cementitious material, while the flexural strength test is also essential for ECC mixtures. Therefore, the compressive strength (f_c') and flexural strength tests were also considered in this study and were tested for both mixtures and for every temperature level.

Figure 3.7. Single group of disc, cube and prism specimen.

3.6.1 Compressive and flexural strength tests

Cube specimens with 100 mm side length were used to evaluate the compressive strength (f_c') as per the recommendations of British standard (BS EN 12390-3, 2009). The average of six cubes was considered as the compressive strength (f_c'). Thus, for

each mixture, and for the six temperatures level and the unheated reference case, 42 cubes were cast in groups of six specimens as shown in Figure 3.7.

On the other hand, the average of six prism specimens was taken to represent the flexural strength (modulus of rupture $f_{ct,fl}$) of each mixture at each temperature level. The prisms were 100×100×400 mm in dimensions, while the test span was 300 mm. The flexural strength was conducted based on British standard (BS EN 12390-5, 2009). As for the compressive strength (f_c'), 42 prisms were cast for each mixture in groups of six specimens as shown in Figure 3.7. Thus, for both mixtures, a total of 84 cubes and 84 prisms were cast and tested for both mixtures to evaluate the thermal behavior of compressive strength (f_c') and flexural strength.

3.6.2 ACI 544-2R repeated impact test

The response of materials and structures can be experimentally evaluated using different types of tests, among which is the drop-weight one. ACI 544-2R (ACI 544.2 R-89, 1999) addressed two types of drop-weight tests. The first is the instrumented drop-weight test which is the most commonly used technique to evaluate the structural and material impact response of structural members. This test is mostly used for reinforced beam and slab elements and requires expensive sensor instrumentation and data acquisition equipment.

On the other hand, the alternative drop-weight impact test is a very simple one that is conducted on small size specimens and requires no instrumentation or any sophisticated measurement systems. This test requires that a drop weight of 4.54 kg is dropped repeatedly on the test specimen from a height of 457 mm until a surface crack becomes visible, then the repeated impacts are resumed until the fracture failure of the specimen.

The numbers of impacts at which the first crack and failure occurred are recorded as the cracking impact number and failure impact number. The test is generally considered as a qualitative evaluation technique, which compares the impact resistance of different concrete mixtures based on their ability to absorb higher or lower cracking and failure impact numbers. Figure 3.8 shows the details of the ACI 544-2R repeated impact test apparatus.

The standard test specimen is cylindrical (disk) with a diameter of approximately 150 mm and a thickness of approximately 64 mm. The standard test is operated manually by hand-lifting the drop weight to the specified drop height and releasing it to be freely dropped by gravity on a steel ball, which rests on the center of the specimen's top surface. The steel ball is used as a load distribution point and is held in place using a special framing system that also holds the concrete disk specimen as illustrated in Figure 3.9. However, it was found in the previous works that the manual operation requires significant effort and is time consuming, especially because at least 6 replication specimens are required to assess the test records due to the high dispersion of this test's results.

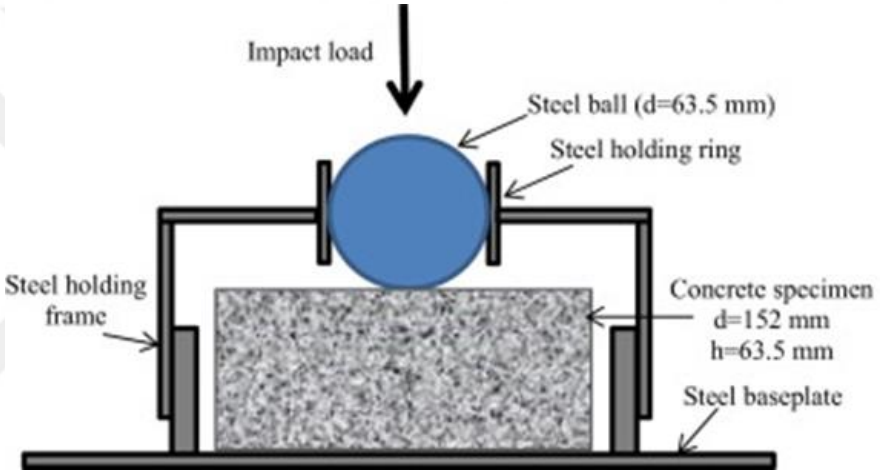

Figure 3.8. The test specimen and the lower portion of the ACI 544-2R RBDWI testing apparatus (Abid, et al., 2020b).

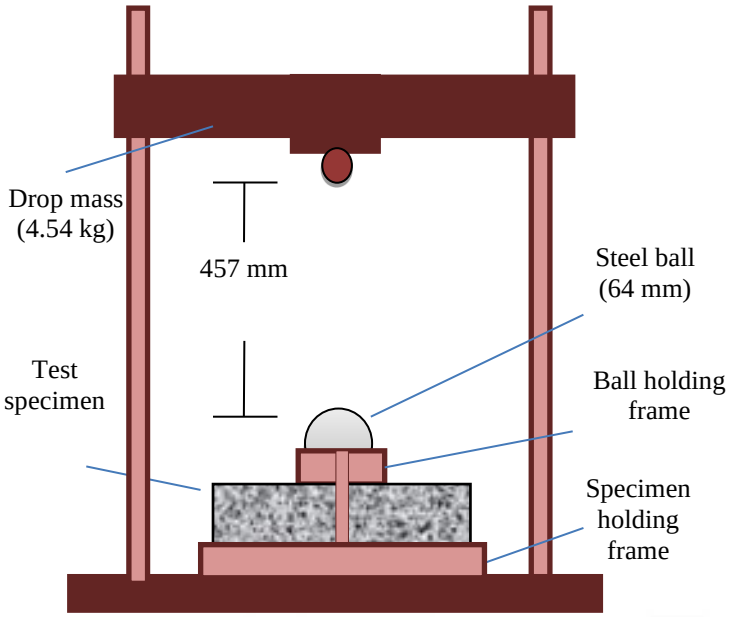

Figure 3.9. Testing apparatus of the ACI 544-2R repeated impact test (Abid, et al., 2020b).

Therefore, an automatic repeated dropping weight impact testing machine was manufactured to afford reliable repeated impact testing with minimized variation of test results. The details of the testing machine are shown in Figures 3.10. The testing machine subject impact loads as per the recommendations of the ACI 544-2R but are operated electrically and impact numbers are counted by a special laser sensor.

(a)

(b)

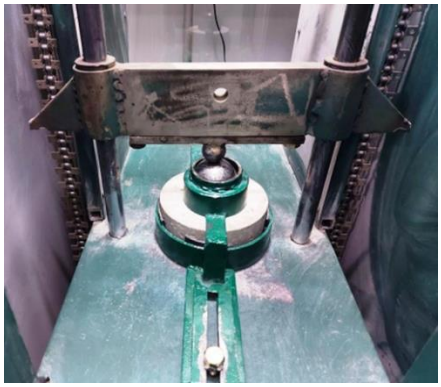

(c)

(d)

Figure 3.10 The automatic repeated impact testing machine (a) general view (b) test cabinet (c) camera system and (d) test control and monitoring unit.

The specimen is tested inside a special isolation cabin (see Figure 3.10b) to reduce the noise of the impact testing. Inside the cabin there is an isolated high-resolution camera that is focused on the testing specimen. The live testing stream from the camera is monitored on a 28 inches wide high-resolution monitor to accurately observe the cracking and failure of the specimen as shown in Figures 3.10c and 3.10d, while the cabin itself is provided with a glass area to visually inspect the testing specimen as clearly shown in Figure 3.10. For each mixture 42 disk specimens were cast. Thus, a

total of 84 specimens as shown in Figure 3.7 were cast, heated and tested to evaluate the thermal response of the repeated impact strength.

3.7 Structural-Scale Drop-Weight Impact Test

To investigate the structural performance of PP-ECC under repeated impact loading, plate specimens were subjected to multiple drop-weight impacts using a specially constructed testing machine. The following subsections describe the used drop-weight electrical testing machine and its instrumentation, the plate specimens, and the test program.

3.7.1 Frame of the drop-weight testing machine

An impact machine based on dropped weight principle was selected since it is able to provide impact velocity by using earth gravity. In the design, a specimen was fixed on top of a steel base. An impactor is elevated and then released from a certain height above the specimen. The impactor would hit the specimen at an impact speed that depends on the dropping height and weight. The kinetic energy of the impactor is then absorbed by the progressive folding of the tested specimen, which reduces the kinetic energy of the impactor until it finally stops.

From the design principle and requirements, the dropped weight impact testing machine was designed. Figure 3.11 shows the drop-weight impact test machine used in this study and is composed of several parts. The first part of the testing machine is the frame that consists of rigid guide columns, base structure and connectors to the base concrete ground. The second part is the impactor assembly that consists of impactor slide, projectile, roller, and weighting mass. The third part is the weight clamping and lifting mechanism, while sensors and the data acquisition system can be considered as the fourth part of the designed drop-weight testing machine.

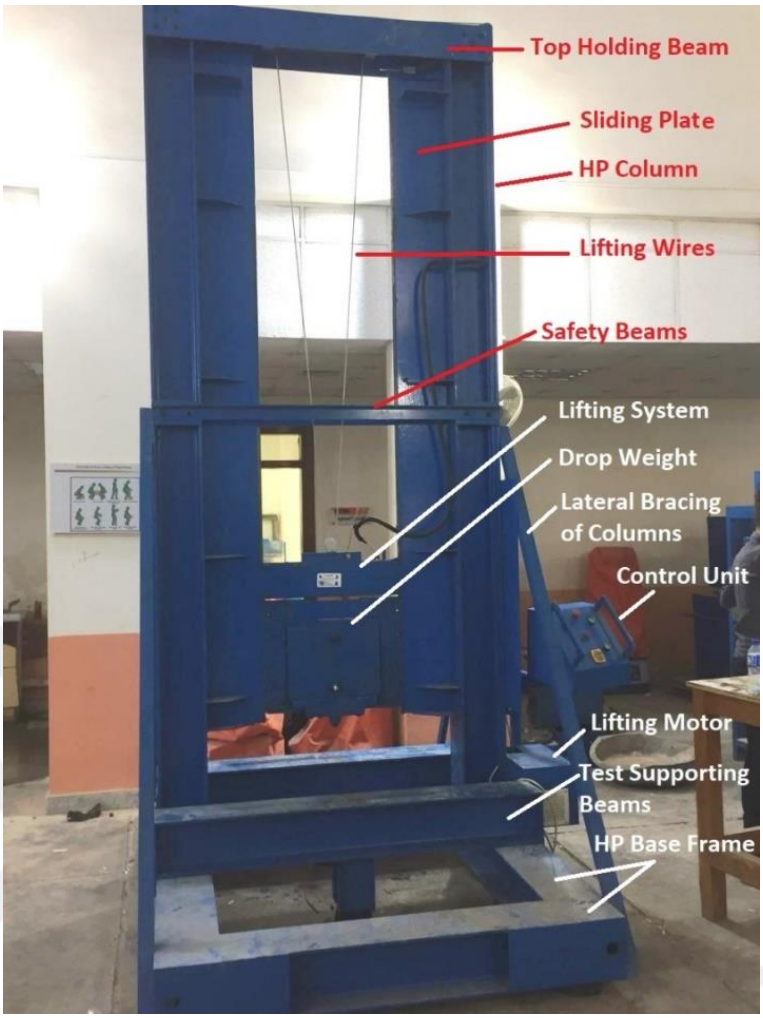

Figure 3.11. The drop-weight impact testing machine.

The columns were designed to act as a guide of the moving impactor assembly and were made of 3.6 m height steel HP-sections. The HP-sections have a web and flange widths of 200 mm and a thickness of 12 mm. The stability of the columns was improved and its effective length was reduced using top, bottom, and mid-height stiffeners. Sliding plates of the drop-weight were directly welded to the columns and were stiffened using steel plates at five locations. The two columns were linked at the top using specially designed linking beam as in Figure 3.11, which was fixed to the columns using stiff plates and 20 bolts.

The columns were mounted on top of a base frame, which was also made from the same steel HP-sections. The base frame composes of four perpendicular HP beams. The columns were attached to the base frame through a stiff base plate and stiff side guest plates using a suitable number of bolts and nets. The columns were also braced

against the base plate using four 100×100×6 mm angles. The base frame is resting on 150 mm diameter circular elastomeric bearing pads. Four pads were used under the corner of the rectangular base frame, while two pads were attached at the thirds of each of the longer beams. On the other hand, one elastomeric bearing pad was used under the mid-length of each of the shorter beams of the base frame as shown in Figure 3.12.

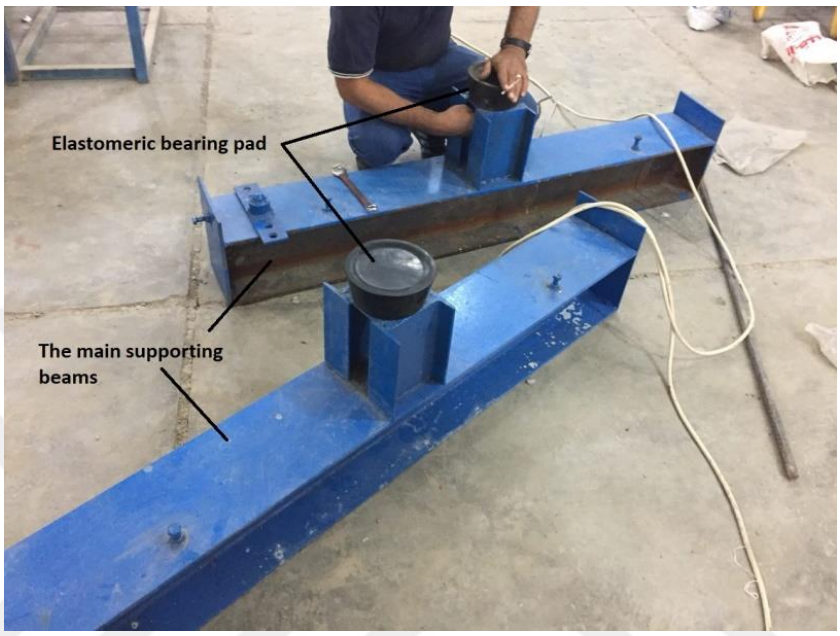

Figure 3.12. The supporting stubs and elastomers of the frame base.

Stiff steel HP beams were used as the main supports of the test specimens. These beams are placed directly on the longer beams of the base frame. To prevent any deformation of the two supporting beams, the beams are designed to directly rests on the reinforced concrete ground similar to the base frame. This was conducted using special mid-length stubs that rest on the elastomeric bearing pads as shown in Figure 3.12.

3.7.2 Sensors and data acquisition

To record the structural performance of the plate specimens, a system of three sensors was used to monitor the real-time impact force, central deflection, and vibration under each impact blow. The dynamic load cell shown in Figure 3.13 with 5000 kg maximum capacity with an accuracy of 0.2% was used to capture the impact force.

Figure 3.13. The dynamic load cell.

The load cell was attached to the impact point that falls directly on the center of the test specimen as shown in Figure 3.14. Thus, the initial impact force and its variation within the very short impact period is recorded as a function of time.

Figure 3.14. The load cell was attached to the impact point that falls.

The deflection under the impact load is recorded using the high accuracy LVDT shown in Figure 3.15, which is placed under the center of the specimen as shown in Figure 3.16. On the other hand, an accelerometer type two demotions double axis, as shown in Figure 3.17 was used to measure the acceleration-time variation under the impact load.

Figure 3.15. The high accuracy LVDT.

Figure 3.16. LVDT is placed under the center of the specimen.

Figure 3.17. Accelerometer used type.

The vibration sensor was directly attached to the boundary plates that frame the testing specimen as shown in Figure 3.18. The data were recorded from the three sensors simultaneously using the LapJack data logger (see Figure 3.19) that was programmed using Lap View software to capture the time-dependent variation of the sensors at a

frequency of not less than 10 kHz, where the capturing speed was set automatic in the programming to allow the data logger a better ability to maximum as best accuracy as possible.

Figure 3.18. The used vibration sensor.

Figure 3.19. Picture of the data acquisition system during data recording.

3.7.3 The plate test specimens

The plate specimens were designed so that they will be easily inserted in and removed out the electrical furnace. Because of the limited furnace internal dimensions, the size of the plates was reduced to 400×400 mm, while the depth was reduced to 80 mm to be compatible with the length side as depicted in Figure 3.20a. The plates were reinforced with four bars with 6 mm diameter each direction as depicted in Figure 3.20a and 3.20b. The formwork was prepared so that each two plates can cast using one wooden formwork as shown in Figure 3.20c.

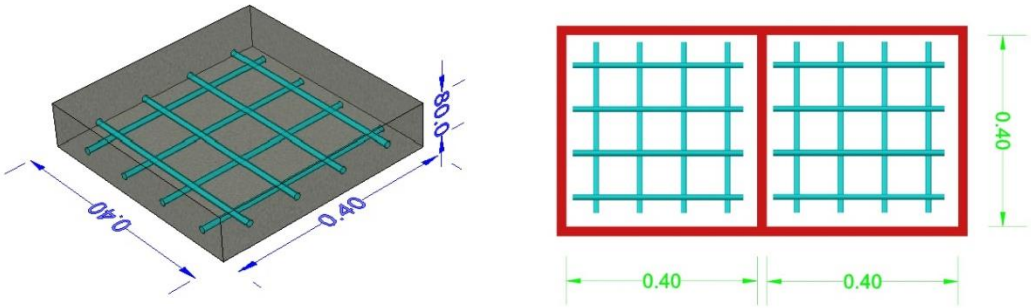

(a) (b)

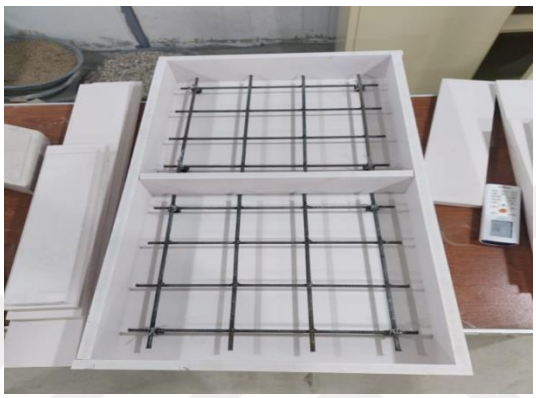

(c)

Figure 3.20. The dimensions and reinforcement of the plate specimens.

A batch of six plates was cast once. Two specimens were cast to perform the impact test without heating, while one specimen was cast for each temperature level. It should be considered that following the conclusions of the first-stage (material-scale) work, three levels of high temperatures of 200, 400, and 600 °C were considered in addition to the reference unheated case. Thus, three specimens were subjected to each level of temperature for each boundary condition case. The sixth specimen from each patch was kept as a recovery specimen in case of explosive exposure damage or any sort of error that may occur during the heating or testing. Figure 3.21a shows the prepared samples before casting of a complete six-specimens patch, while Figure 3.21b shows the casting of plate specimen patch and Figure 3.21c shows a group of cast plates with their associated compressive strength (f_c') cubes.

(a)

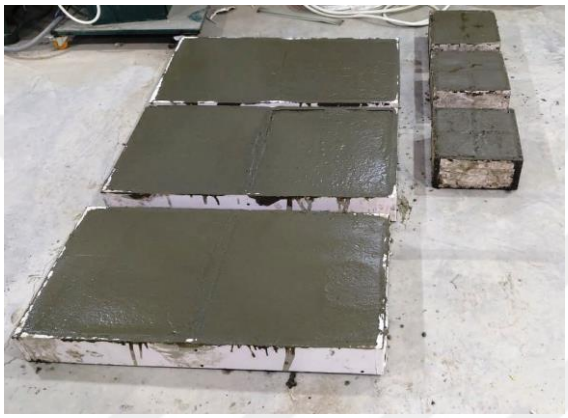

(b)

(c)

Figure 3.21. The specimens' preparations.

3.7.4 Test setup

To evaluate the effect of end-restriction degree on the structural behavior under fire conditions, three end boundary conditions were considered in this study for the tested plates. The first boundary condition is the four-corners clamped case as shown in Figure 3.22a, which represents the simple supporting system. The second boundary condition is the two-ends restricted that is illustrated in Figure 3.22b, while the third boundary condition is the four-ends restricted that represents the continuous or fixed-ended slabs as illustrated in Figure 3.22.

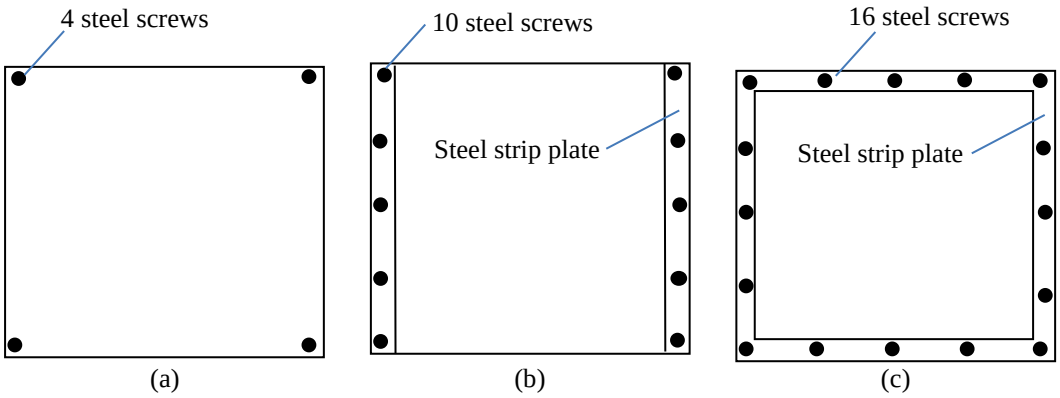

Figure 3.22. Boundary conditions of the plate specimens (a) four-ends clamped (b) two-ends restricted (c) four-ends restricted.

Before testing the specimen is inserted in the holding steel-box frame. For the simple span case, the corners are clapped using tightened screws and small steel plates as shown in Figure 3.23.

Figure 3.23. Four-corners clamped setup of test plates (simple supports).

For the two-ends restricted, 30 mm wide strip steel plates are placed on two opposite sides of the test specimens, then clamped at five points along each side with tightened screws that are welded to the box-frame as shown in Figure 3.24. The same procedure but using for strip steel plates along the four end-sides of the test specimen as shown in Figure 3.25. As the plate setup becomes ready, the sensors and their connection to data logger are checked and the test is initiated as shown in Figure 3.26.

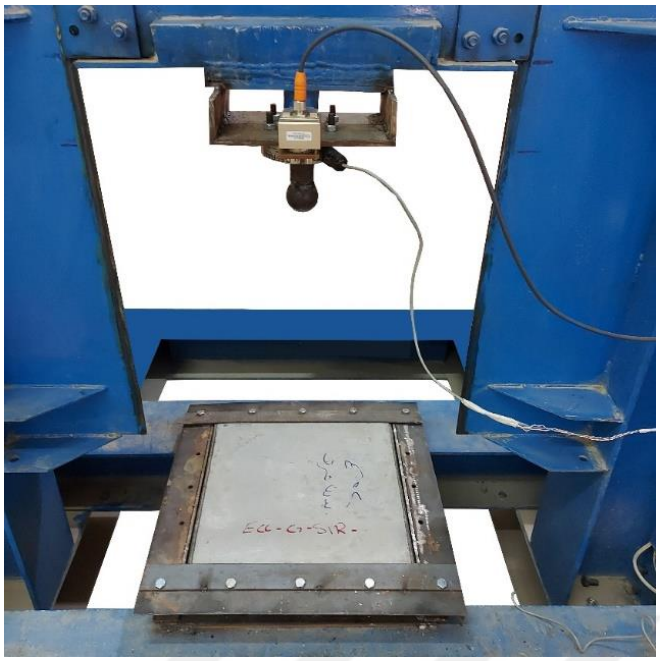

Figure 3.24. Tow-ends restricted setup of test plates.

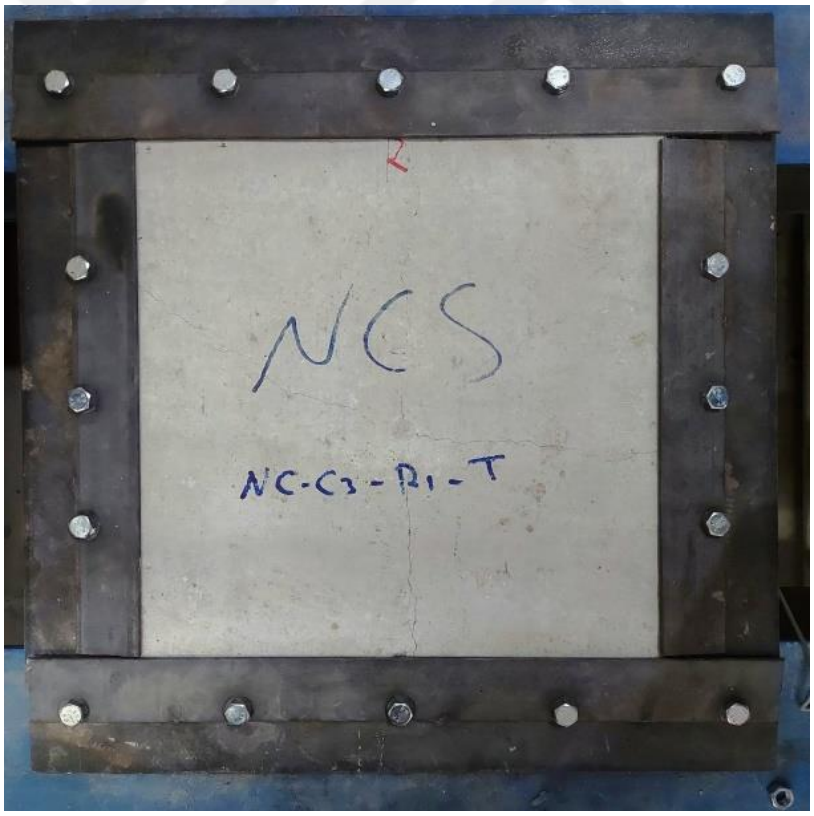

Figure 3.25. Four-ends restricted setup of test plates.

(a) (b)

Figure 3.26. Test setup of the drop-weight impact plate specimens.

3.8 Heating and Cooling Regimes

Seven specimen patches of material-scale stage and four specimen patches of the structural-scale stage were cast and cured in water tanks under the same conditions for 28 days. The curing tanks were set to a temperature level of approximately 20 to 23 °C After which, the specimens were left to air dry for a few hours, and the specimens that would be heated were then dried in an electrical oven at approximately105 °C for 24 hours. After the specimens were naturally air-cooled, six of the seven material-scale patches were heated to temperatures of 100, 200, 300, 400, 500, and 600 °C using the electrical furnace shown in Figure 3.27, while the seventh patch was left as a reference unheated one.

Figure 3.27. An interior view of the used electrical furnace.

On the other hand, the drop-weight plate specimens (structural-scale stage) were heated to three levels of temperatures of 200, 400, and 600 °C in addition to the reference specimens. The steel cage shown in Figure 3.28a was used to reduce the destructive effects of the concrete explosive failure on the internal walls and heaters of the furnace as shown in Figure 3.28b. The specimens were placed in small groups and were placed on special thermal insulation spacers from the base as shown in Figure 3.29 to allow for a uniform and balanced heating for all specimens.

(a) (b)

Figure 3.28. Protection of the electrical furnace using a steel cage (a) the steel box-cage (b) the final internal view of the furnace.

Figure 3.29. Placement of test specimens inside the furnace.

The heating process followed the heating and cooling procedure shown in Figure 3.30, where the specimens were heated steadily at a heating rate of approximately 4 °C /min till the target temperature. Then after, the specimens were thermally saturated at this temperature for one hour to ensure the thermal steady-state condition (Phan & Carino,1998; Husem, 2006). Finally, the furnace door was opened to allow for the natural air cooling of the specimens. As their temperature reduced, the specimens were left in the laboratory environment and tested in the next day.

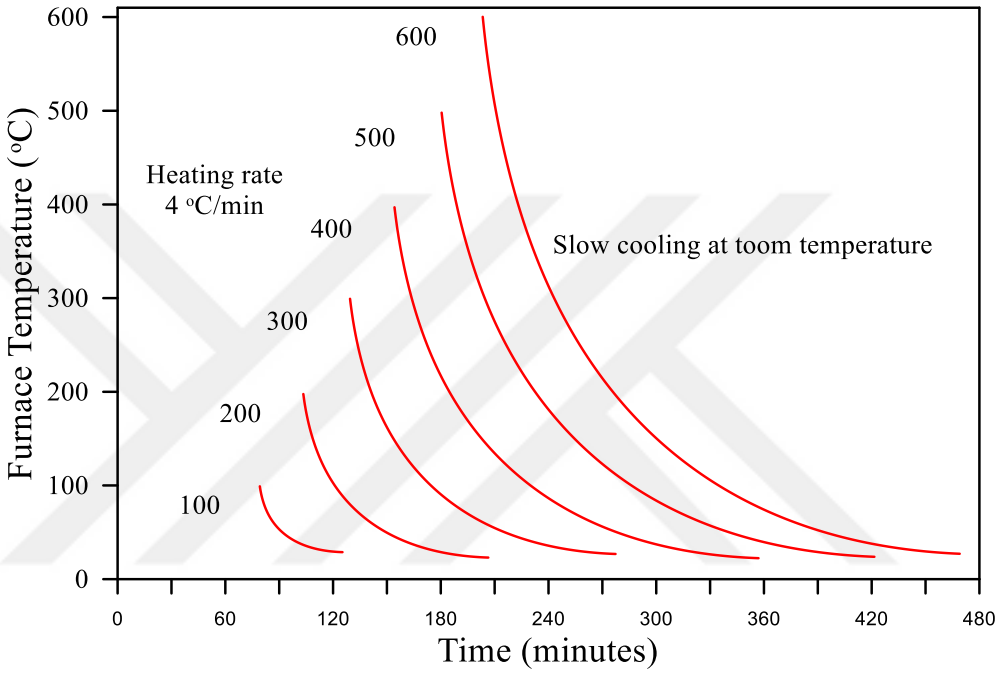

Figure 3.30. Heating and cooling regime of the electrical furnace.

CHAPTER FOUR

RESULTS AND DISCUSSION OF MATERIAL-SCALE TESTS

4.1 General

Material control is an essential part of structural design and structural research development. Therefore, material control tests have to be considered among the experimental program of structural concrete research to support a better understanding of the structural behavior, which is basically built on knowledge of the used materials' properties and behavior.

As the aim of this work is to investigate the material-scale and structural-scale impact performance of ECC before and after being subjected to elevated temperature levels in the case of structural fires, the temperature-dependent behavior of compressive strength (f_c') and flexural strength was investigated as preceded in the previous chapter. The scope of this chapter is to present the results and related discussions of the following:

- The temperature-dependent behavior of the compressive strength (f_c') of NC and ECC mixtures and its relation with weight loss after exposure to the designed temperature targets.
- The temperature-dependent behavior of the flexural strength of NC and ECC mixtures and its relation with weight loss after exposure to the designed temperature targets.
- The temperature-dependent behavior of the ACI 544-2R repeated impact strength of NC and ECC mixtures and its relation with weight loss after exposure to the designed temperature targets.
- The fracture mechanism of the repeated impact specimens of NC and ECC and the effect of high temperatures on this mechanism.

4.2 Compressive Strength Results

The compressive strength (f_c') and cube weight loss (W_l) results of the NC and PP-ECC specimens at the different temperature exposure levels of 100, 200, 300, 400, 500, and 600 °C in addition to reference specimens are listed in Tables 4.1.

Table 4.1. Compressive strength and cubes weigh loss results of NC and ECC.

Temperature	NC		ECC	
	Compressive strength (f_c') (MPa)	**Percentage weight loss** (%W_l)	**Compressive strength** (f_c') (MPa)	**Percentage weight Loss** (%W_l)
Room	43.19	0.00	57.47	0.00
100	43.85	0.75	55.02	1.56
200	35.08	2.56	44.80	8.97
300	42.31	4.88	43.41	10.39
400	35.08	4.99	40.49	12.35
500	33.52	5.09	34.30	13.43
600	21.58	6.36	29.53	14.92

4.2.1 Normal concrete compressive strength results

The residual compressive strength (f_c') values after exposure to 100, 200, 300, 400, 500, and 600 °C in addition to that at ambient temperature are shown in Figure 4.1. The Figure 4.1 also shows the percentage reduction in strength due to temperature exposure. It is obvious that a slight strength gain of approximately 1.5% was recorded at 100 °C, where the compressive strength (f_c') after exposure to this temperature was 43.9 MPa, which is higher than before heating (43.2 MPa). This initial strength gain was reported by previous researchers (Phan & Carino, 2003) and is attributed to the increase of material density due to the evaporation of free pore water and the increase of hydration products owing to the accelerated pozzolanic reaction. The strength gain is represented as a negative percentage reduction in Figure 4.1.

After exposure to 200 °C, the compressive strength (f_c') was recorded as 35.1 MPa with a percentage reduction of approximately 18.8%, while a noticeable percentage strength recovery was recorded at 300 °C. The residual compressive strength (f_c') at 300 °C was 42.3 MPa and the percentage reduction was only approximately 2.1%.

Hence, more than 16% strength recovery was gained as the temperature was increased from 200 to 300 °C As temperature increases beyond 200 °C, the removal of water from the surfaces of the cement gel particles induces higher attraction surface forces (Vander Val's forces), which might increase the ability of the microstructure to absorb higher compression stresses (Arna'ot, et al., 2017).

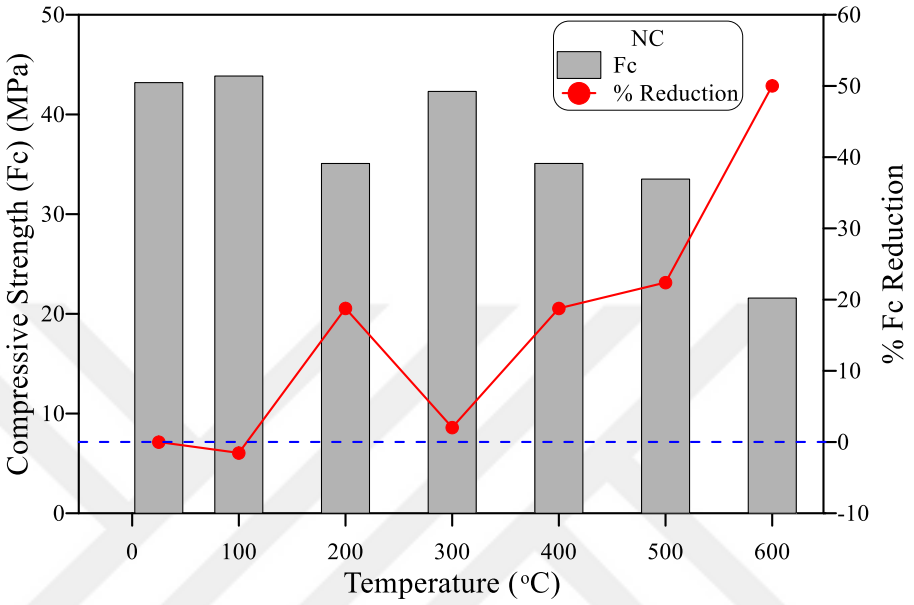

Figure 4.1. Compressive strength-temperature behavior of NC.

Beyond 300 °C, the compressive strength (f_c') exhibited a continuous decrease in strength with the increase of temperature where the percentage strength reductions were 18.8, 22.4, and 50.0% after exposure to 400, 500, and 600 °C. The significant strength drops after 500 °C is attributed to the volume changes that take place due the shrinkage of cement pastes and expansion of the aggregate particles, which deteriorates the bond between the two materials (Sultan & Alyaseri, 2020). The dehydration of cement and decomposition of calcium hydroxide also leads to destructive effects (Murali, et. al., 2020)

Figure 4.2 shows the relationship between compressive strength (f_c') and percentage weight loss of the same cube specimens after exposure to 100 to 600 °C high temperatures. The percentage weight loss was calculated by dividing the weight loss (weight before heating-weight after heating) by the original specimen weight before heating, with the result multiplied by 100. Figure 4.2 shows that three stages can be recognized in the percentage weight loss relation with temperature. In the first stage,

the slope of the percentage weight loss was high after exposure to the sub-high temperature range (100 to 300 °C), which indicates early high weight loss. This weight loss can be attributed to the evaporation of the free pore water before 200 °C and the absorbed water in the cement gel particles.

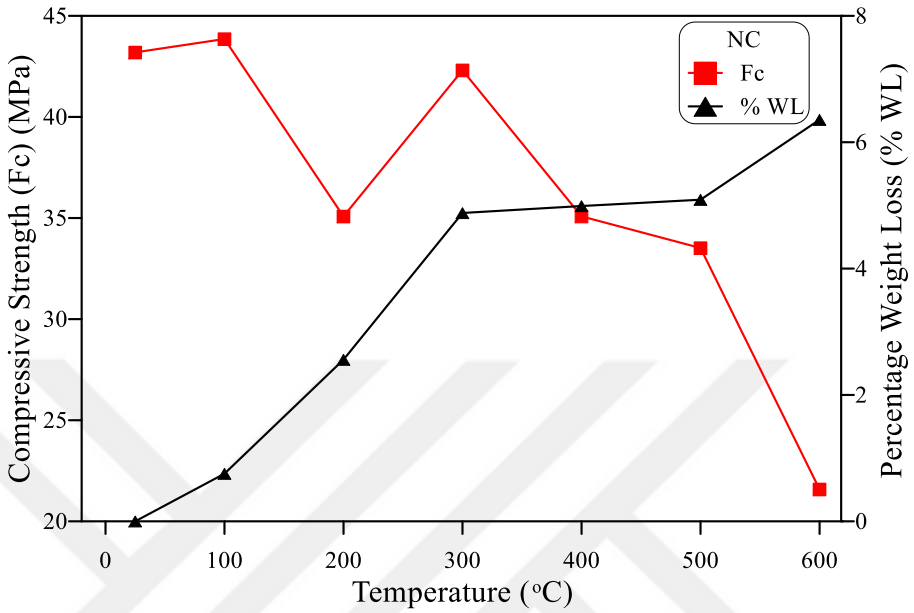

Figure 4.2. Compressive strength-weight loss relation of NC at high temperature.

The second stage, which is a semi-stabilization stage with a very small positive slope, is related to the strength recovery and low reduction between 300 and 500 °C, where the microstructure is still not very affected by the chemical and physical changes due to temperature exposure. Finally, the weight loss starts another high-slope reduction region after 500 °C, where the cement matrix was cracked owing to the chemical changes, and the bond between cement and aggregate_was almost lost due to the different thermal movements (Murali, et. al., 2021).

Excluding the initial strength gain at 100 °C and the strength recovery at 300 °C, it can be said that the strength loss can be related to the loss in weight. The differences between strength loss and weight loss in these regions are attributed to the different behaviors of concrete under the different applied stresses, where it was stated that the residual tensile strength of concrete, for example, has a different behavior with temperature than that of compression strength. As weight loss is a stress-free measurement, there would be some expected differences with load tests.

4.2.2 ECC compressive strength results

Figure 4.3 illustrates the influence of heating to the adopted various temperature levels on the compressive strength (f_c') of the ECC specimens. Previous studies showed that the concrete compressive strength (f_c') of ECC (Shang, & Lu, 2014). increased in some cases after exposure to temperatures in the range of 100 to 300 °C, or exhibited a partial recovery after exposure to 300 °C Such a behavior did not occur in this study where the compressive strength (f_c') of ECC exhibited continuous decrease as temperature increased. However, the strength reduction after exposure to 100 °C was limited to approximately 4% as shown in Figure 4.3, where the compressive strength (f_c') decreased from 57.5 to 55.0 MPa. Another notice is that the strength reduction at 200 °C is comparable to that at 300 °C, where the strength reduced to 44.8 and 44.4 MPa, respectively, exhibiting percentage decreases of 22 and 24.4%, respectively. Similar continuous reduction of compressive strength (f_c') of ECC with temperature was also reported by previous studies (Sahmaran, et. al., 2010; Sahmaran, et. al., 2011).

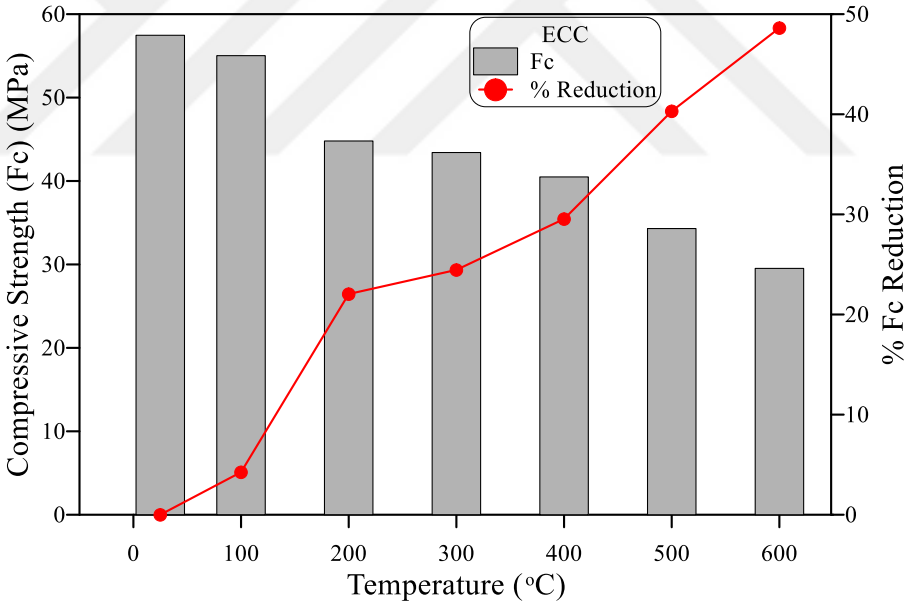

Figure 4.3. Compressive strength-temperature behavior of ECC.

A further decrease was recorded when the heating temperature was increased to 400 °C However, this additional decrease was small compared to the initial one, where the percentage reduction after exposure to 400 °C was 29.5%. When the specimens were heated to higher temperatures of 500 and 600 °C, significant strength degradation was noticed with residual compressive strengths (f_c') of 34.4 and 29.5 MPa, respectively.

This means that the strength losses were 40.3 and 48.6% after exposure to 500 and 600 °C, respectively, compared to the strength of the unheated specimens. On the other hand, the percentage strength reduction of NC was less than that of ECC after exposure to 200 and 400 °C.

The denser microstructure of ECC compared to NC is considered as the main cause of the further strength reduction between 200 and 400 °C ECC comprises a much larger amount of very fine binder, fine silica sand, no coarse aggregate and lower water/cementitious material content, which in turn lowers the porosity of ECC compared to NC. The evaporation of free pore water below 200 °C induces a pore pressure inside the microstructure. The dissipation of this pressure in NC specimens due to the higher porosity relieves the internal thermal stresses, while these stresses are higher in ECC due to the denser microstructure. As a result, ECC suffered higher compressive strength (f_c') losses at 200 to 400 °C. Previous researchers (Netinger, et al., 2011) reported that the total volume of the 0.1 micrometer and larger pores in ECC reduces after exposure to 400 °C, which is attributed to the pozzolanic reaction of the un-hydrated fly ash and other cementitious materials.

Such reaction would induce unfavorable volume changes due to the production of more CSH gel, which results in microstructural cracking leading to further strength degradation. The dehydration of hydrated products after exposure to temperatures higher than 400 °C is the main cause of the steep strength reduction at 600 °C, where this process leads to the degradation of the microstructure due to the increase of pore size and number and the further volume changes' micro-cracking. Sahmaran et al. (2011) reported a significant increase in the volume and size of pores of ECC after exposure to 600 °C and higher, where the porosity increased by 9% after exposure to 600 °C, which is large enough compared to 5% after exposure to 400 °C, while the pore size increased by at least 300% after 600 °C exposure.

Figure 4.4 shows the relationship between compressive strength (f_c') and percentage weight loss of the same cube specimens after exposure to the 100 to 600 °C high temperatures. The percentage weight loss was calculated by dividing the weight loss (weight before heating-weight after heating) by the original specimen weight before heating, with the result multiplied by 100. Figure 4.4 shows that three stages can be recognized in the percentage weight loss relation with temperature. In the first stage,

the slope of the percentage weight loss was high after exposure to the sub-high temperature range (100 to 300 °C), which indicates early high weight loss. This weight loss can be attributed to the evaporation of the free pore water before 200 °C and the absorbed water in the cement gel particles.

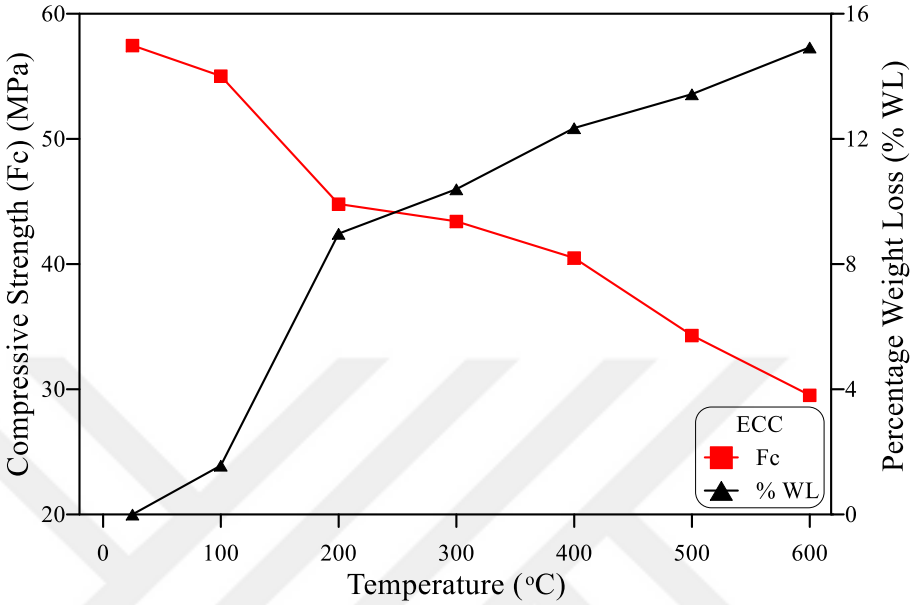

Figure 4.4. Compressive strength-weight loss relation of ECC at high temperature.

4.2.3 Flexural strength results

The flexural strength ($f_{ct,fl}$) results of NC and ECC specimens at all temperature exposure levels in addition to reference specimens are listed in Tables 4.2 in addition to the weight losses recorded for the same tested prisms after exposure to all temperature levels.

4.2.3.1 NC flexural strength results

The residual flexural strength records (modulus of rupture) of the tested prisms are visualized in Figure 4.5, which also visualizes the percentage reduction in flexural strength as a ratio of the unheated strength. Figure 4.5 explicitly shows that a similar strength gain was recorded for the flexural strength at 100 °C to that of compressive strength (f_c'). However, the percentage increase was higher, where the unheated flexural strength was 3.7 MPa, while that after exposure to 100 °C was approximately 4.1 MPa with a percentage increase of approximately 10.10 %, which is depicted in

Figure 4.5 as a negative percentage reduction. The same reason discussed in the previous section for compressive strength (f_c') could be the source of this increase in flexural strength. Then after, a continuous strength deterioration was recorded as the temperature increased beyond 100 °C Where the residual modulus of rupture values was approximately 2.9, 2.4, 2.2, 1.6, and 0.3 MPa with respective percentage reductions of approximately 22.5, 35.1, 41.6, 57.3 and 91.2 % after exposure to 200, 300, 400, 500, and 600 °C.

Table 4.2. Flexural strength and corresponding prisms weigh loss results of NC and ECC.

Temperature	NC		ECC	
	Flexural strength ($f_{ct,fl}$) (MPa)	**Percentage weight loss** ($\%W_l$)	**Flexural strength** ($f_{ct,fl}$) (MPa)	**Percentage weight loss** ($\%W_l$)
Room	3.70	0.00	6.94	0.00
100	4.07	0.73	7.78	1.11
200	2.87	2.57	5.75	4.76
300	2.40	5.13	5.63	10.07
400	2.16	5.25	4.32	11.32
500	1.58	6.10	2.98	13.61
600	0.32	7.64	2.32	14.73

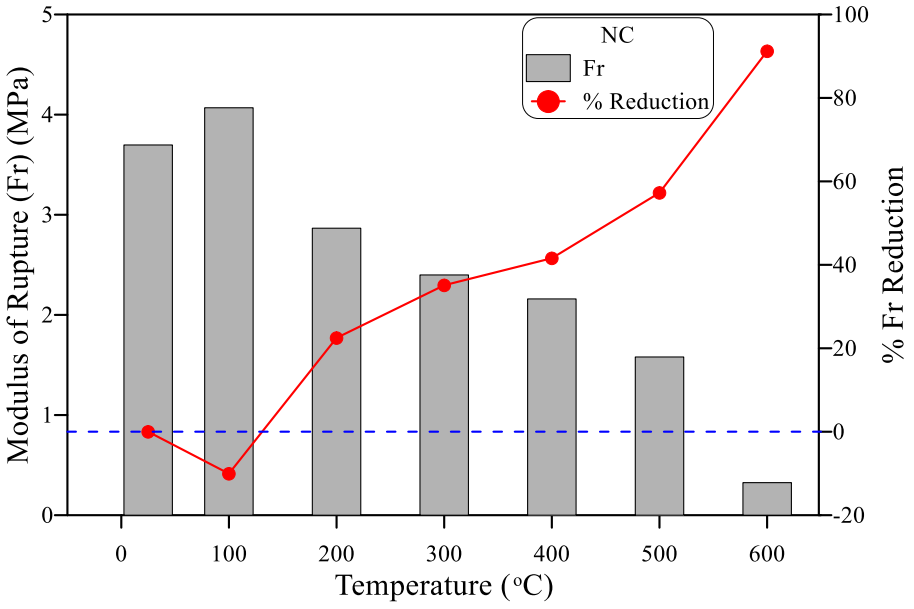

Figure 4.5. Flexural strength-temperature behavior of NC.

It can be noticed that the strength recovery recorded for compressive strength (f_c') at 300 °C was not recorded for flexural strength, which reflects the positive effect of physical attraction forces at this temperature to sustain higher compressive stresses (f_c'), while such effect was insignificant under the flexural tensile stresses. Another notice is the faster deterioration of flexural strength compared to compressive strength (f_c'), which is directly related to the weak microstructural response of concrete to tensile stresses.

The weight loss for the same prisms was recorded and from which the percentage weight loss was calculated, which is depicted in Figure 4.6 against the residual modulus of rupture. The Figure 4.6 also shows that a similar three-stage behavior can be recognized for the prism specimens to that recorded for cube specimens, where the slope of the percentage weight loss was higher before 300 °C and beyond 500 °C, while it was lower between them. Similarly, excluding the high residual flexural strength recorded at 100 °C, the strength reduction curve exhibited a similar three-slope behavior to that of weight loss, where the percentage reduction slope was high from 100 to 300 °C and from 500 to 600 °C, while it was semi-stabilized between 300 and 400 °C for both the flexural strength and weight loss as shown in Figure 4.6. The similar trend confirms the strong relation between weight loss and strength reduction after high temperature exposure.

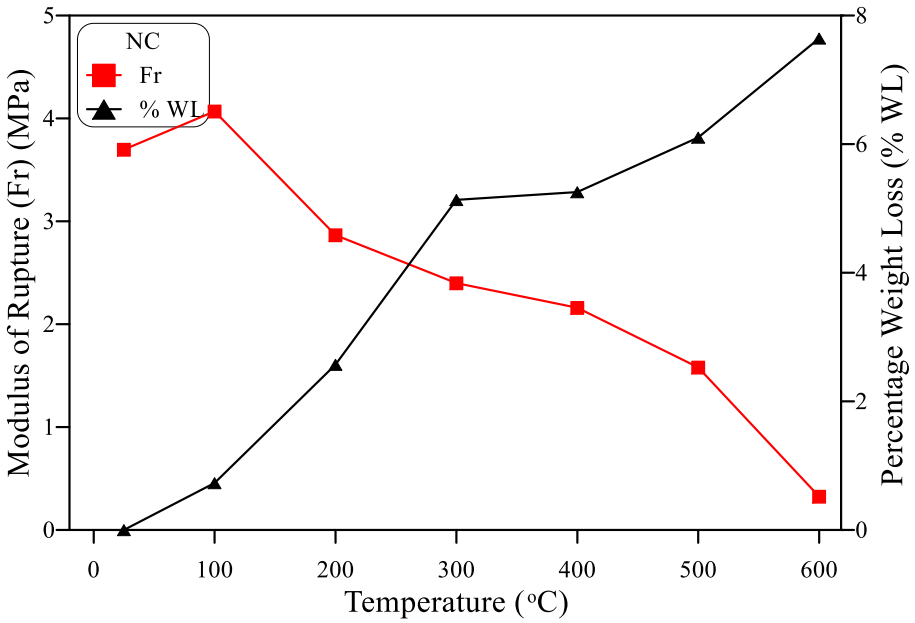

Figure 4.6. Flexural strength-weight loss relation of NC at high temperature.

4.2.3.2 ECC flexural strength results

The flexural strength was tested using the four-point bending setup to determine the modulus of rupture (MOR). The unheated ECC specimens exhibited the multi-cracking ductile behavior as shown in Figure 4.7 and Figure 4.8a, where all specimens showed more than five cracks that extended from the bottom surface of the beam specimen vertically towards the top loading points as the load was increased. Finally, one of these cracks was opened wider leading to the failure of the specimen. This cracking behavior assures the ductile performance of the adopted PP-based ECC.

Figure 4.7. multi-cracking failure of tested prisms.

(a)

(b)

Figure 4.8. Failure of tested prisms (a) unheated specimens (b) heated to 100 °C.

A similar cracking and failure performance was also recorded for the specimens exposed to 100 °C as depicted in Figure 4.8b. However, the number of cracks was lesser than those in the unheated specimens. After exposure to 200 °C, the specimens exhibited a brittle failure with only one crack that widened quickly under loading increase as shown in Figure 4.9a, while the specimens exposed to 300 °C exhibited a clear sudden brittle failure similar to that of NC as shown in Figures 4.9b, which is the same trend of behavior for the higher temperatures of 400, 500, and 600 °C as shown in Figures 4.9c through 4.9e.

(a)

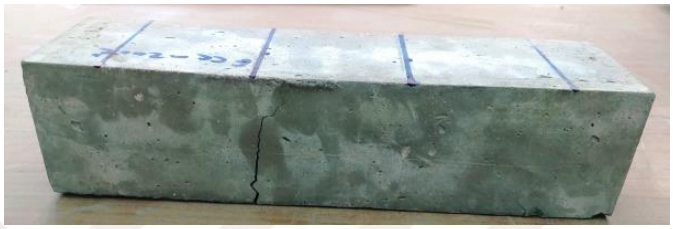

(b)

(c)

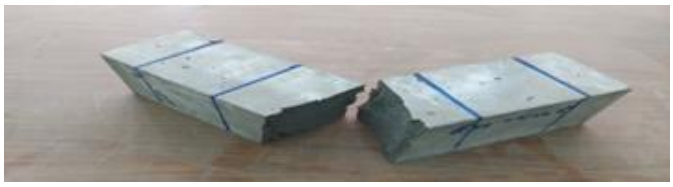

(d)

(e)

Figure 4.9. Failure of tested prisms exposed to different temperatures (a) 200 °C, (b) 300 °C, (c) 400 °C, (d) 500 °C and (e) 600 °C.

Another notice is that the visual examination after failure revealed that the PP fibers were clearly bridging the two sides of the cracks of the unheated specimens and those exposed to 100 °C, which explains their ductile behavior. On the other hand, such bridging activity was not observed for specimens exposed to higher temperatures due to the melting of the PP fibers at slightly below 200 °C, which in turn explains the brittle failure of these specimens.

Figure 4.10 shows the flexural strength behavior of with temperature increase. Similarly, the Figure 4.10 also shows the percentage difference in flexural strength compared to the reference unheated record. It can be seen in the Figure 4.10 that the flexural strength of the tested PP-ECC was not significantly affected by heating to temperatures up to 300 °C, while it exhibited a continuous decrease when exposed to higher temperatures up to 600 °C.

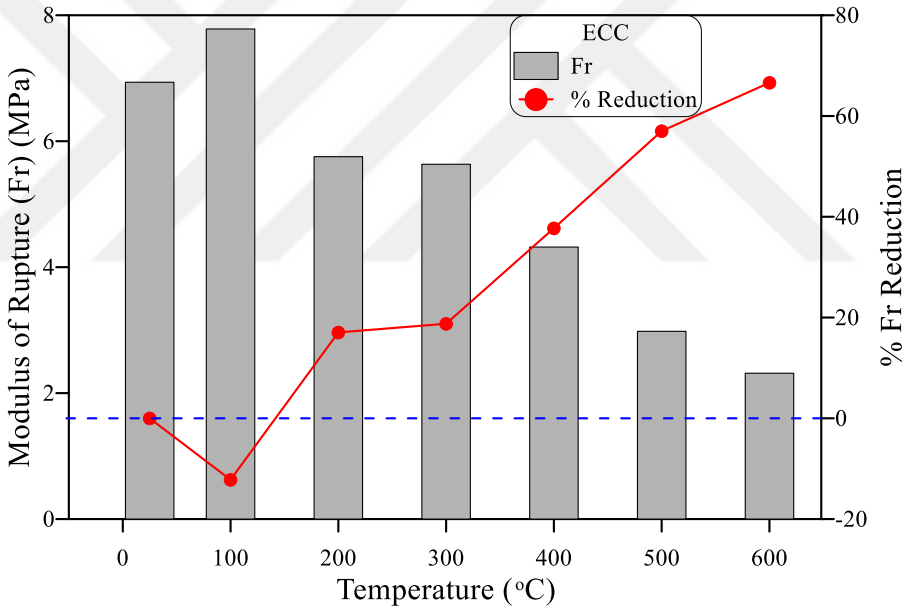

Figure 4.10. Flexural strength-temperature behavior of ECC.

The recorded flexural of the reference unheated specimens was 6.94 MPa, while after exposure to 100 °C, this value increased to 7.78 MPa recording a percentage increase of 12.2% compared to the reference record. However, after exposure to 200 and 300 °C, the flexural strength reduced by 17 and 18.8%, respectively as clearly depicted in Figure 4.10. Exposure to 400, 500, and 600 °C reduced the flexural strength to 4.32, 2.98, and 2.32 MPa, respectively, recording percentage decreases of approximately 38, 57, and 67%, respectively. Thus, the flexural strength kept within an approximately

20 % difference with the unheated specimens when exposed to sub-high temperatures up to 300 °C, while increasing the temperature by an additional 100 °C approximately duplicates this reduction and starts a new stage of strong deterioration.

The increase in strength at 100 °C can be attributed to the densification of the material due to the vaporization of free pore water, while the melting of fibers after 200 °C left open micro-tubes inside the matrix that reduced its stiffness and weakened its structure (Şahmaran, et al., 2011). Consequently, the strength was less than that before heating. The obtained trend of results in this study agrees with records reported by previous researchers (Çavdar, 2012). However, the percentages of increase after 100 °C exposure and decrease after exposure to 200 °C and higher were different owing to the different mixtures, fiber types, heating regimes, and other reasons. Where for instance, Yu et al., (2017) reported a percentage decrease of approximately 50% for ECC reinforced with PVA fibers after exposure to 200 °C, while the percentage decrease at the same temperature was only 25% for specimens reinforced with both PVA and steel fibers. On the other hand, Wang & Chouw, (2017). reported a partial recovery at 100 °C after an initial decrease at 50 °C, followed by a significant decrease after exposure to temperatures of 200 °C and higher.

The continuous decrease in the flexural strength after high-temperature exposure beyond 300 °C is generally attributed to the volumetric changes in the cement matrix, and the bond loss between binder and filler after 400 °C due to their different thermal properties. In addition, most of the degradation at higher temperatures is attributed to the chemical reactions after 400 °C (dehydration of CSH) and the increased porosity as discussed in the previous section. As the flexural strength depends on the capability of concrete to withstand tensile stresses, the initial flexural strength was apparently higher for ECC owing to the crack bridging activity of PP fibers, in addition to the higher content of cementitious materials. However, this bridging activity diminished after exposure to temperatures higher than 200 °C due to the melting of PP fibers.

Figure 4.11 shows that similar three-stage behavior can be recognized for the prism specimens to that recorded for cube specimens, where the slope of the percentage weight loss was higher before 300 °C and beyond 500 °C, while it was lower between them. Similarly, excluding the high residual flexural strength recorded at 100 °C, the strength reduction curve exhibited a similar three-slope behavior to that of weight loss,

where the percentage reduction slope was high from 100 to 300 °C and from 500 to 600 °C, while it was semi-stabilized between 300 and 400 °C for both the flexural strength and weight loss as shown in Figure 4.11. A similar trend confirms the strong relation between weight loss and strength reduction after high-temperature exposure.

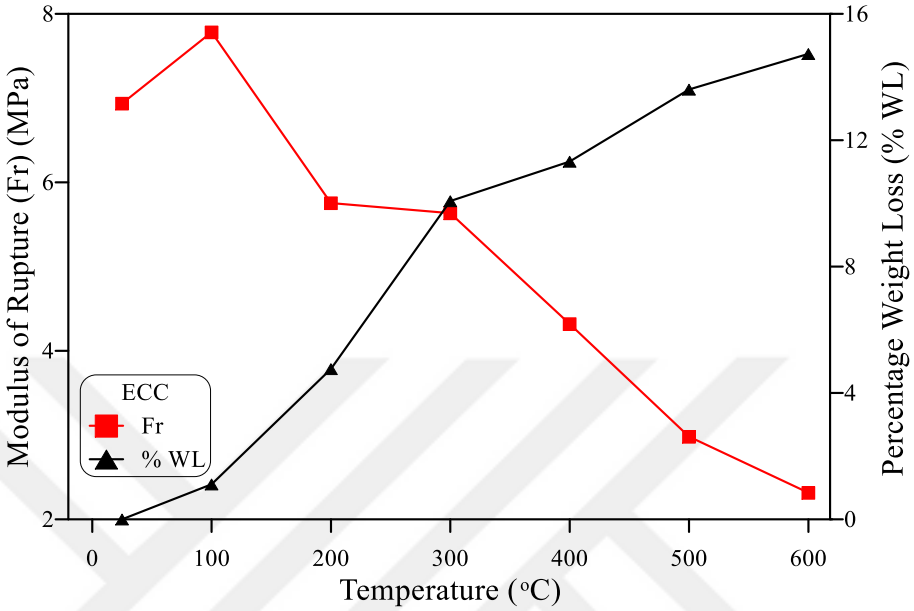

Figure 4.11. Flexural strength-weight loss relation of ECC at high temperature.

4.2.4 Results of the ACI 544-2R Repeated Impact Test

The obtained average impact numbers of six disk specimens at the cracking stage (N_{cr}) and failure stage (N_f) in addition to their corresponding weight losses of the same specimens are listed in Tables 4.3, which shows the results of NC and ECC mixtures before heating and after heating to temperature levels of 100 to 600 °C.

4.2.5 NC repeated impact results

4.2.6 Cracking and failure impact numbers of NC

The obtained impact numbers are listed in Table 4.3, while Figures 4.12 and 4.13 show the post-high temperature exposure response of cracking (N_{cr}) and failure (N_f) impact numbers, respectively. Figure 4.12 shows that after exposure to 100 °C, the cracking number did not affect noticeably, where this number decreased from 55 to 53.7 with a percentage decrease of only 2.4% Similarly, N_f was decreased by no more than 3.5% as illustrated in Figure 4.13. Considering the known high variation of the ACI 544-2R

repeated impact test (ACI 544.2 R-89, 1999), it can be said that the impact resistance was not affected by heating to 100 °C, which is also confirmed by the comparison of the individual impact numbers in Table 4.3, where the retained impact numbers for some specimens where higher after exposure to 100 °C than before heating. For instance, an individual cracking impact number of 60 was recorded for specimens heated to 100 °C, which is higher than all recorded numbers before heating for ECC.

Table 4.3. Impact numbers and corresponding disk weight loss results of NC and ECC.

Temperature	NC			ECC		
	Cracking Impact Number (N_{cr})	**Failure Impact Number** (N_f)	**Percentage Weight Loss** ($\%W_l$)	**Cracking Impact Number** (N_{cr})	**Failure Impact Number** (NS_f	**Percentage Weight Loss** ($\%W_l$)
R	55.00	57.17	0.00	43.33	259.33	0.00
100	53.67	55.17	0.73	51.00	313.00	0.51
200	14.17	15.17	3.62	41.50	256.67	6.88
300	6.50	7.50	4.40	26.00	44.67	9.60
400	3.00	4.00	4.85	19.50	24.00	11.07
500	2.17	3.00	5.89	10.33	11.67	13.55
600	1.00	2.17	6.21	8.83	9.83	14.08

As discussed in the previous sections, the compressive strength (f_c') and flexural strength were increased after exposure to 100 °C temperature. The strength gain was reported to be due to the shrinkage of concrete pore holes after the evaporation of pore water, which resulted in denser media. The slow preheating of specimens in an electrical oven at 100 °C might also help to minimize the reduction in impact strength at this temperature.

Where the free pore water was partially evaporated during the initial heating phase resulting in stress relief during the second (furnace) quick heating phase, which kept the microstructural deterioration minimal. It should be mentioned that the oven's slow preheating is essential to prevent any sort of thermal explosive failure during heating,

which would be harmful to the furnace and other specimens in the furnace. The preheating process was a typical procedure followed by many literatures' experimental studies, where it was reported that thermal explosive spalling is probable at temperatures in the range of 300 to 650 °C (Phan & Carino, 2003).

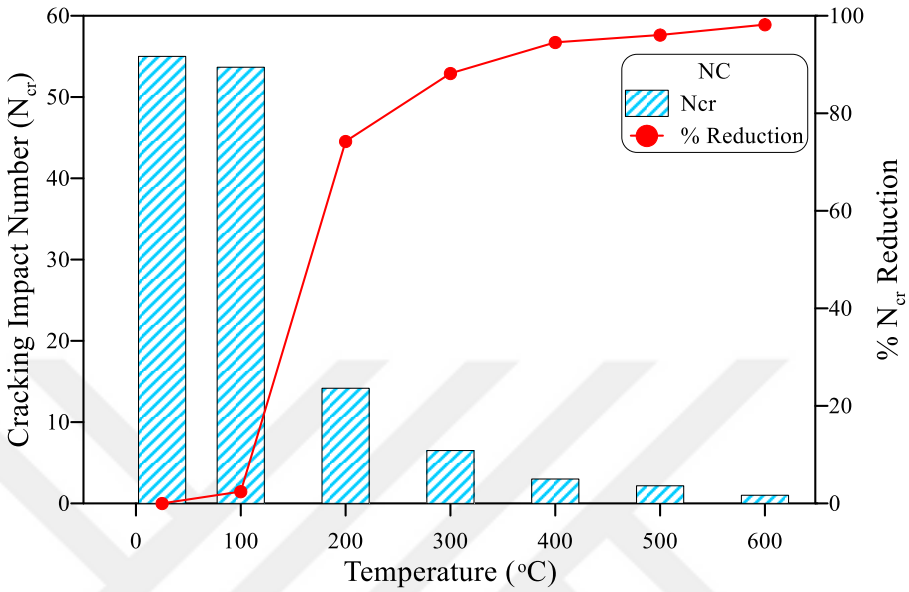

Figure 4.12. Cracking impact number-temperature behavior of NC.

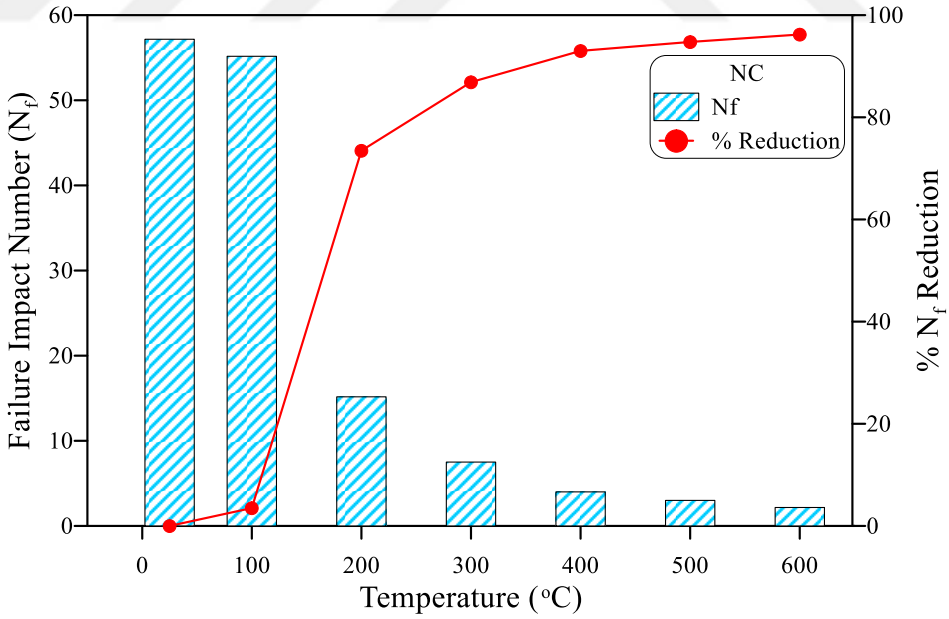

Figure 4.13. Failure impact number-temperature behavior of NC.

The strength of the material to resist impact forces dropped sharply after exposure to 200 °C, where the loss in impact resistance in terms of N_{cr} and N_f reached 74.2 and

73.5%, respectively. This reduction is dramatic and is much higher than the losses in compressive, flexural and tensile strengths according to the literature and the current study results. Where previous studies showed that the normal compressive strength (f_c') range of NC after exposure to 200 °C falls between 70 and 110% of the unheated strength.

Similarly, it is widely addressed in the literature that the modulus of elasticity of NC would be higher than 70% of the unheated values (Murali, et. al., 2020). Phan & Carino (2003) reported that for the case of unstressed residual compressive strength test, which is the heating procedure followed in this research, initial strength gain or minor loss is the usual trend of NC up to 200 °C The residual impact strength of the higher temperatures followed the same excessive strength drop as shown in Figures 4.12 and 4.13. The residual cracking impact strength after exposure to 300, 400, 500, and 600 °C were 11.8, 5.5, 3.9, and 1.8% of the original unheated strength respectively. Similarly, the residual failure impact strength was 13.1, 7.0, 5.2, and 3.8% after exposure to 300, 400, 500, and 600 °C, respectively.

Two points should be discussed here, the strength reduction behavior with temperature and the high drop in strength. It is obvious that impact strength follows a similar trend of reduction with temperature to the flexural strength, where both flexural and impact strength showed stable response at 100 °C, followed by a continuous decrease until the approximate fading of strength at 600 °C This might be attributed to the type of stresses caused by the repeated impacts in concrete, where the received impact forces tend to cause a fracture surface then transferred into tensile stresses that try to open the cracks until the breakage failure. The higher strength reduction can also be attributed to the nature of impact loads, where a sudden concentrated loading is induced within a very short time leading to higher stress concentration and hence faster deterioration.

As soon as the microstructure is internally fractured by the initiation of microcracks, only a few further concentrated drops are required to induce the surface cracking and failure of the specimen. Since the microstructure of the cement paste, the aggregate particles, and the bond between them are negatively affected by the preceding heating phase of the specimens, the quick fracture of these specimens is expected under impact drops.

Figure 4.14 compares the behaviors of residual impact strength in terms of impact numbers of the disc specimens and the percentage weight loss of the same specimens. It can be said that the trend of impact strength reduction is related to that of the percentage weight loss, where the same minor reduction is clear in the Figure 4.14 after exposure to 100 °C for both the strength and the weight loss, followed by a steep drop from 100 to 200 °C Then after, a continuous decrease in strength and increase in weight loss are obvious from 300 to 600 °C, the percentage strength is much higher than the percentage weight loss at each temperature, however, the behavior of reduction with temperature increase is quite similar.

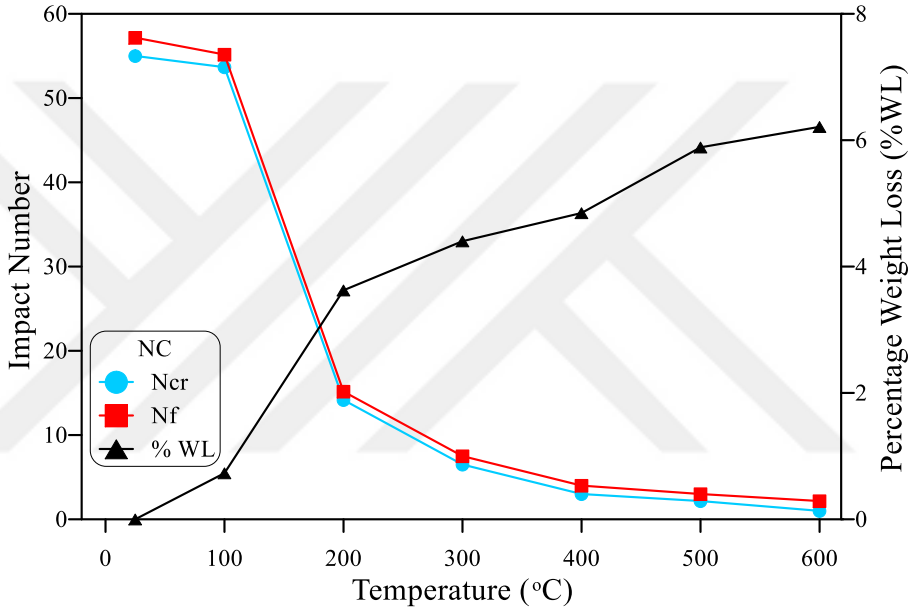

Figure 4.14. Impact number-weight loss relation of NC at high temperature.

4.2.7 Impact ductility of NC

One of the structural physical quantities that are used to define the response of flexural members under loads is ductility, which is a kind of quantitative measurement to define the capacity of the member to sustain plastic deformations (Abbass, et al.,2020). A similar definition was also used in previous studies to estimate the plastic range of repeated impact that the specimen can withstand before failure. The impact ductility index (DI) can thus be defined as the ratio of the failure impact number to the cracking impact number (DI=N_f/N_{cr}), which agrees with the original definition of flexural ductility, where it is defined as the ratio of the ultimate deflection to the deflection at the yielding of the tension steel bars (Abbass, et al.,2021).

As shown in Figure 4.15, limited ductility index numbers were recorded in general, where DI was approximately 1.0 before heating and after heating to 100 to 300 °C, which was in the range of 1.03 to 1.15, while it was slightly higher than 1.0 after exposure to 400 and 500 °C (1.33 and 1.38, respectively). It should be noted that the lowest possible DI value is 1.0. These low DI values reflect a brittle behavior, where the failure occurred after one or few additional impact blows after cracking, therefore, the value of N_f was very close to that of N_{cr}. The low ductility is expected for NC mixtures that are not reinforced with reinforcing bars or fibers, which is attributed to the very low tensile capacity of concrete. Understanding the evolution of stresses under impact blows would explain this trend. Where the concentrated compressive stresses received at the top surface center from the impactor are transferred through the microstructure along all diagonal directions as tensile stress waves. As soon as the ultimate tensile strength is reached and the crack is formed, the failure becomes imminent by the quick propagation and fracture of the specimens after a very limited number of additional impact blows.

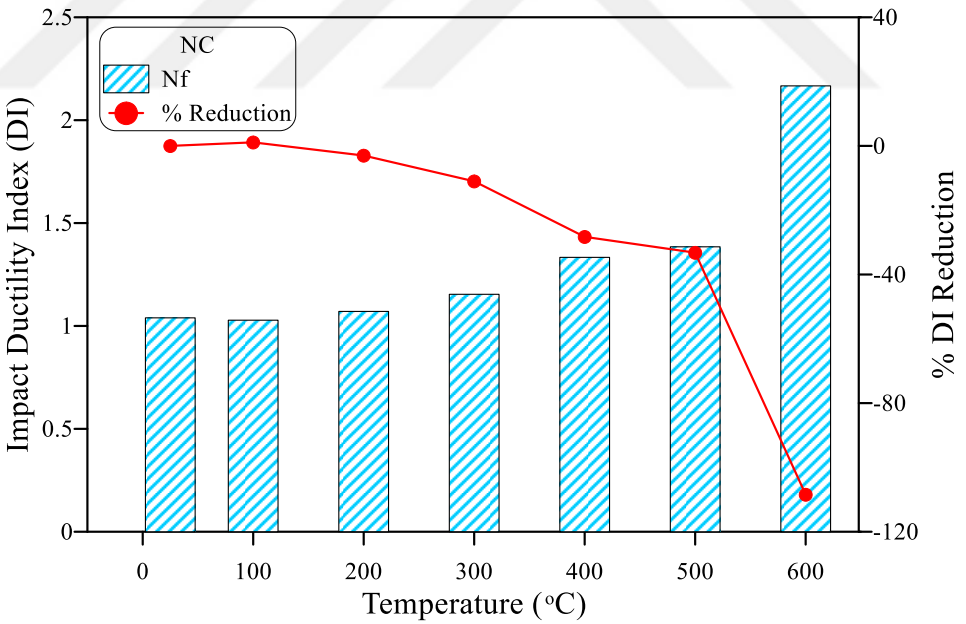

Figure 4.15. Impact ductility index-temperature behavior of NC.

Although the DI record at 600 °C was higher than the other records, it still lowers within the brittleness index range. The higher DI at 600 °C is attributed to the very low retained N_{cr} at this stage, which occurred after only one impact blow owing to the

serious material thermal deterioration. The recorded N_f was only 2.17, which means that failure occurred after approximately one additional impact blow. However, as DI is a simple division operation, the very low N_{cr} resulted in higher DI, which means that it in this case only has a mathematical meaning but not a true physical meaning.

4.2.8 Failure patterns of NC

Pictures for the disc specimens at room ambient temperature (R) and after exposure to 100, 200, 300, 400, 500, and 600 °C are shown in Figures 4.16 through 4.22 both before and after impact testing. The fracture and failure of the reference unheated specimens align with what was reported in previous studies for plain concrete, where after several repeated blows, a small diameter central fracture zone was created under the concentrated compression impacts via the top surface's steel ball. After a few more blows, the internal cracks propagated to the surface forming a surface cracking of two or three radial cracks from the central fracture zone, which formed the failure shape that occurred after a few additional blows as shown in Figure 4.16.

(a) (b)

Figure 4.16. Reference unheated NC disk specimens (a) before testing (b) after testing.

Figures 4.17 to 4.19 show that the specimens heated up to 300 °C exhibited a similar cracking and fracture behavior to that of the unheated specimens. However, at 200 and 300 °C, the cracking and failure sound softer where the fracture started at much lower impact numbers and the central fracture zone was smaller. The fracture of the specimens heated to temperatures above 400 °C is different. The material became too

weak to absorb the applied impact energy after being heated, where the cement paste became softer, the crushing strength of the aggregate particle was reduced and the bond between them was almost lost.

(a) (b)

Figure 4.17. NC disk specimens subjected to 100 °C (a) before testing (b) after testing.

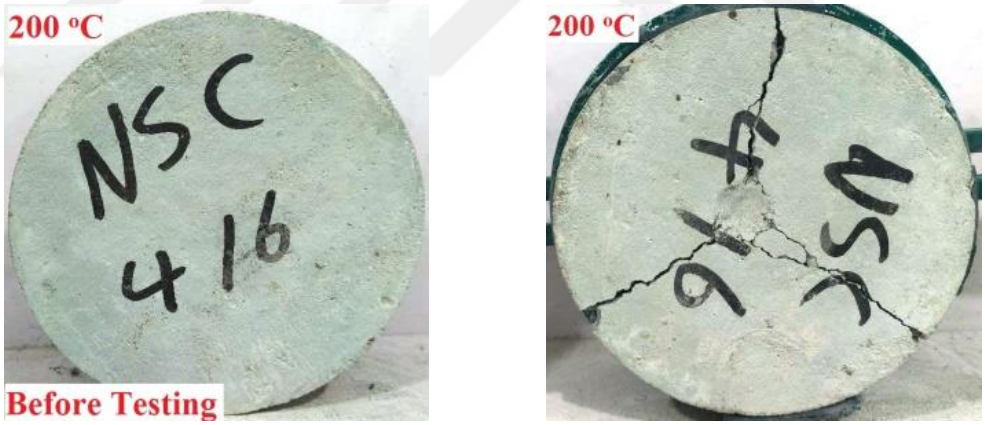

(a) (b)

Figure 4.18. NC disk specimens subjected to 200 °C (a) before testing (b) after testing.

(a) (b)

Figure 4.19 NC disk specimens subjected to 300 °C (a) before testing (b) after testing.

Due to these effects, internal thermal cracks were formed in the whole volume of the specimens. Therefore, for the specimens exposed to 400, 500, and 600 °C, only 3, 2, and 1 impact were enough to cause the already existing cracks to appear on the surface. As a result, the central fracture zone was barely formed and a higher number of major cracks (4 or 5) were formed accompanied by more hair cracks as shown in Figures 4.20 - 4.22.

(a) (b)

Figure 4.20. NC disk specimens subjected to 400 °C (a) before testing (b) after testing.

(a) (b)

Figure 4.21. NC disk specimens subjected to 500 °C (a) before testing (b) after testing.

(a) (b)

Figure 4.22. NC disk specimens subjected to 600 °C (a) before testing (b) after testing.

4.3 ECC Repeated Impact Results

4.3.1 Cracking and failure impact numbers of ECC

Figure 4.23 shows the recorded cracking number (N_{cr}) at each temperature and the temperature-dependent percentage reduction in N_{cr} based on the record of the unheated specimens. It is obvious in the Figure 4.23 that ECC specimens retained higher N_{cr} after exposure to 100 °C than that of the reference unheated specimens. On the other hand, a slight decrease in N_{cr} was recorded after exposure to 200 °C, while a serious decrease occurred after exposure to temperatures of 300 °C and higher. The retained N_{cr} records after exposure to 100 and 200 °C were 51 and 41.5 blows,

respectively, while the reference unheated N_{cr} was 43.3. Hence, the cracking impact number increased by 17.7% after exposure to 100 °C and decreased by 4.2 after being heated to 200 °C. However, the exposure to 300, 400, 500, and 600 °C decreased the retained N_{cr} by 40.0, 55.0, 76.2, and 79.6%, respectively, as depicted in Figure 4.23.

Following a similar behavior with temperature increase, the failure impact number (N_f) of specimens exposed to 100 °C was higher than the corresponding reference unheated n_f as shown in Figure 4.24. This increase was also followed by a slight decrease after exposure to 200 °C However, the decrease of N_f after heating to 300 °C was much higher than its corresponding N_{cr}, which reflects the much higher effect of heating at this temperature on the failure impact resistance than the cracking impact resistance.

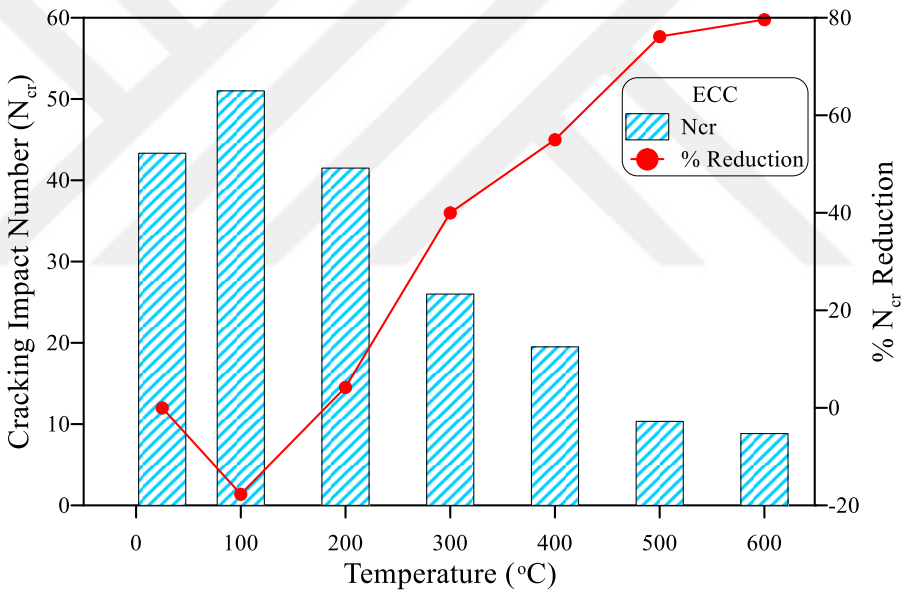

Figure 4.23. Cracking impact number-temperature behavior of ECC.

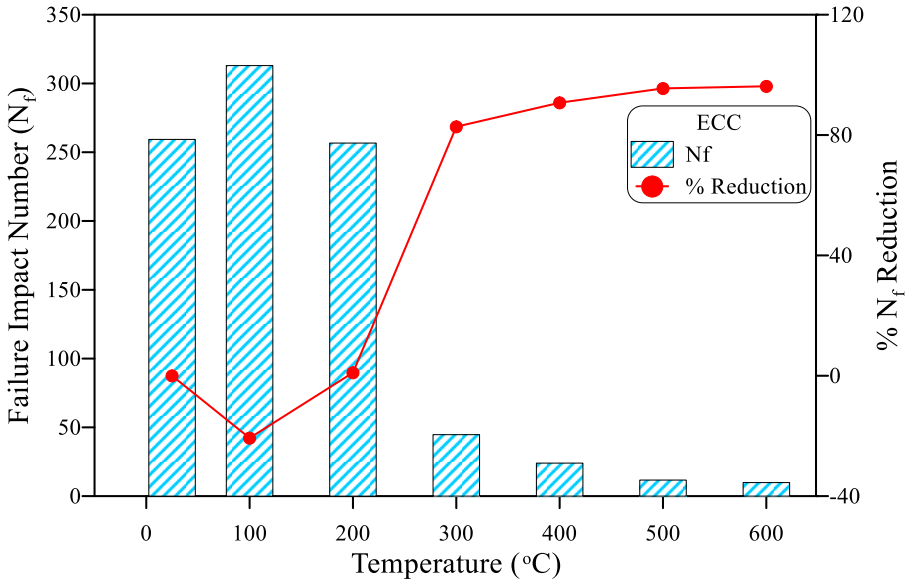

Figure 4.24. Failure impact number-temperature behavior of ECC.

The retained N_f values were 313, 256.7, and 44.7 after exposure to 100, 200, and 300 °C, respectively, while the reference N_f was 259.3 blows. This means that n_f increased by approximately 21% after 100 °C exposure, while almost keeping the same as the reference N_f with a slight decrease of 1% after exposure to 200 °C On the other hand, a serious N_f drop of approximately 83% was recorded for the specimens heated to 300 °C, which was a harsh start of a continuous harmful deterioration after exposure to temperatures higher than 200 °C The percentage reductions in N_f after exposure to 400, 500, and 600 °C were 90.8, 95.5 and 96.2%, respectively. This means that after exposure to a temperature of 400 °C, the impact strength almost vanishes, which may cause a sudden impact failure.

The higher reduction after exposure to 300 °C and higher is attributed to the microstructural changes that occurred at this temperature, where the complete melting of PP fibers left behind open micro-tubes that composed a network of connected continuous pores, which increased the porosity of the material and made it more brittle. Sahmaran et al., (2011) indicated that the increase in PVA-ECC porosity was minimal (0.2%) before fiber melting at 200 °C, while the complete melting of fibers increased the porosity to 5% and more after exposure to higher temperatures. Similarly, the increase in pore diameter was minimal after exposure to 200 °C, while exposure to 400 °C resulted in an increase in pore diameter by about 50%, which explains the

minor decrease in N1 and N2 after exposure to 200 °C and the significant decrease after exposure to 300 °C. Bhat et al., (2014) reported an increase in the tensile strength of PVA-ECC after exposure to 100 °C, which was attributed to the initial moisture loss due to the free pore water evaporation (form larger pores and capillary pores), and the hydration of the free fly ash that was not hydrated during the curing period, which is in turn attributed to the large amount of fly ash used in ECC. It should also be noticed that fibers were still working at 100 °C, while the weakening of the bridging activity of fibers after exposure to 200 °C (due to partial melting). It was also reported that the moisture loss was less than 3% after 100 °C exposure, while it was more than 7% after exposure to 200 °C (Bhat et al., 2014).

Figure 4.25 displays a comparison of the characteristics of residual impact strength between the disc specimens' impact counts and their percentage weight loss. It can be concluded that the impact strength reduction trend and the percentage weight loss trend are associated. Both the strength and the weight loss clearly decrease after exposure to 100 °C, and then there is a sharp decline from 100 to 200 °C. After that, it is evident that strength is continuously declining and weight loss is increasing between 300 and 600 °C. Indeed, at every temperature, the percentage strength is significantly higher than the percentage weight loss; nevertheless, the reduction behavior becomes more comparable as the temperature rises.

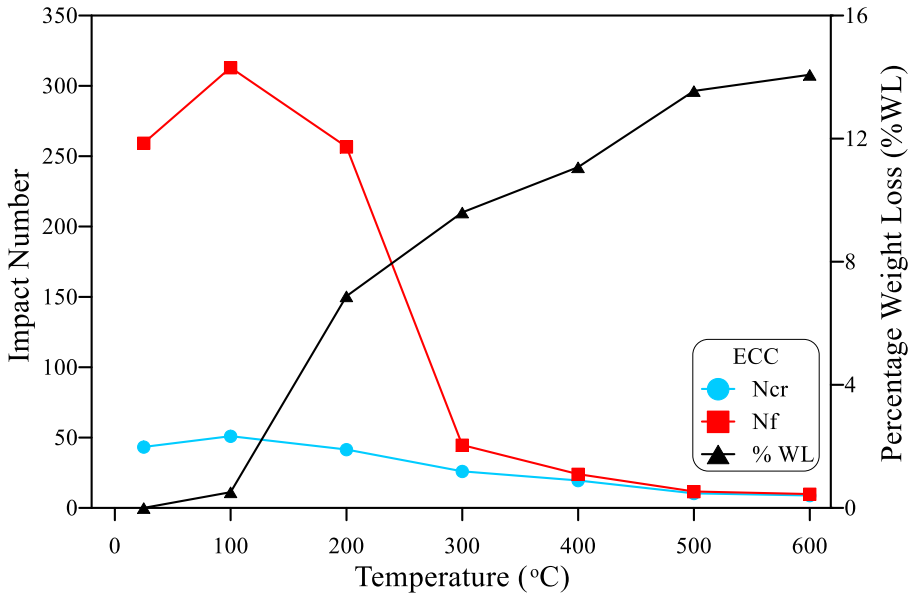

Figure 4.25. Impact number-weight loss relation of ECC at high temperature.

4.3.2 Impact ductility of ECC

As preceded in the previous sections, N_{cr} and N_f records did not suffer serious deteriorations after exposure to 100 and 200 °C, where these values were slightly higher at 100 °C and slightly lower at 200 °C than those of the reference specimens. This behavior was reflected in the impact ductility, where as shown in Figure 4.26, the ductility index values (DI) were almost the same at the three temperatures, which were 6.0, 6.1, and 6.2 at room temperature, 100 and 200 °C, respectively. These results reflect the ability of specimens heated to temperatures up to 200 °C to withstand significant impact numbers after surface cracking. Oppositely, the ductility index of the specimens exposed to higher temperatures of 300, 400, 500, and 600 °C deteriorated significantly to only 1.72, 1.23, 1.13, and 1.11, respectively. This reduction in DI is attributed to the serious microstructural effects of temperature and melting of fibers that led to a sharp drop in N_f.

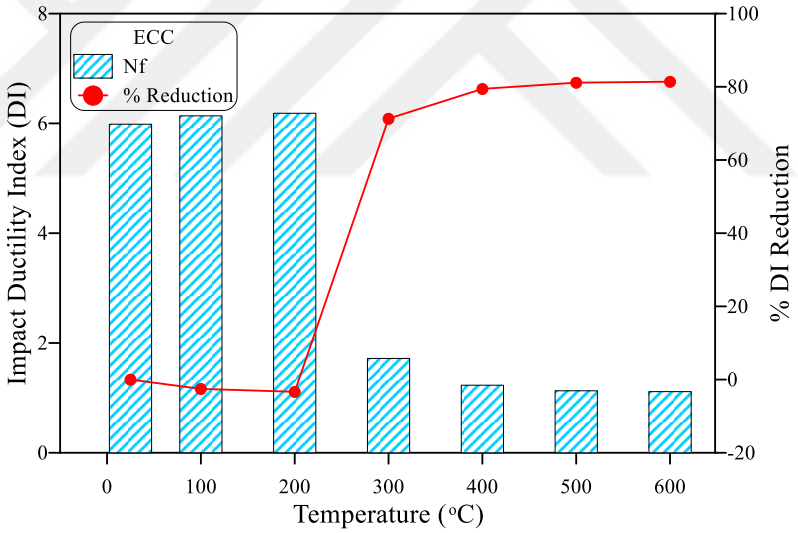

Figure 4.26. Impact ductility index-temperature behavior of ECC.

4.3.3 Failure patterns of ECC

To completely evaluate the impact behaviors of test samples the failure patterns of each sample are determined, as shown in Figure 4.27 to Figure 4.33.

(a) (b)

Figure 4.27. Reference unheated ECC disk specimens (a) before testing and (b) after testing.

(a) (b)

Figure 4.28. ECC disk specimens subjected to 100 °C (a) before testing (b) after testing.

(a) (b)

Figure 4.13. ECC disk specimens subjected to 200 °C (a) before testing (b) after testing.

(a) (b)

Figure 4.30. ECC disk specimens subjected to 300 °C (a) before testing (b) after testing.

(a) (b)

Figure 4.31. ECC disk specimens subjected to 400 °C (a) before testing (b) after testing.

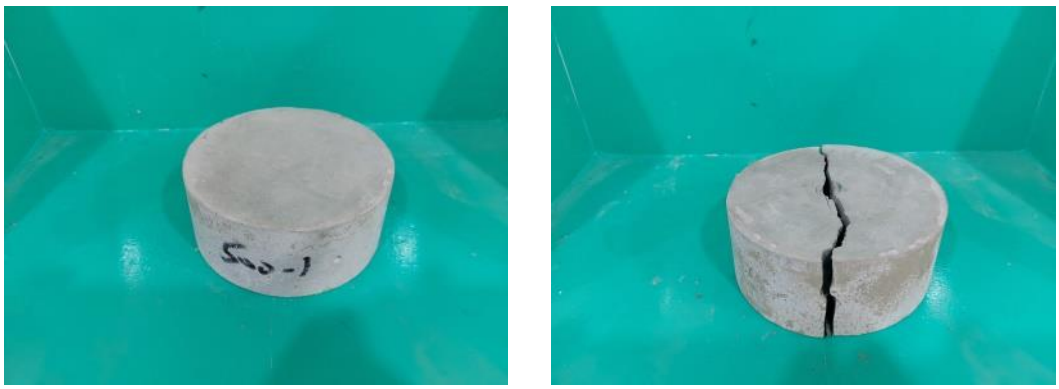

(a) (b)

Figure 4.32. ECC disk specimens subjected to 500 °C (a) before testing (b) after testing.

(a) (b)

Figure 4.33. ECC disk specimens subjected to 600 °C (a) before testing (b) after testing.

4.3.4 Comparison of ECC and NC repeated impact results

The comparison of ECC and NC impact test samples can be summarized at Table 4.3. It shows that, for NC, after exposure to 100 °C, the cracking number did not affect noticeably, where this number was decreased with a percentage decrease of only 2.4%. Similarly, Nf was no more than 3.5%. It can be said that the impact resistance did not affect by heating to 100 °C. The strength of impact forces dropped sharply after exposure to 200 °C, where the loss in impact resistance in terms of Ncr and Nf reached 74.2 and 73.5%, respectively, The residual cracking impact strength after exposure to 300, 400, 500 and 600 °C where respectively 11.8, 5.5, 3.9 and 1.8% of the original unheated strength. Similarly, the residual failure impact strength was 13.1, 7.0, 5.2 and 3.8% after exposure to 300, 400, 500 and 600 °C respectively. Figures 4.35 and 4.36 show the comparison of ECC and NC cracking and failure impact numbers.

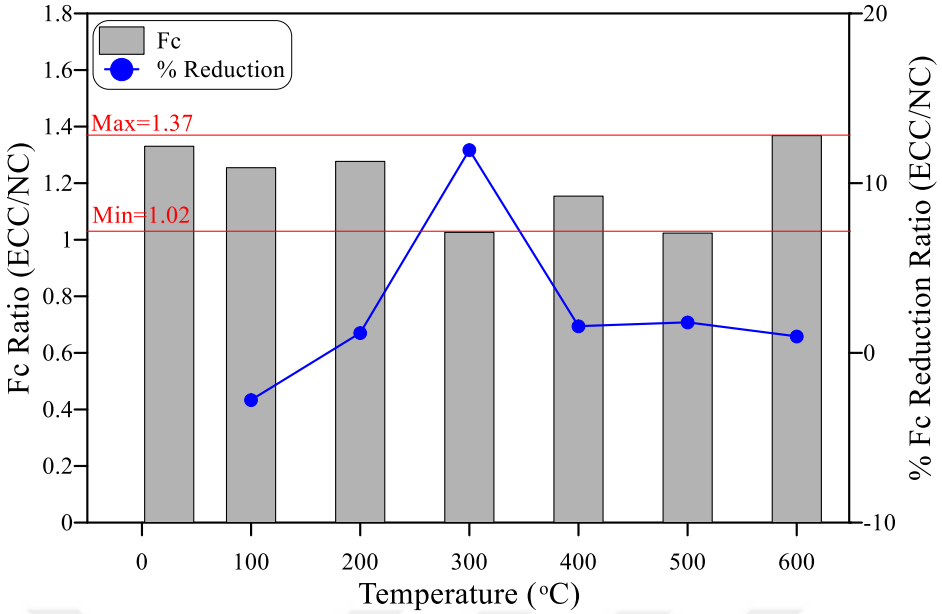

Figure 4.34. Comparison of ECC and NC compressive strengths (f_c').

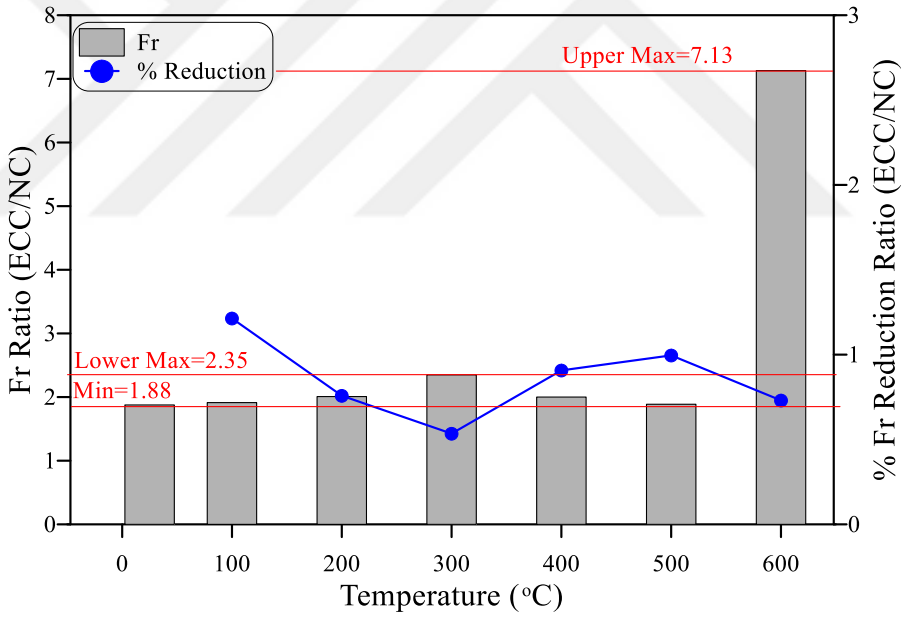

Figure 4.35. Comparison of ECC and NC flexural strengths.

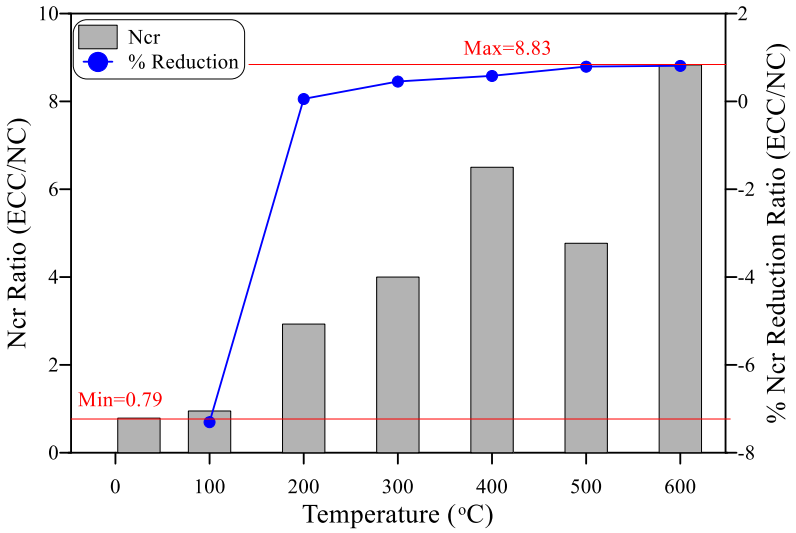

Figure 4.14. Comparison of ECC and NC cracking impact numbers.

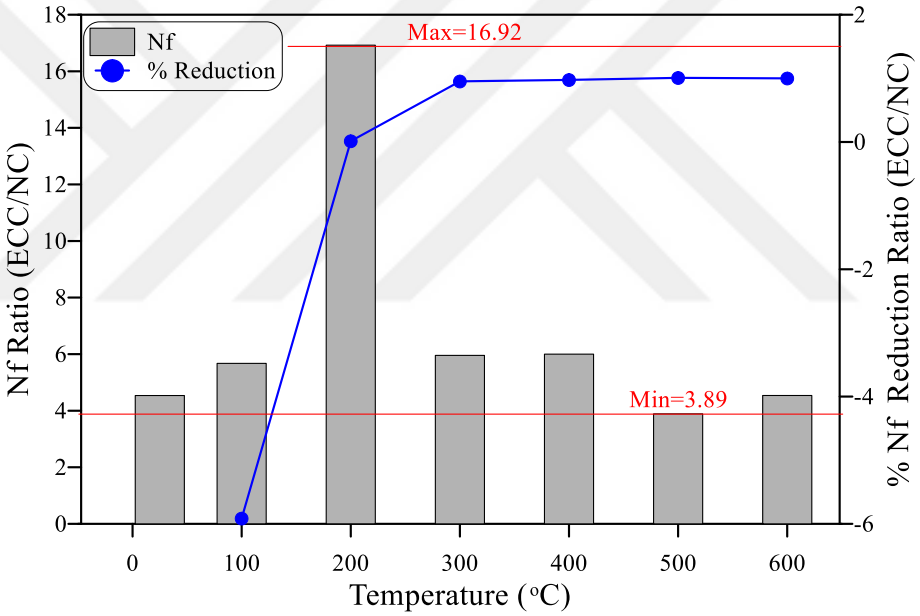

Figure 4.37. Comparison of ECC and NC failure impact numbers.

CHAPTER FIVE

RESULTS AND DISCUSSION OF PLATE SPECIMENS

5.1 General

The results from a load cell, LVDT, and accelerometer were collected simultaneously at fixed time intervals of 3 ms. the data logger could capture more than 10k records per second; therefore, the selected time step was appropriate to ensure compatible data recording without serious issues.

The following sections discuss the obtained results from plate specimens in terms of recorded physical quantities and considering the test variables. As disclosed in Chapter 3, the major variables of plate impact tests are the type of material, heating temperature level, and end boundary conditions, while the drop weight energy was kept constant by using fixed drop weight and drop height. Two plate groups, each of 15 specimens were cast and prepared for testing. The first is NC, while the second is PP fiber-based-ECC. The plate specimens of each group were divided into three subgroups according to three boundary conditions (degree of fixity), which are four-restrained ends, two-restrained ends, and clamped cases as detailed in Chapter 3. Three specimens were prepared from each group to test the residual impact capacity after exposure to different levels of high temperatures of 200, 400, and 600 °C, and one specimen was tested at room temperature as a reference specimen, while the fifth specimen was kept aside to replace any failed test.

The discussion of the results is presented in the following sections based on the obtained test records, which are the impact number at failure (n_f), retained impact force, and central deflection. It should be remembered that each specimen was subjected to subsequent constant-energy impact blows, and time variations of impact force, central deflection, and acceleration were recorded for each blow.

There was no specific trend of acceleration-time variation, while the maximum recorded accelerations for all blows of all tested materials were in the range of approximately 8 to 12 g. The time variations of impact force and deflection are briefly presented in section 5.2, while sections 5.3 through 5.5 present the effect of test variables on the failure impact number, maximum impact force, and deflection, for each impact blow and each plate specimen.

5.2 Variation of Impact Force and Deflection Results with Time

The recorded time variations of impact force and deflection with time were noticed to have approximately no specific trend of variation when subsequent time steps are compared, while the envelopes of these variations show approximately similar trends. Therefore, it was found to be more efficient to present representing sample curves instead of presenting a huge number of curves for each impact blow for the 24 tested plates. Figure 5.1 shows the impact force-time variations of the NC plate with four-ends restricted case at all temperature levels recorded for the first impact blow, while Figure 5.2 shows the variation of deflection with time for the same specimen considering the first impact blow.

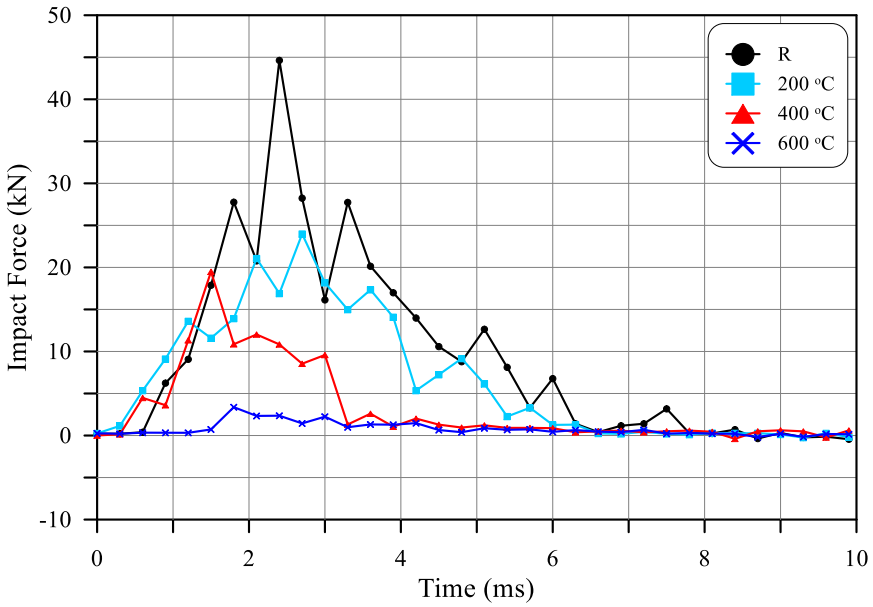

Figure 5.1. Impact force-time variation of NC 4-ends restricted plates of the first impact blow.

The test recording was started at the time of the load releasing order, where the load is released a few seconds after that for safety purposes, and continued for a few more seconds. However, it was found that the effective impact wave and hence the waves of recorded quantities extend for approximately 0.1 ms. Therefore, as shown in the two following figures, the time is presented for only 0.1ms from the whole test period.

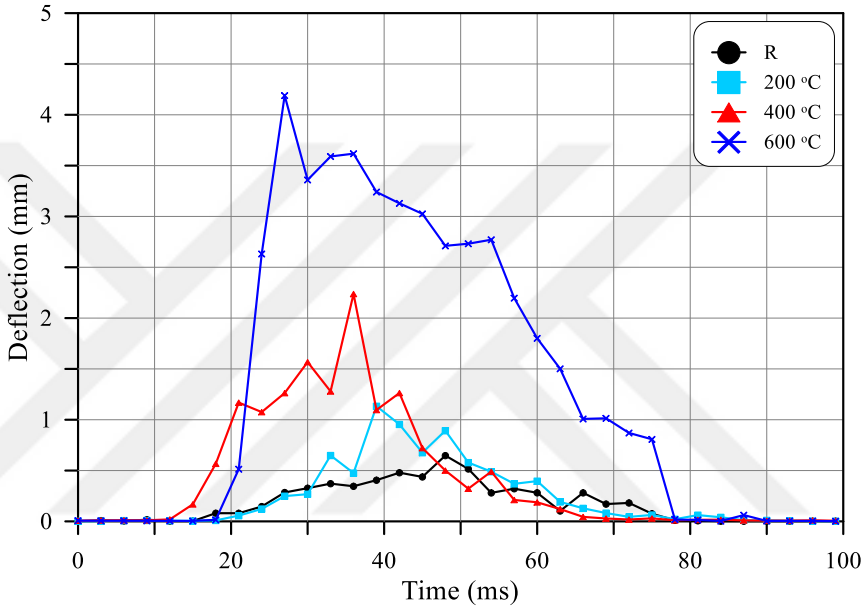

Figure 5.2. Deflection-time variation of NC 4-ends restricted plates of the first impact blow.

It is shown in Figure 5.1 that the reference specimen that was tested without heating retained the highest impact force envelope and that the force envelope decreases as temperature increases. There is no recognized specific oscillation trend. However, a common notice is that for all curves, the variation of the force at the start of the wave is minimal, where the maximum force is reached at no more than 20 ms after the start of the impact wave. On the other hand, the descending or decay part after the maximum force is longer for all temperatures.

Figure 5.2 shows that deflection increases with the increase of temperature and the specimen exposed to 600 °C exhibited noticeably higher temperature envelop compared to other specimens, which is compatible with their noticeably lower impact forces shown

in Figure 5.1. For this specimen, the concrete degraded significantly so that its stiffness and surface hardness were extremely weakened so that approximately the whole subjected impact energy from the falling weight was relieved via local deformation.

On the other hand, the opposite stands for the case of reference specimens that absorbed most of the impact energy by sustaining high impact force with minimal deformations as shown in Figures 5.1 and 5.2, respectively. Comparing the two figures, it can also be noticed that there is a small-time lag of approximately 10 to 30 ms between the recorded times of maximum force and maximum deflection, which is understood as deflection a sort of energy response that occurs after the force action.

5.3 Failure Impact Numbers

Increasing the impact number till failure reflects a higher resistance to impact loads, where all specimens are subjected to constant drop weight and drop height. Thus, the specimens with higher energy capacity would absorb a higher number of impact blows before failure.

Figure 5.3 shows the effect of temperature on the retained impact numbers of NC plates. As shown in the figure, the retained numbers of impact blows of NC specimens before heating were in the range of 8 to 13 depending on the boundary condition. Exposing the specimens to 200 °C decreased the failure impact numbers to a range of 4 to 5 blows, while the retained numbers were slightly lower (3 to 4) after exposure to 400 °C On the other hand, heating the plates to 600 °C decreased the number of impact blows required to fail the plates to only 1 or 2 blows as shown in Figure 5.3.

Three concluding remarks can be drawn from these results. The first is that increasing the temperature continuously decreases the sustained number of impacts till failure, while the second remark is that exposing the specimens to a temperature range of 200 to 400 °C has approximately an equivalent effect, where the impact resistance for most cases decreased by approximately 50 to 70% compared to unheated plates.

On the other hand, the third remark is that exposing the specimens to as high as 600 °C leads to further destructive effects, where in some cases, the residual impact strength in terms of failure impact number was approximately 15% or lower. This behavior is

expected due to the physical and chemical changes that occur in concrete after exposure to high temperatures as discussed in Chapter 4 for the small-size disk specimens.

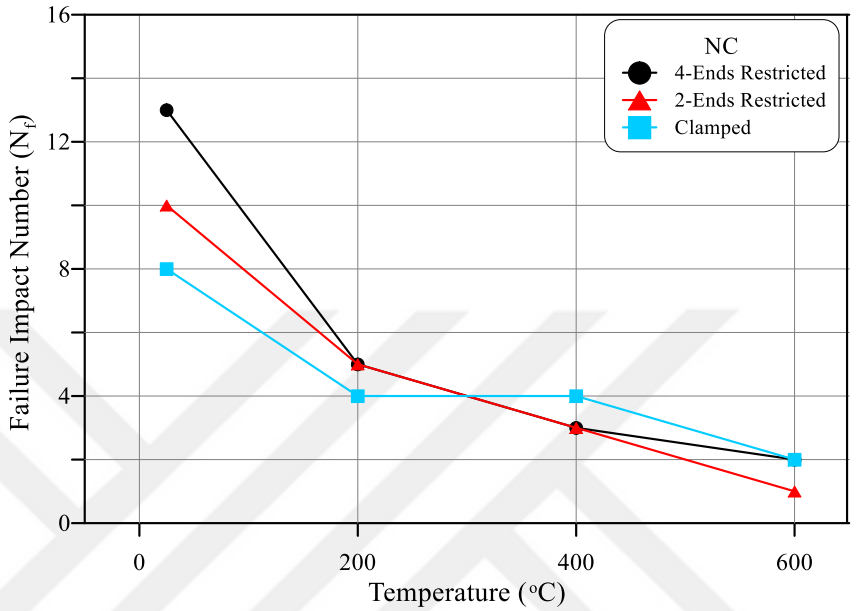

Figure 5.3, Failure impact number-temperature relations of NC plates for different boundary cases.

The results of the ECC plates shown in Figure 5.4 confirm and better clarify the drawn remarks for the NC specimens. The residual impact numbers of the ECC plates after exposure to 200 and 400 °C were in the ranges of approximately 15 to 20% and 9 to 12%, respectively, which means that percentage deteriorations of more than 80% and 88% occurred after exposure to 200 and 400 °C On the other hand, the specimens exposed to 600 °C deteriorated by more than 94% and retained only 3 to 6% of their original impact strength in terms of failure impact number. The greater deterioration of ECC compared to NC can be attributed to the much denser cementitious matrix that prevents the dissipation of water vapor and hence thermal stresses are induced resulting in more severe deterioration of the microstructure.

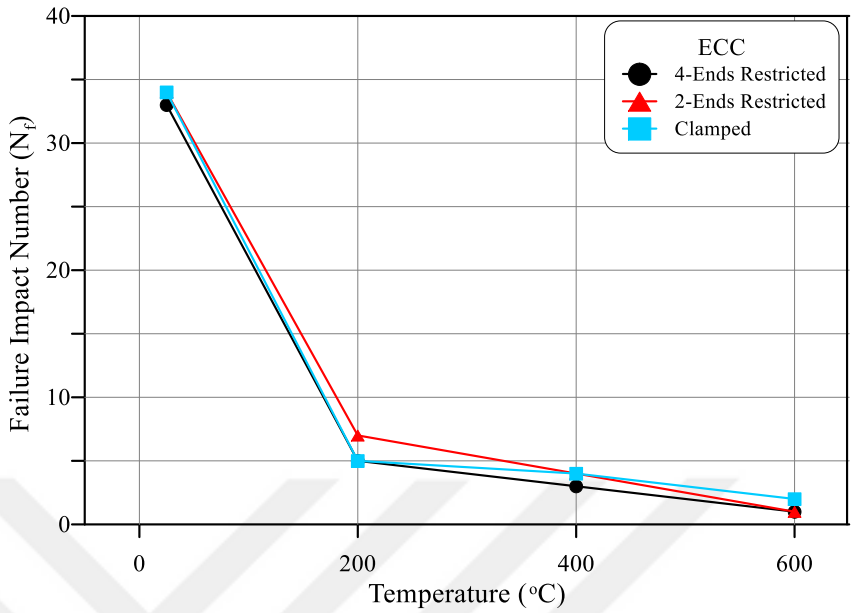

Figure 5.4. Failure impact number-temperature relations of ECC plates for different boundary cases.

Comparing NC and ECC microstructures, it is expected that ECC can withstand significantly higher tensile stresses owing to the large amount of cementitious materials, very fine filler, and the presence of fibers. Thus, the results shown in Figure 5.5 are self-explained, where considering the adopted flexural impact setup; the failure of the test plates is controlled by the tensile strength of tested specimens at the bottom face. Since; the flexural strength of ECC is way higher than that of NC; the retained impact numbers of ECC unheated plates were much higher than their corresponding NC plates. As shown in Figure 5.5, ECC reference specimens retained from 33 to 34 impact blows for the three boundary cases, while NC specimens retained only 8 to 13 impact blows. Hence, the impact strength of ECC specimens in terms of resisted impact blows was approximately 250 to 425% higher than that of NC plates.

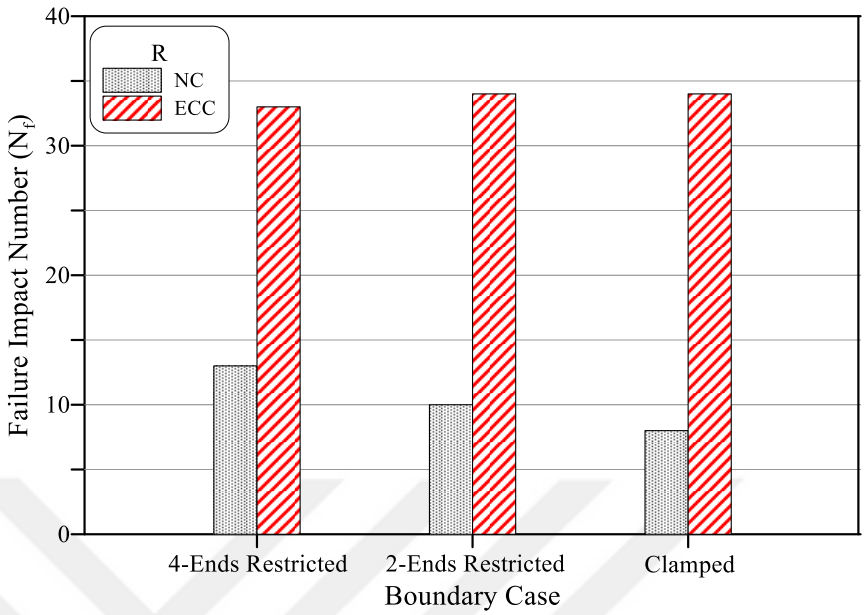

Figure 5.5. NC and ECC failure impact numbers of different boundary cases at room temperature.

As shown in Figures 5.6 to 5.8, as temperature increases, the differences between retained impact numbers of NC and ECC plates become narrower, where after exposure to 200 and 400 °C, ECC specimens retained 100 to 140% compared to NC specimens. This is because of the faster degradation of ECC compared to NC due to its denser matrix as discussed earlier. When the specimens were exposed to 600 °C, the ECC plates degraded at a much higher rate compared to corresponding NC plates reaching even lower impact numbers as shown in Figure 5.8.

The effect of boundary condition or end fixity degree is illustrated in Figure 5.5 for both NC and ECC unheated specimens. The figure shows obviously that for NC specimens, the retained impact number increased with the increase of end fixity degree, where n_f was 8 for clamped plate, while it increased to 10 and 13 for two-end restrained and four-end restrained plates, respectively. On the other hand, there was no such trend for ECC specimens, where the recorded n_f for the four-end restrained plate was 33, while it was 34 for the other two cases. Figures 5.6 to 5.8 show that there is no specific effect trend of end condition on n_f records of plates exposed to high temperatures. However, it can be

said that for ECC specimens, the four-end restrained case exhibited the lowest impact number records at almost all temperature levels.

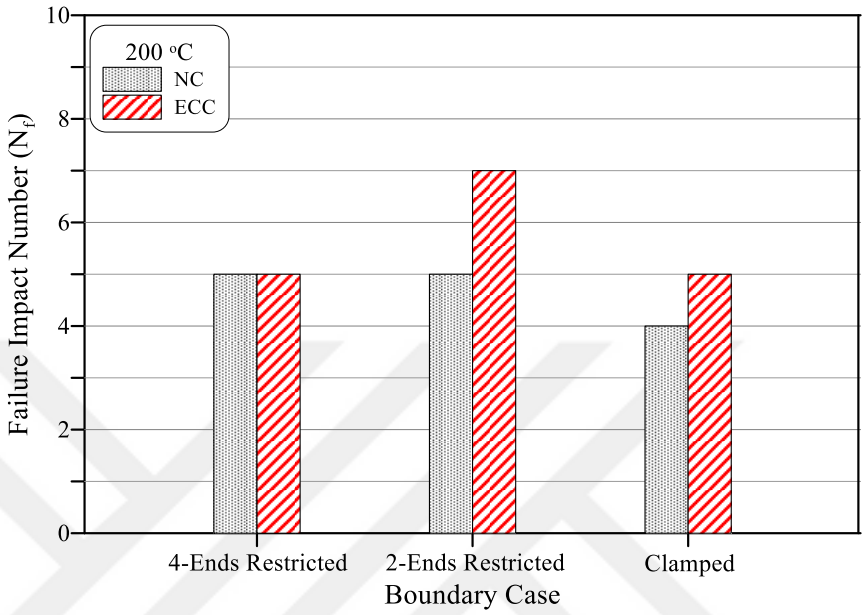

Figure 5.6. NC and ECC failure impact numbers of different boundary cases at 200 °C.

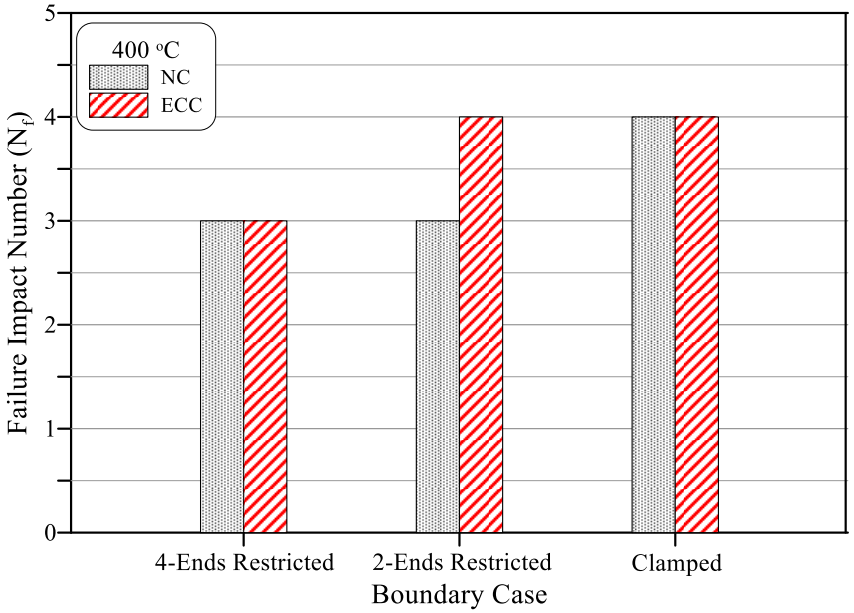

Figure 5.7. NC and ECC failure impact numbers of different boundary cases at 400 °C.

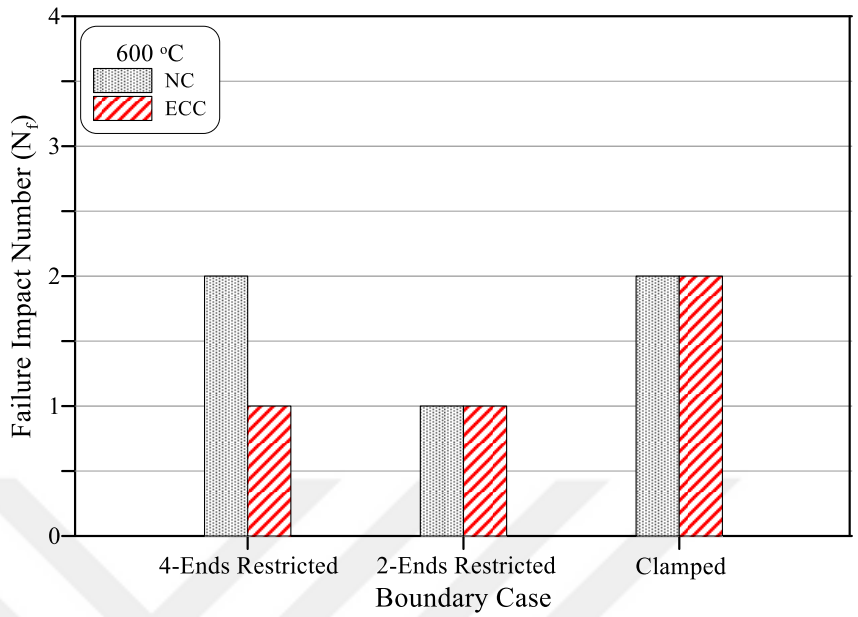

Figure 5.8. NC and ECC failure impact numbers of different boundary cases at 600 °C.

5.4 Impact Force Results

As depicted in Figure 5.1, the impact force was recorded during the testing time for each impact blow. The maximum recorded impact force for each impact blow is shown in Figures 5.9 to 5.11 for NC plates, while Figures 5.12 to 5.14 show the variation of impact force with impact blow for ECC plates at all temperatures. The observation of Figures 5.9 to 5.11 reveals that retained impact force decreases almost smoothly with the increase of impact blow number for all temperatures and regardless of end conditions. Subjecting a plate to an impact force that does not fail, would affect the microstructure by inducing concentrated compressive stresses at the center of the top face, which in turn results in a tensile stress wave around the loading point and across the plate thickness.

On the other hand, the flexural test setup subjects the lower part of the plate below the neutral axis to flexural tensile stresses and the top surface to compressive flexural stresses. These stresses would weaken the microstructure and cause cracking, which reduces the load-carrying capacity of the plate. Therefore, it is expected that the recorded impact force decreases after each additional impact blow.

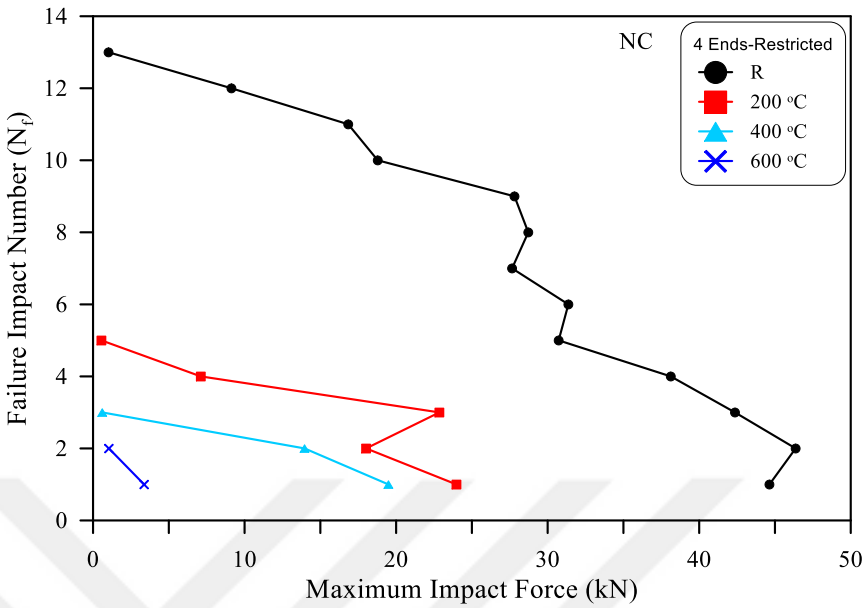

Figure 5.9. NC failure impact number-impact force relations at different temperatures for 4-ends restricted case.

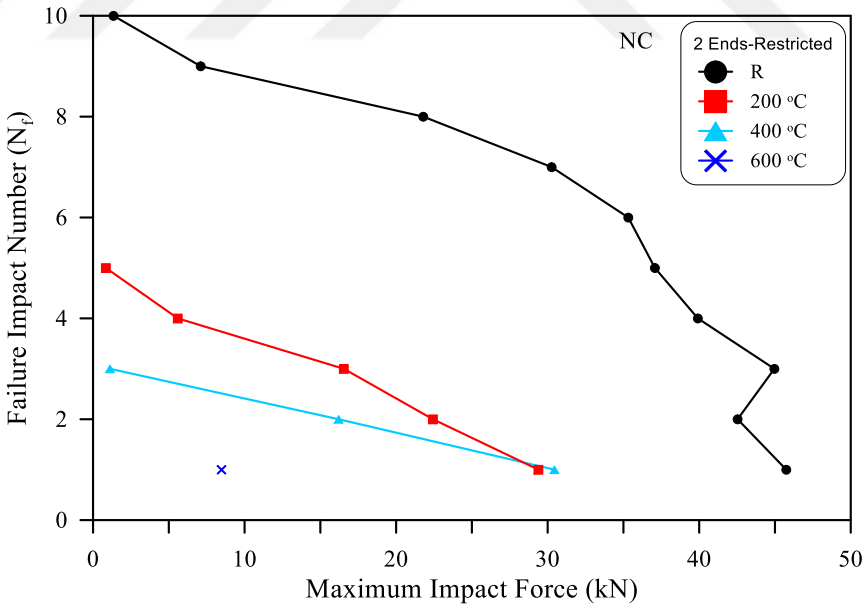

Figure 5.10 NC failure impact number-impact force relations at different temperatures for 2-ends restricted case.

However, as depicted in Figures 5.9 to 5.11, some minor fluctuations reveal a slightly higher impact force than what was recorded in the previous time step. This action can be

attributed to the heterogeneous microstructure of concrete. Due to the higher recorded impact blows, this fluctuation is more obvious for ECC plates as shown in Figures 5.12 to 5.14. However, the envelope of the curves refers to an obvious decrease in impact force as the number of impact blows increases for all temperatures and all boundary cases.

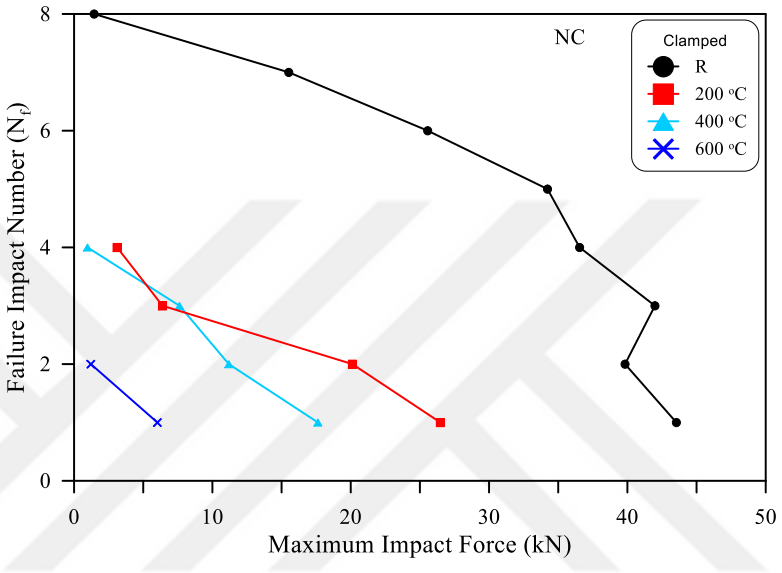

Figure 5.11. NC failure impact number-impact force relations at different temperatures for clamped case.

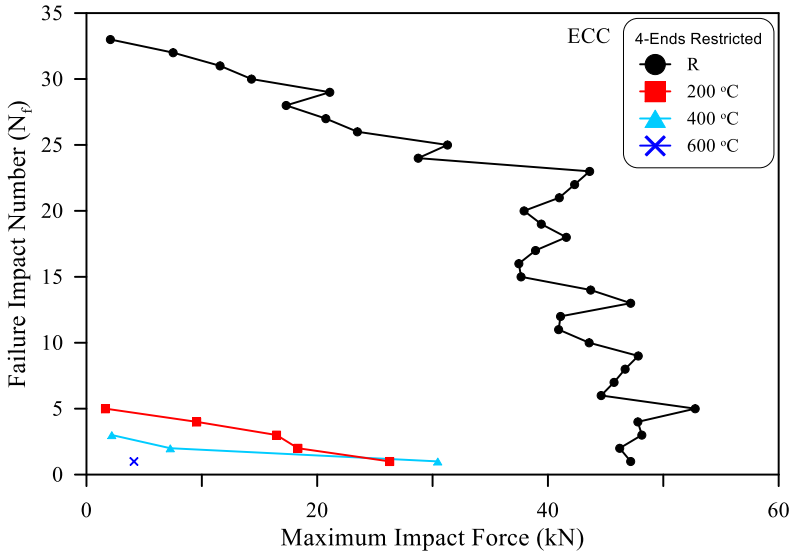

Figure 5.12. ECC failure impact number-impact force relations at different temperatures for 4-ends restricted case.

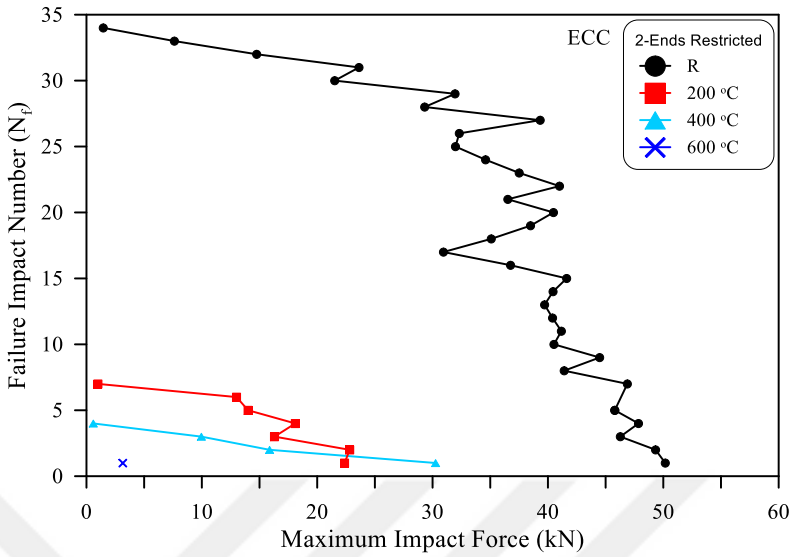

Figure 5.13. ECC failure impact number-impact force relations at different temperatures for 2-ends restricted case.

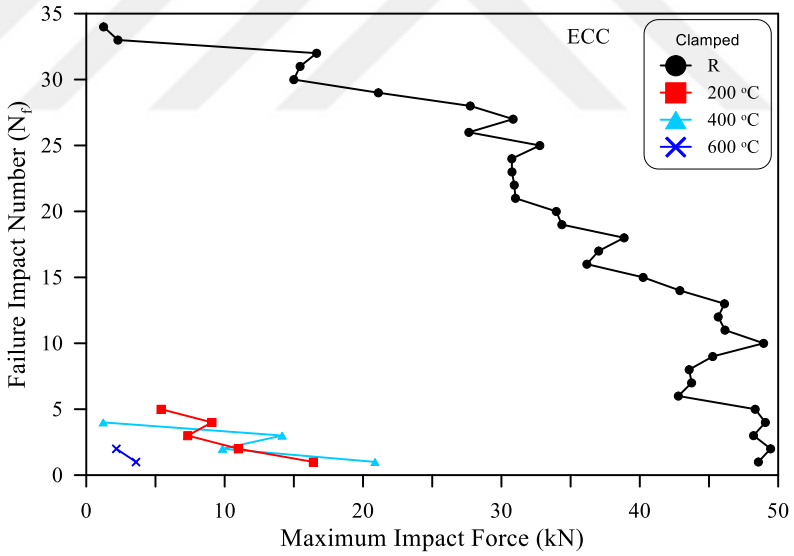

Figure 5.14. ECC failure impact number-impact force relations at different temperatures for clamped case.

To evaluate the effect of temperature and boundary conditions on impact forces, the absolute maximum recorded impact forces for each specimen from all impact blows were collected and presented in Figures 5.15 to 5.20. It is worth mentioning that the maximum impact force was mostly recorded at the first impact blows. However, in very few cases,

the maximum was recorded in the second impact, which was slightly higher than that recorded at the first impact blow.

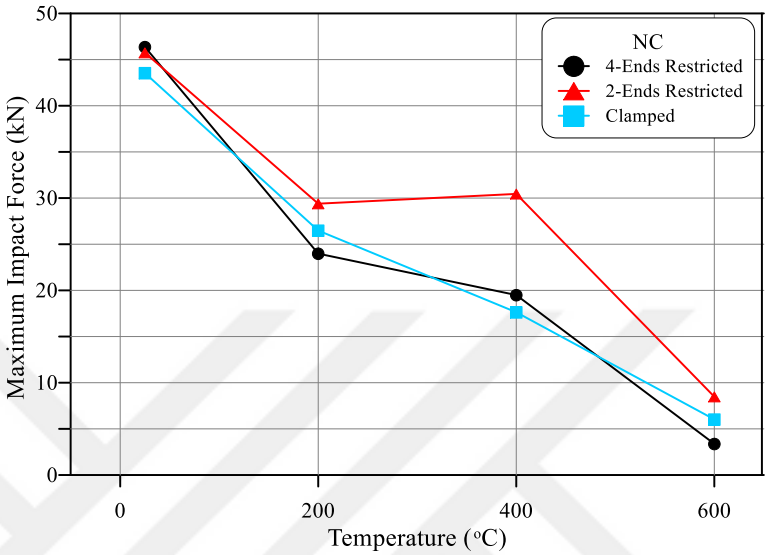

Figure 5.14. Maximum impact force-temperature relations of NC plates for different boundary cases.

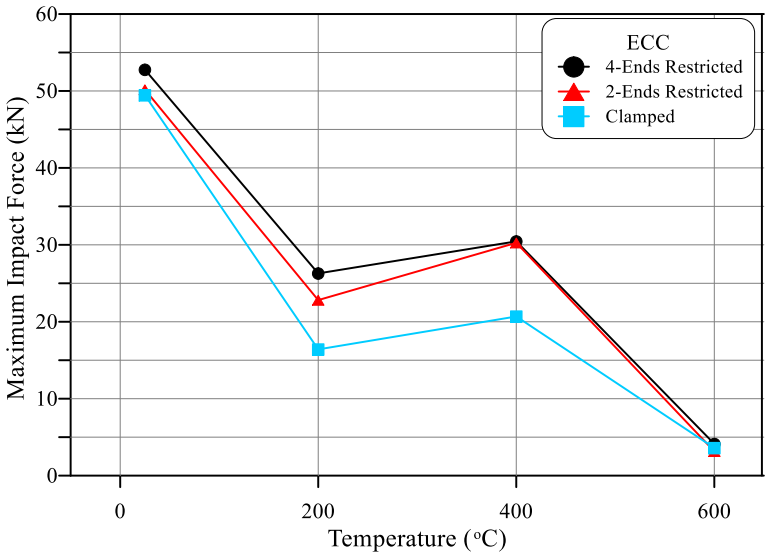

Figure 5.16. Maximum impact load -temperature relations of ECC plates for different boundary cases.

It is clear in Figures 5.15 and 5.16 that the retained impact forces of heated specimens are less than those of their corresponding unheated ones, which is attributed to the destructive effects of high temperature on concrete microstructure as discussed earlier for the impact numbers. The figures show that impact forces drop significantly after exposure to 200 °C and approximately hold an equivalent level of deterioration after exposure to 400 °C, with a slight decrease or increase. Thus, a semi-stabilized region can be clearly noticed in Figures 5.15 and 5.16 between 200 and 400 °C Finally, a destructive drop occurs after exposure to 600 °C This behavior is noticed for both NC and ECC plates regardless of the boundary condition.

However, a distinguished difference between NC and ECC can be recognized in the semi-stabilized region, where ECC plates recovered slightly higher impact forces at 400 °C compared to 200 °C, where such behavior is not a general case for NC plates. For ECC plates, the specimens exposed to 200 °C retained 45.5 to 49.8% of the impact force of corresponding unheated specimens, while this range was 57.7 to 60.3% after exposure to 400 °C On the other hand, the percentage retained impact forces of NC specimens exposed to 200 and 400 °C were in the ranges of 51.7 to 64.2% and 42.0 to 66.6%, respectively.

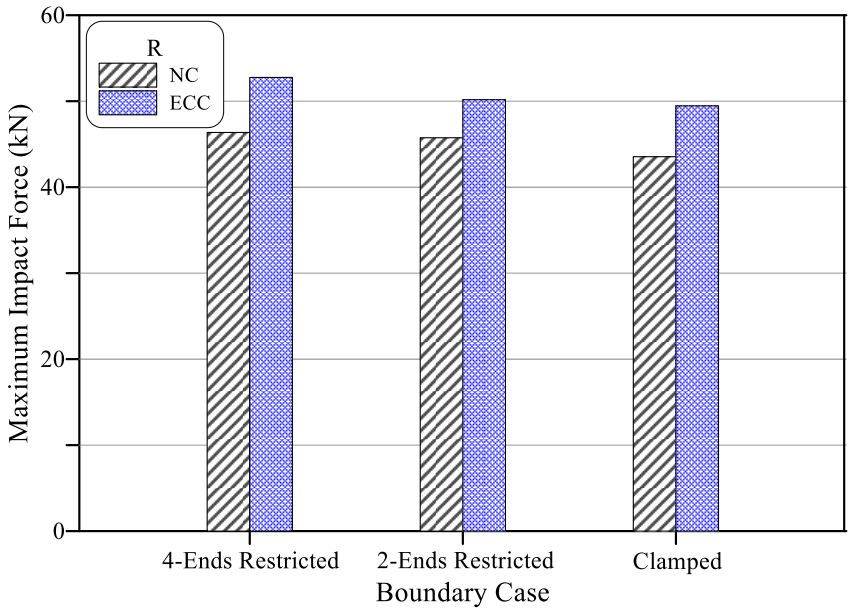

Figure 5.17. NC and ECC maximum impact forces of different boundary cases at room temperature.

Figure 5.17 shows that despite the small differences, stiffer end restriction leads to higher absorbed impact forces for unheated specimens, where the four-ends restricted plates retained the highest impact force records followed by the two-ends restricted plates, while clamped specimens retained the lowest impact forces for both NC and ECC plates. As shown in Figure 5.17, compared to the case of four-ends restriction, the two ends restricted plate and clamped plate retained 1.3 and 6.1% lower impact forces, respectively, for the NC plate, and 4.9 and 6.3%, respectively, for the ECC plate. This result explains that a higher degree of end fixity reduces the end rotation and limits the mid-span deflection, which means that a smaller part of the impact energy is dissipated in the form of deformations. Thus, a larger part of the impact energy from the drop weight is absorbed by the material and transformed as increased impact force. Due to the effect of temperature on the microstructure of the material, the effect of end conditions on heated specimens is not as clear as for reference unheated specimens as shown in Figures 5.18 to 5.20. However, it can be noticed that ECC plates could exhibit the same behavior after exposure to 200 °C and 400 °C, while no such trend was recorded for plates exposed to 600 °C or for NC heated plates. The degradation of the material after high-temperature exposure might weaken the edges of plates so that the end rotation cannot be restricted effectively.

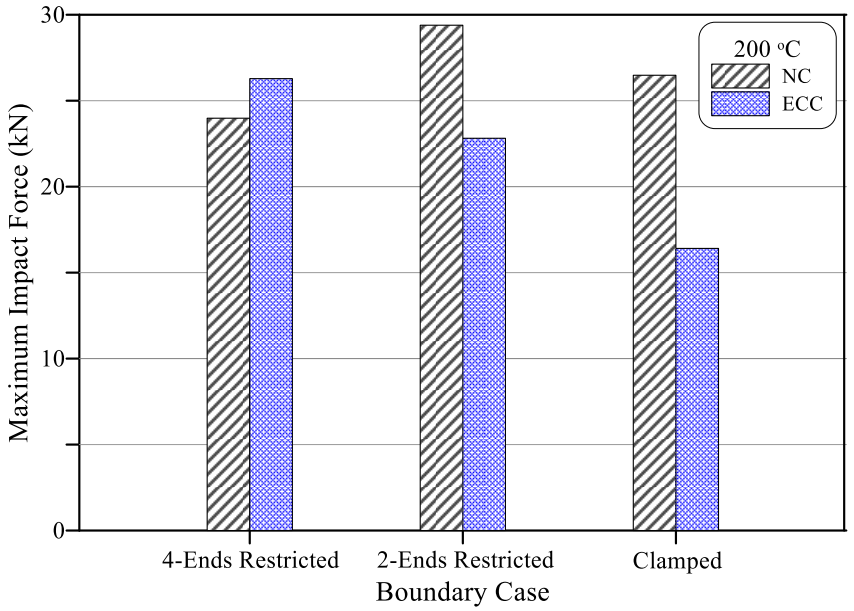

Figure 5.18. NC and ECC maximum impact forces of different boundary cases at 200 °C.

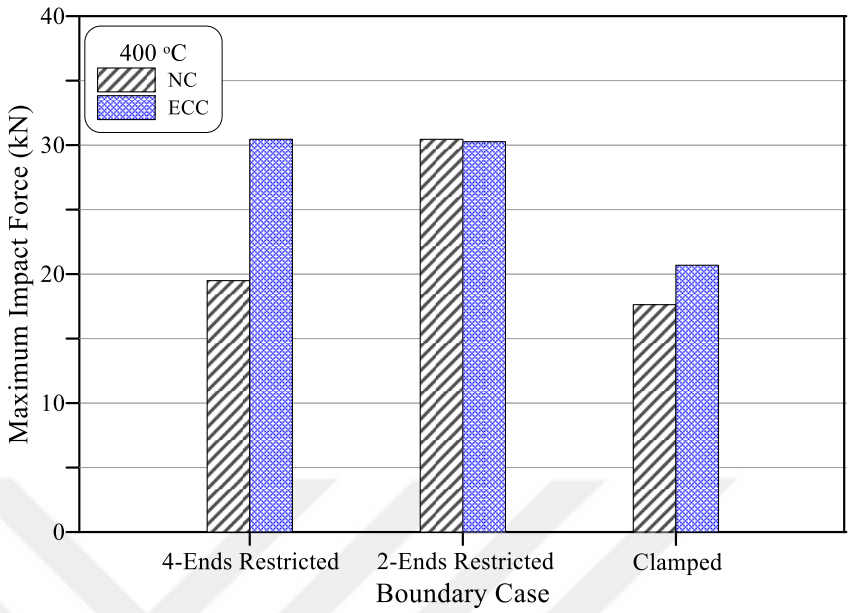

Figure 5.19. NC and ECC maximum impact forces of different boundary cases at 400 °C.

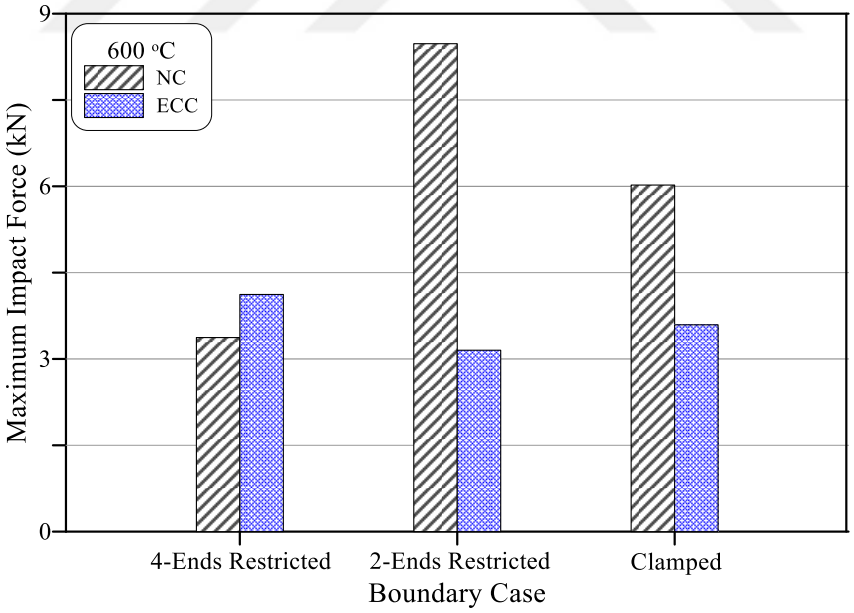

Figure 5.20. NC and ECC maximum impact forces of different boundary cases at 600 °C.

5.5 Deflection Results

The variation of deflection with each subsequent impact blow is shown in Figures 5.21 through 5.23 for NC plates and Figures 5.24 through 5.26 for ECC plates. The figures show that the deflection was small after the first blow and increased after each subsequent blow. This result is compatible with the impact force results discussed in Figures 5.9 through 5.14, where each impact blow has its own degree of negative effect on the microstructure and consequently on the total strength of the material.

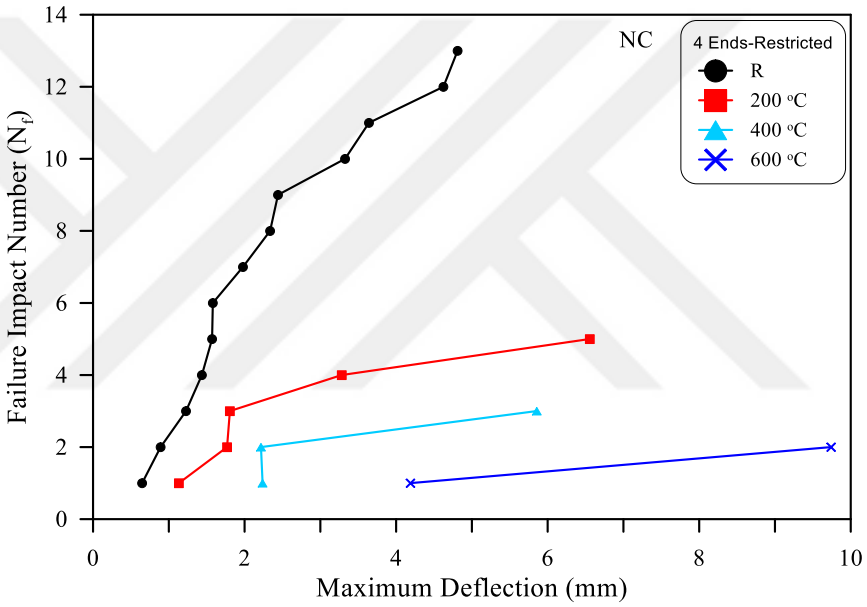

Figure 5.21. NC failure impact number-maximum deflection relations at different temperatures for 4-ends restricted case.

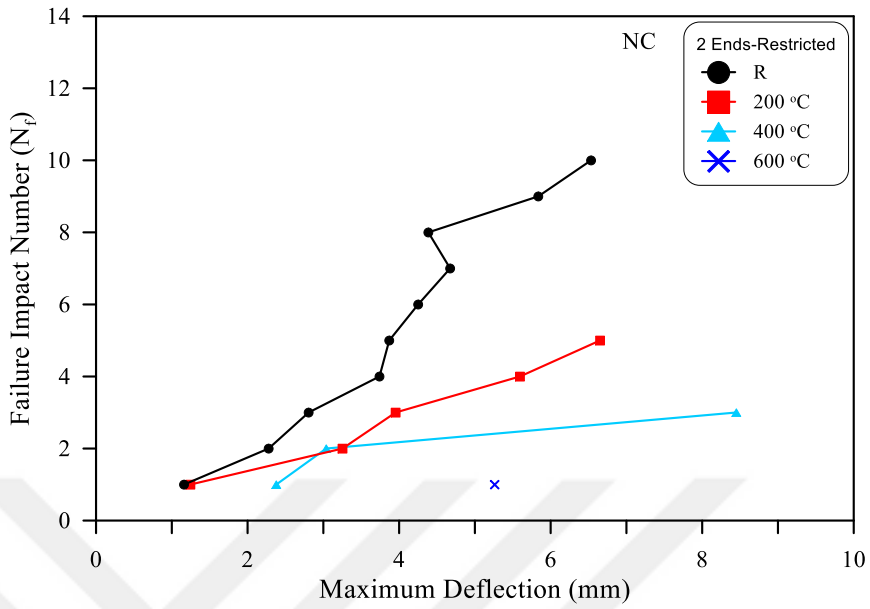

Figure 5.22. NC failure impact number-maximum deflection relations at different temperatures for 2-ends restricted case.

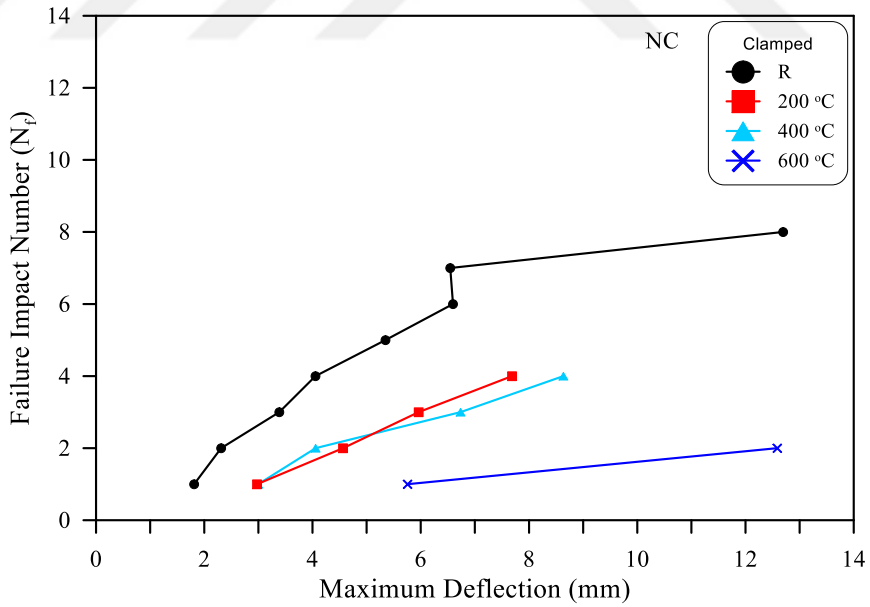

Figure 5.23. NC failure impact number-maximum deflection relations at different temperatures for clamped case.

Decreasing the strength with the increase in the number of blows decreases the modulus of elasticity of the material, which is directly reflected as a weaker stiffness and hence a

larger deformation, where the amount of dissipated impact energy via cracking and deflection gradually increases as more impact blows are subjected. As for the impact force records, and despite that the total envelope of the curves reflects the above discussed trend, fluctuation of some results can also be observed in many cases, where lower deflections were recorded in subsequent blows as shown in Figures 5.24 - 5.26. This fluctuation is again attributed to the heterogeneity of concrete.

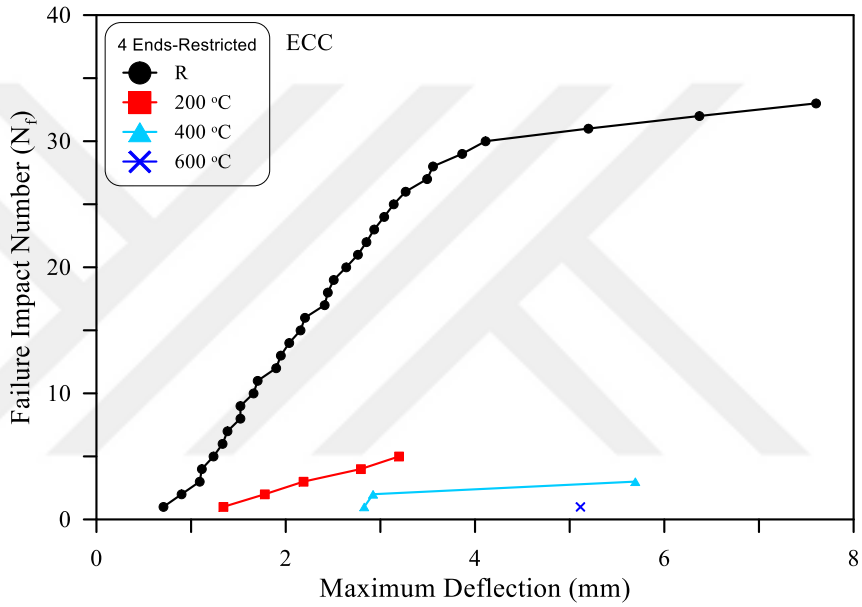

Figure 5.24. ECC failure impact number-maximum deflection relations at different temperatures for 4-ends restricted case.

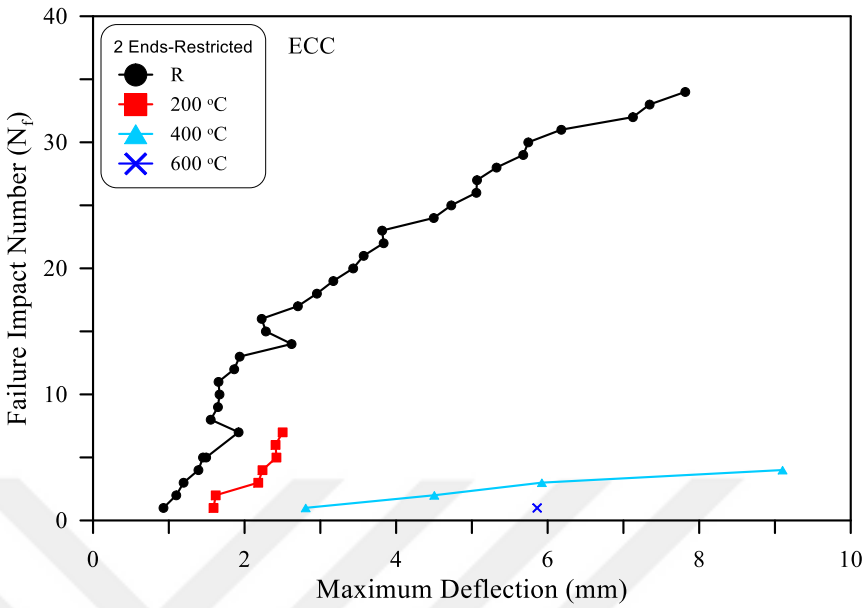

Figure 5.25. ECC failure impact number-maximum deflection relations at different temperatures for 2-ends restricted case.

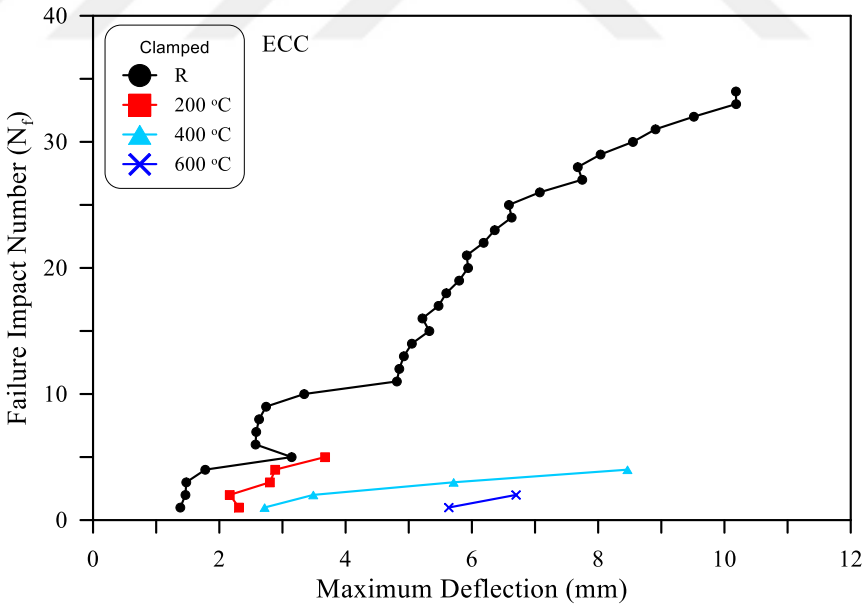

Figure 5.26. ECC failure impact number-maximum deflection relations at different temperatures for clamped case.

Figures 5.27 through 5.32 visualize the effect of boundary conditions on deflection records of NC and ECC plates before and after exposure to high temperatures. The results are

compared for the first, third, and fifth impact blows. Figure 5.27 clearly shows that higher restriction at plate boundaries reduces the recorded deflection values. It is clear in the figure that clamped plates exhibited the highest deflections, while four-ends restricted plates recorded the lowest deflections. For the unheated specimens, the recorded deflections due to the first impact blow were 0.65, 1.16, and 1.81 mm for four-ends restricted, two-ends restricted, and clamped NC plates, respectively. Similar sequences were also maintained after exposure to higher temperatures, where the recorded deflections were respectively 1.13, 1.24, and 2.97 mm; 2.24, 2.38, and 3.00 mm; 4.19, 5.26, and 5.76 mm for plates exposed to 200, 400, and 600 °C, respectively.

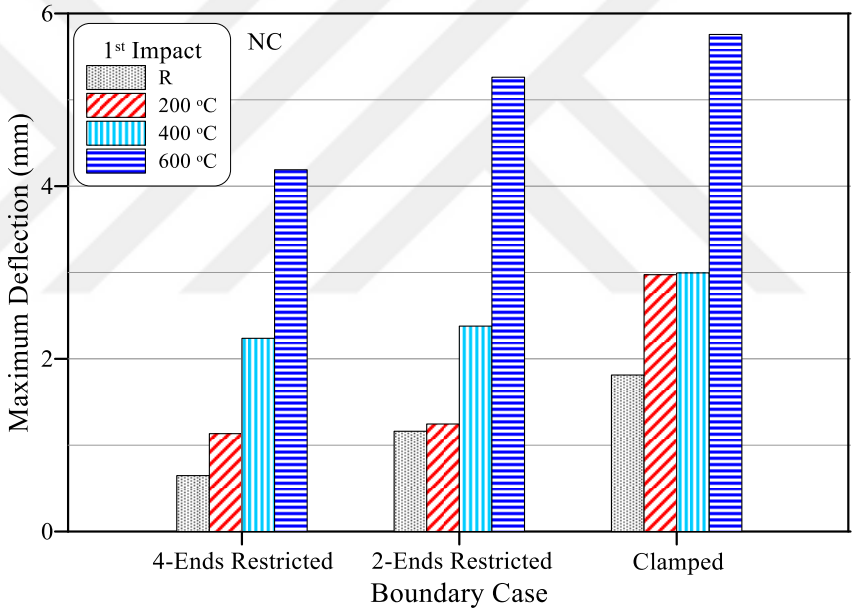

Figure 5.27. NC first impact maximum deflections for different boundary cases at different temperatures.

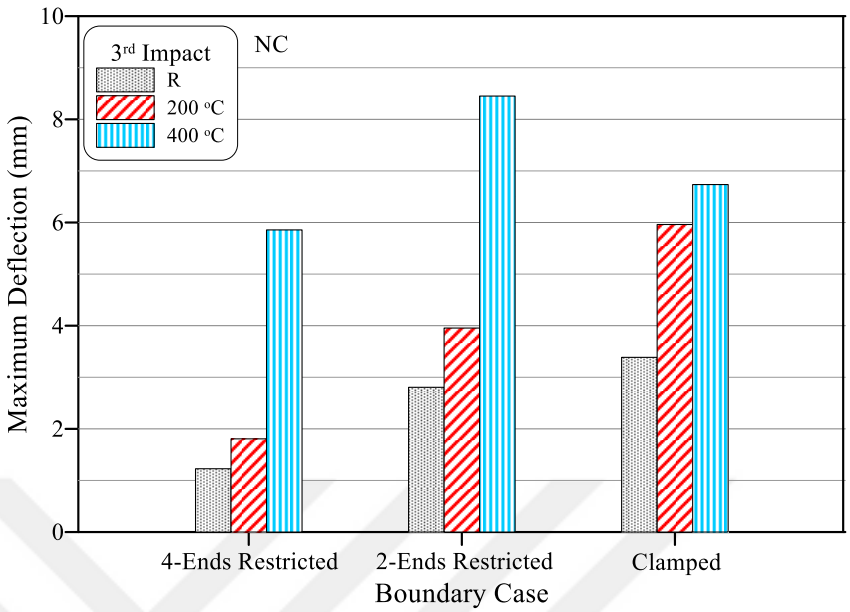

Figure 5.28. NC third impact maximum deflections for different boundary cases at different temperatures.

The same trend still stands for deflection records of the third and fifth impact blows but with limited exceptions. Figure 5.27 shows that for unheated NC plates and those heated to 200 °C, the same trend of end-restriction effect was recorded, while an exception was recorded at 400 °C. On the other hand, it is shown in Figure 5.28 that as for the first impact, more restriction at the plate edges reduces the recorded deflection regardless of temperature at the fifth impact. The exception explains that plate edges of some heated specimens might be thermally affected and weakened so that end rotation could occur due to corner fracturing of these edges in some cases. It is worth mentioning that some missing data are obvious within the third and fifth impact figures due to the failure of specimens subjected to 600 °C or even those subjected to lower temperatures under a smaller number of impact blows. The deflection records of ECC specimens shown in Figures 5.30 through 5.32 reflect a similar trend of results to that of NC plates but with a more frequent exception that two-ends restricted plates record slightly higher deflection than that of four-ends restricted plates.

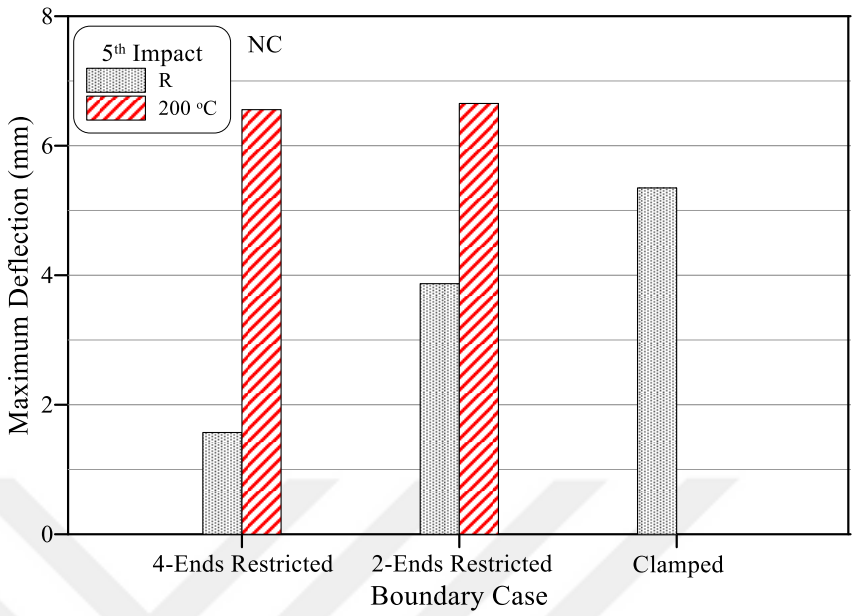

Figure 5.29 NC fifth impact maximum deflections for different boundary cases at different temperatures.

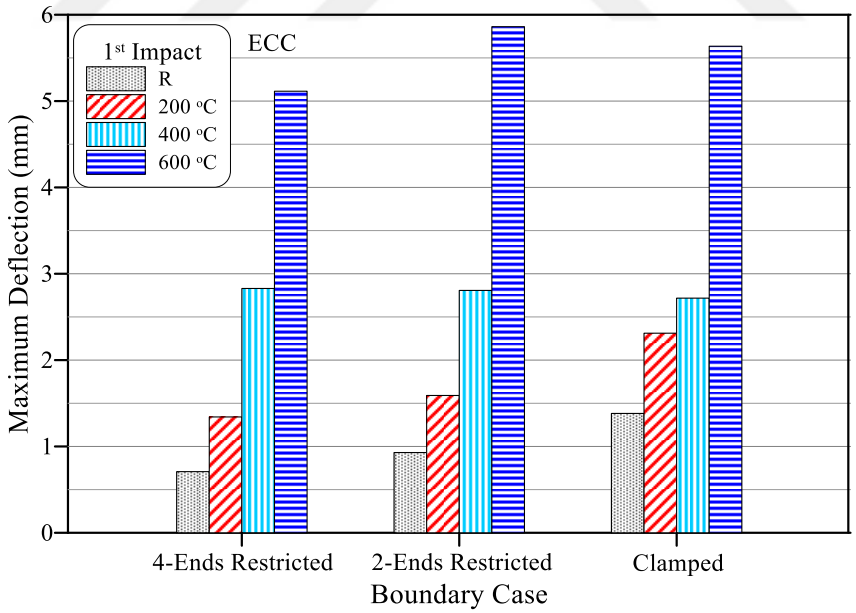

Figure 5.30. ECC first impact maximum deflections for different boundary cases at different temperatures.

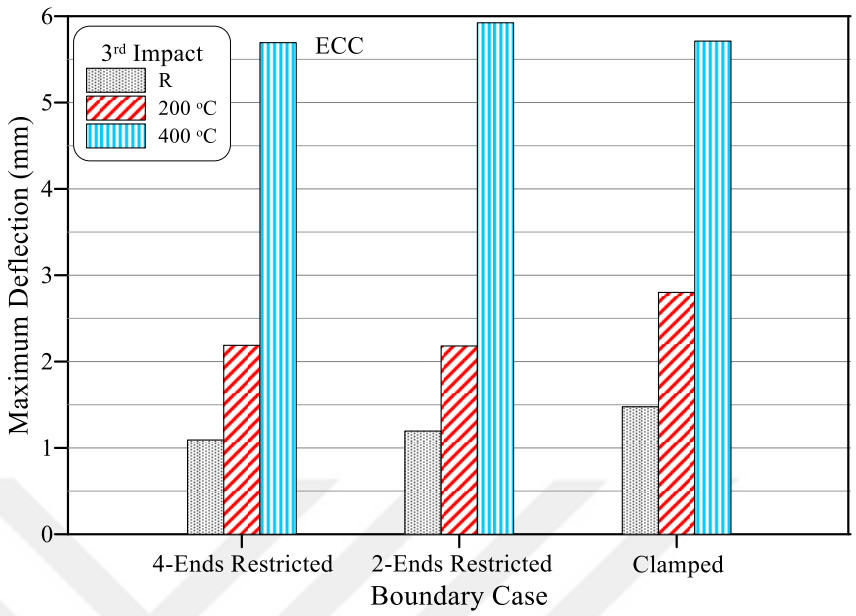

Figure 5.31. ECC third impact maximum deflections for different boundary cases at different temperatures.

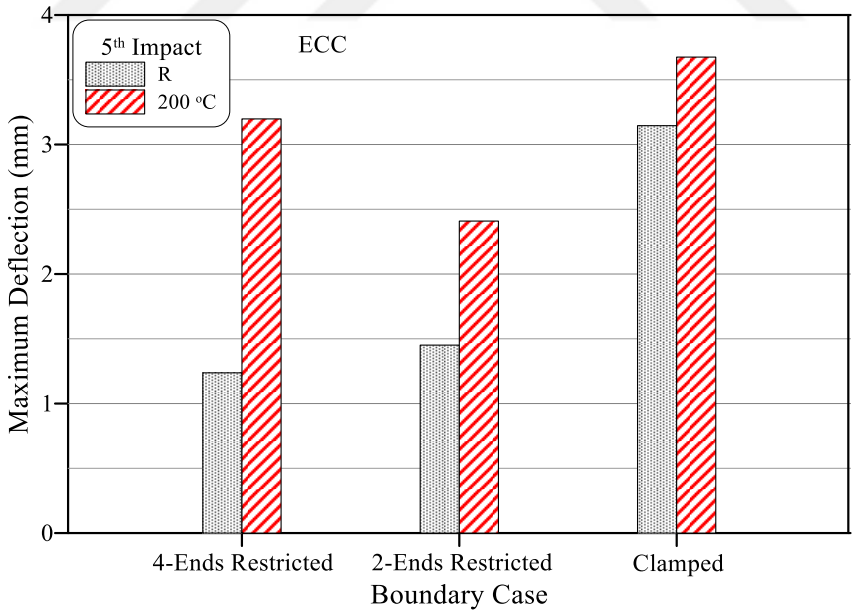

Figure 5.32. ECC fifth impact maximum deflections for different boundary cases at different temperatures.

Figures 5.33 to 5.35 illustrate the effect of temperature exposure on deflections of NC plates recorded at the first, third, and fifth impact blows, while Figures 5.36 to 5.38 visualize those of ECC plates. The figures show clearly that heated specimens exhibited higher deflections compared to unheated ones, and that the deflections increase with temperature increase. Considering the first impact blow of NC plates shown in Figure 5.33, the recorded deflections for the four-ends restrained plate were 0.65, 1.13, 2.24, and 4.19 mm for room, 200, 400, and 600 °C exposures, respectively. A very similar sequence was also recorded for the case of a two-ends restricted plate as shown in Figure 5.33, while the recorded deflection at 400 °C was 3.00 mm, which is slightly higher than that of 200 °C (2.97 m) for the case of clamped plate. However, the basic trend of deflection increases with temperature increase still stands. Similar behavior of the three groups is also shown for the recorded deflections under the third impact blow (Figure 5.34) and fifth impact blow (Figure 5.35).

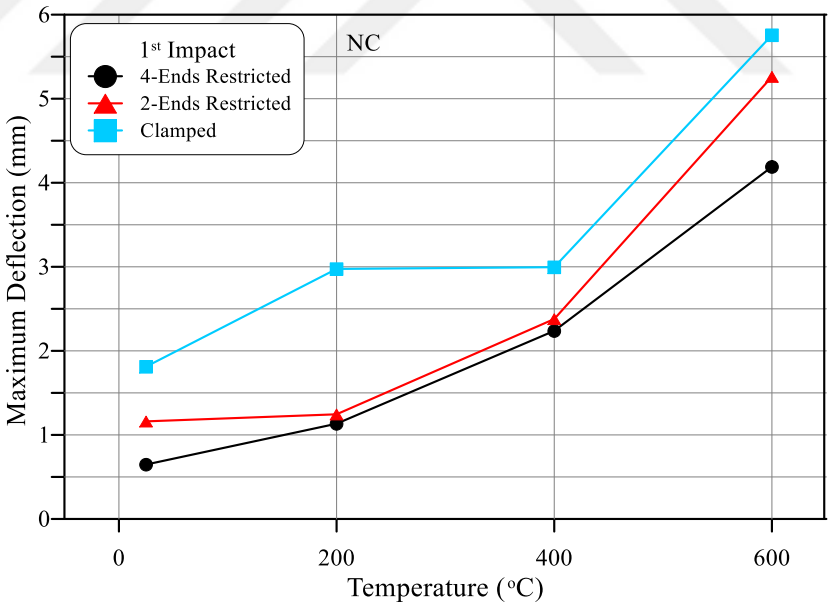

Figure 5.33. NC maximum deflections-temperature relations for different boundary cases at first impact.

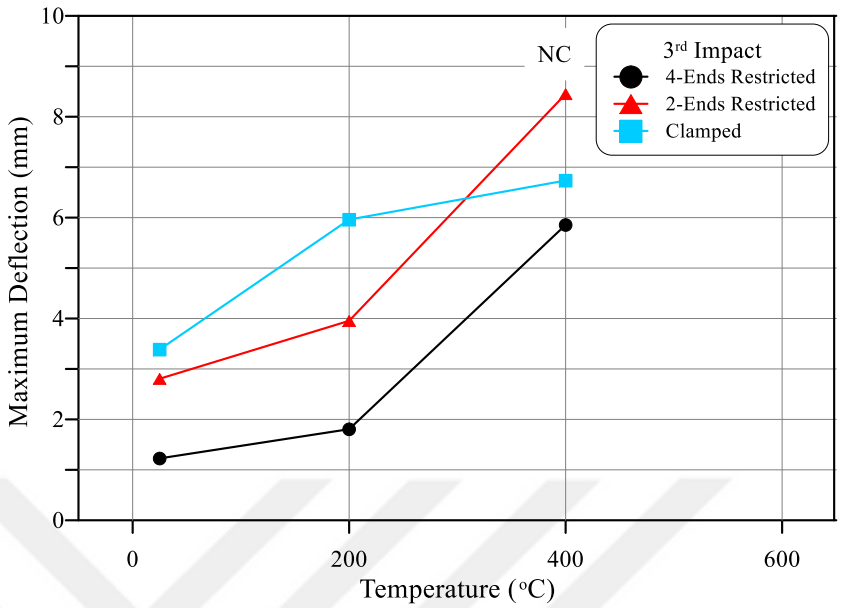

Figure 5.34. NC maximum deflections-temperature relations for different boundary cases at third impact.

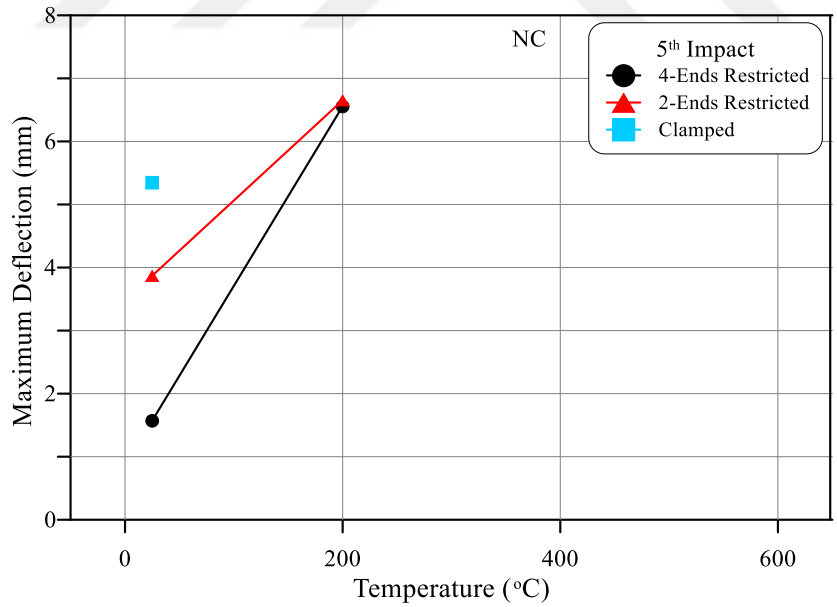

Figure 5.35. NC maximum deflections-temperature relations for different boundary cases at the fifth impact.

As discussed earlier, exposing the plate specimens to high temperatures causes permanent microstructural effects due to a combination of physical and chemical changes that

deteriorate the sectional stiffness. The degree of deterioration develops with exposing the plates to higher temperature levels, which led to the recorded continuous increase of deflection with temperature increase. The variation of deflection with temperature of ECC specimens followed a very similar trend to that discussed for NC specimens. In general, deflection increases with temperature increase regardless of the number of impact blows (first, third, or fifth), and the deflection difference between 200 and 400 °C is smaller than between other temperatures.

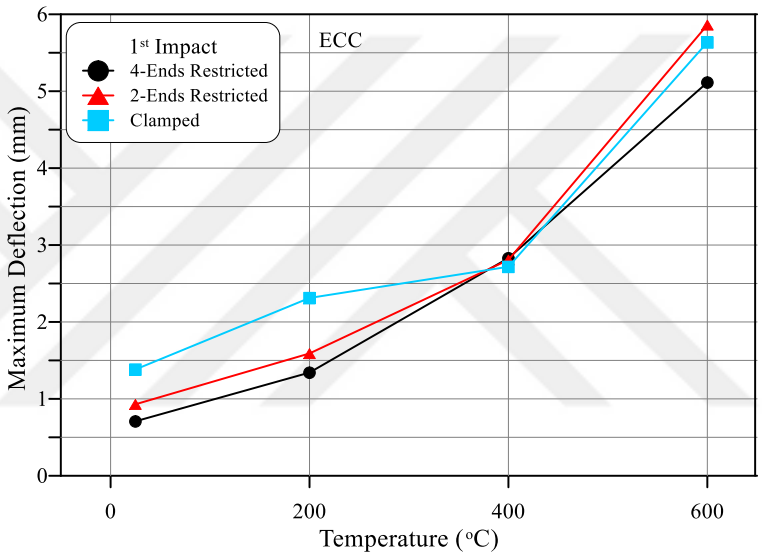

Figure 5.36. ECC maximum deflections-temperature relations for different boundary cases at first impact.

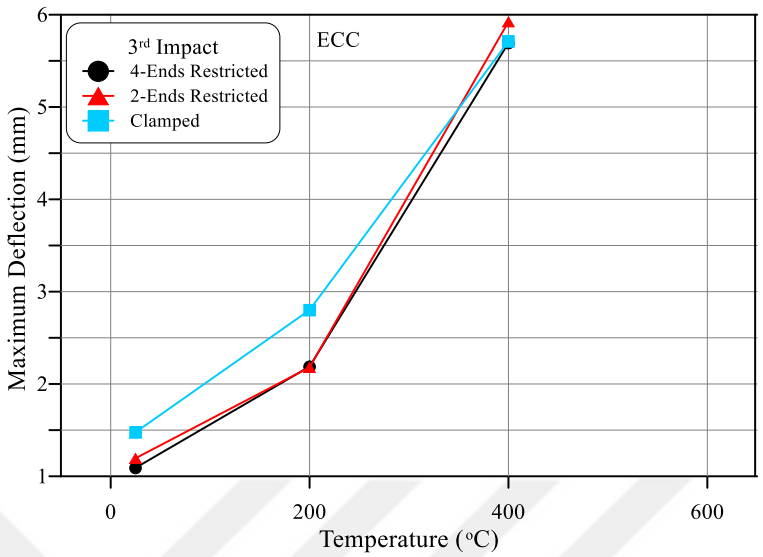

Figure 5.37. ECC maximum deflections-temperature relations for different boundary cases at third impact.

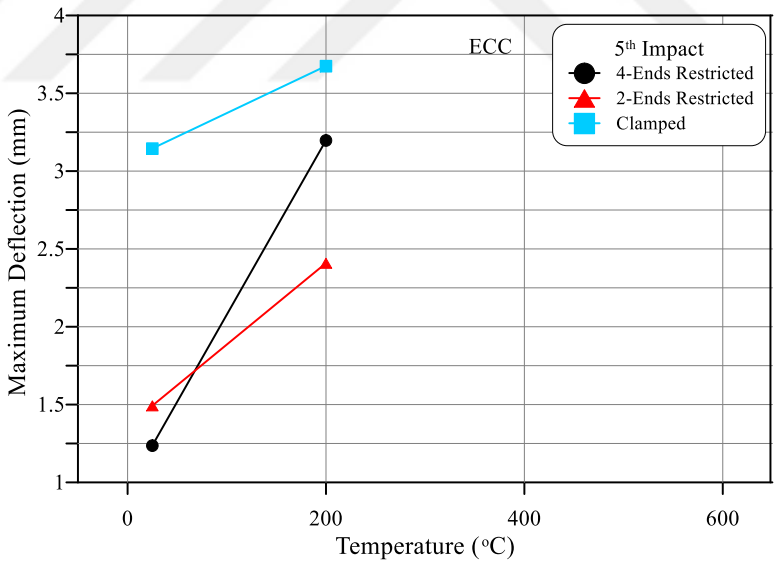

Figure 5.38. ECC maximum deflections-temperature relations for different boundary cases at the fifth impact.

5.6 Cracking and Failure Patterns

Figures 5.39 to 5.50 present pictures for all tested specimens before testing to visualize the effect of heating, and for the top and bottom surfaces after failure. Comparing

subfigure (a) from Figures 5.39 to 5.50, it can be seen that there are no obvious surface effects of temperature on NC specimens subjected to 200 ℃ However, a close observation of these plates revealed the presence of very few and very tiny surface thermal cracking that reflects the vaporization of free water from matrix voids and cement gel pores and its induced shrinkage.

The surface thermal cracks were slightly more obvious for specimens exposed to 400 °C, while an obvious cracking can be clearly observed on the surface of NC specimens subjected to 600 °C. This cracking is due to the dramatic chemical changes and the breakage of bonds between cement paste and aggregate particles that occur after exposure to approximately 400 °C. (Varona, et al., 2020; Amin & Khan, 2020)

The decomposition of calcium silicate hydrates after 450°C deteriorates the microstructure extremely (Arna'ot et al. 2017a; Chu et al., 2016), which leads to a noticeable surface cracking after exposure to 600 °C.

(a) (b) (c)

Figure 5.39. Pictures of NC four-ends restricted unheated reference plate (a) before testing (b) top surface after testing (c) bottom surface after testing.

(a) (b) (c)

Figure 5.40. Pictures of NC four-ends restricted plate heated to 200 °C (a) before testing (b) top surface after testing (c) bottom surface after testing.

(a) (b) (c)

Figure 5.15. Pictures of NC four-ends restricted plate heated to 400 °C (a) before testing (b) top surface after testing (c) bottom surface after testing.

(a) (b) (c)

Figure 5.42. Pictures of NC four-ends restricted plate heated to 600 °C (a) before testing (b) top surface after testing (c) bottom surface after testing.

(a) (b) (c)

Figure 5.16. Pictures of NC two-ends restricted unheated reference plate (a) before testing (b) top surface after testing (c) bottom surface after testing.

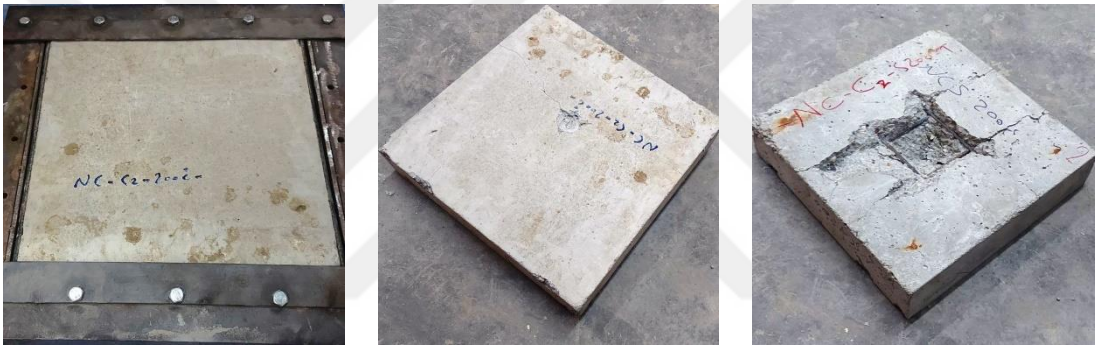

(a) (b) (c)

Figure 5.44. Pictures of NC two-ends restricted plate heated to 200 °C (a) before testing (b) top surface after testing (c) bottom surface after testing.

(a) (b) (c)

Figure 5.45. Pictures of NC two-ends restricted plate heated to 400 °C (a) before testing (b) top surface after testing (c) bottom surface after testing.

(a) (b) (c)

Figure 5.46. Pictures of NC two-ends restricted plate heated to 600 °C (a) before testing (b) top surface after testing (c) bottom surface after testing.

(a) (b) (c)

Figure 5.47. Pictures of NC clamped unheated reference plate (a) before testing (b) top surface after testing (c) bottom surface after testing.

(a) (b) (c)

Figure 5.48. Pictures of NC clamped plate heated to 200 °C (a) before testing (b) top surface after testing (c) bottom surface after testing.

(b) (b) (c)

Figure 5.49. Pictures of NC clamped plate heated to 400 °C (a) before testing (b) top surface after testing (c) bottom surface after testing.

(a) (b) (c)

Figure 5.50. Pictures of NC clamped plate heated to 600 °C (a) before testing (b) top surface after testing (c) bottom surface after testing.

The same subfigures for ECC specimens (Figures 5.51 to 5.62) show a similar cracking trend to that recorded for NC specimens. However, the effect of exposure to 400 and 600 °C can be said to be more severe in ECC specimens, where the surface cracking was more obvious than in NC specimens. This might be attributed to the denser microstructure of ECC due to the considerably higher amounts of fine materials. As a result, the dissipation of water vapor pressure from gel pores before 200 °C becomes more difficult compared to NC specimens, which induces larger thermal stresses within the microstructure causing more obvious cracking after heating to higher temperatures.

Sahmaran. et.al., (2010) reported that the porosity of ECC specimens exposed to 400 °C increased by 5%, while after exposure to 600 °C, the porosity increased by 9% and the pore size increased by 300%.

As clarified in Chapter 3, the load is subjected to the top surface of test plates via a steel ball impactor. Therefore, the central point of all NC and ECC specimens is fractured showing the concentrated compressive stress effect of the falling ball as shown in subfigures (b) of Figures 5.39 to 5.62. The central fracture zone is accompanied in most cases by two or more diagonal cracks on the top surface that reflect the spread of the impact wave effect along all directions.

The major effect of impact loads is transferred as flexural tensile stresses that are dissipated over the bottom surface in forms of deflection and cracking as shown in subfigures (c) of Figures 5.39 to 5.62. The bottom surface cracking increased with the increase of impact blows number and was concentrated on the central surface area, then spread towards the corners and edges.

The specimens heated to higher levels of temperature revealed more severe cracking, where the effect of flexural stresses propagated and widened the already existing thermal cracks and initiated more cracking baths through the deteriorated media. This behavior is most clear after exposure to 600 °C in Figure 5.46 for NC plates and Figure 5.58 for ECC plates.

Generally, the impact force decreased and deflection increased with the increase of temperature for both NC and ECC plates. NC plates exhibited an increase in impact strength with the increase of end fixity, while no specific trend was recognized for ECC plates with end conditions.

(a) (b) (c)

Figure 5.51. Pictures of ECC four-ends restricted unheated reference plate (a) before testing (b) top surface after testing (c) bottom surface after testing.

(a) (b) (c)

Figure 5.52. Pictures of ECC four-ends restricted plate heated to 200 °C (a) before testing (b) top surface after testing (c) bottom surface after testing.

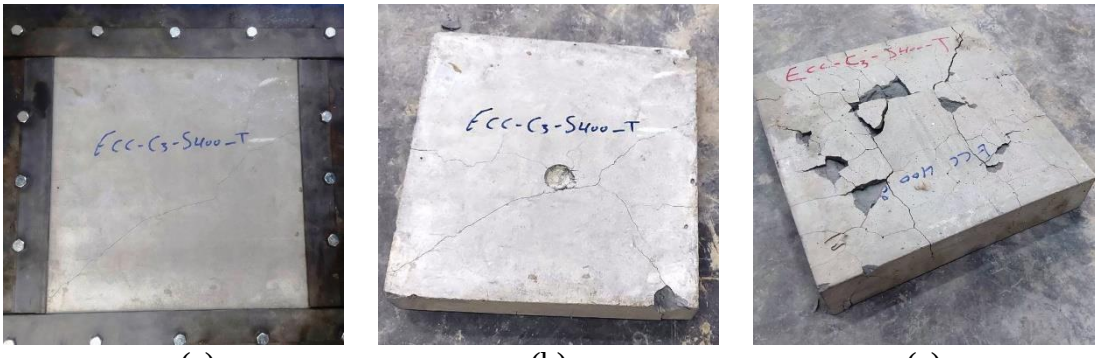

(a) (b) (c)

Figure 5.53. Pictures of ECC four-ends restricted plate heated to 400 °C (a) before testing (b) top surface after testing (c) bottom surface after testing.

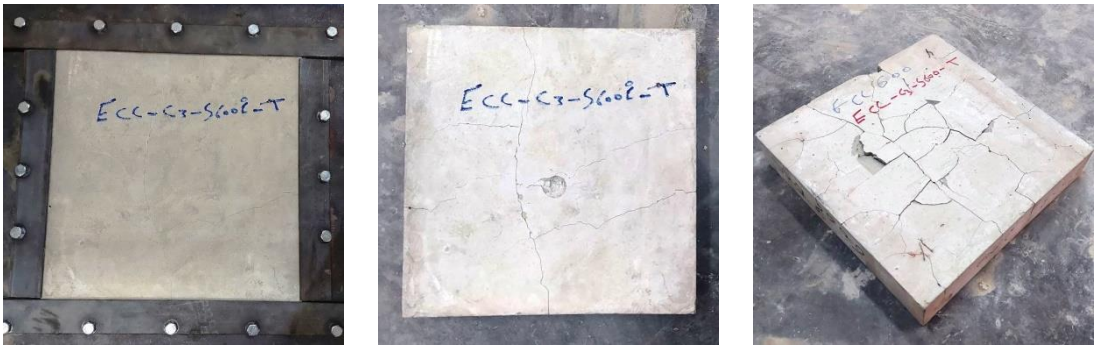

(a) (b) (c)

Figure 5.54. Pictures of ECC four-ends restricted plate heated to 600 °C (a) before testing (b) top surface after testing (c) bottom surface after testing.

(a) (b) (c)

Figure 5.55. Pictures of ECC two-ends restricted unheated reference plate (a) before testing (b) top surface after testing (c) bottom surface after testing.

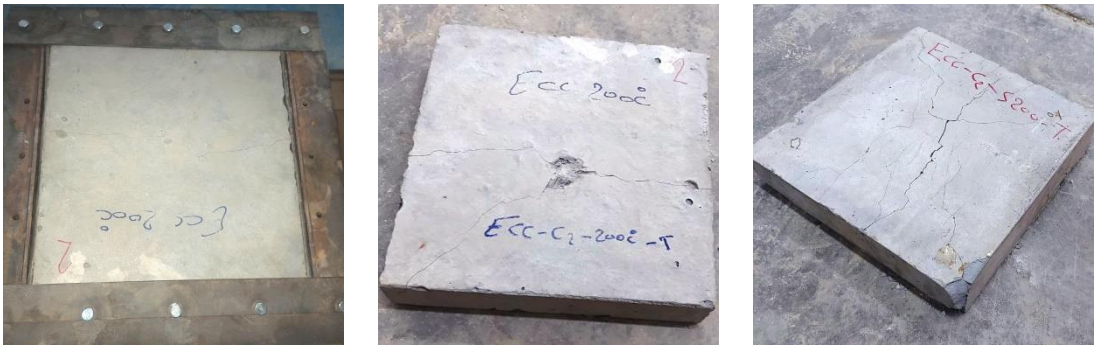

(a) (b) (c)

Figure 5.56. Pictures of ECC two-ends restricted plate heated to 200 °C (a) before testing (b) top surface after testing (c) bottom surface after testing.

(a) (b) (c)

Figure 5.57 Pictures of ECC two-ends restricted plate heated to 400 °C (a) before testing (b) top surface after testing (c) bottom surface after testing.

(a) (b) (c)

Figure 5.58. Pictures of ECC two-ends restricted plate heated to 600 °C (a) before testing (b) top surface after testing (c) bottom surface after testing.

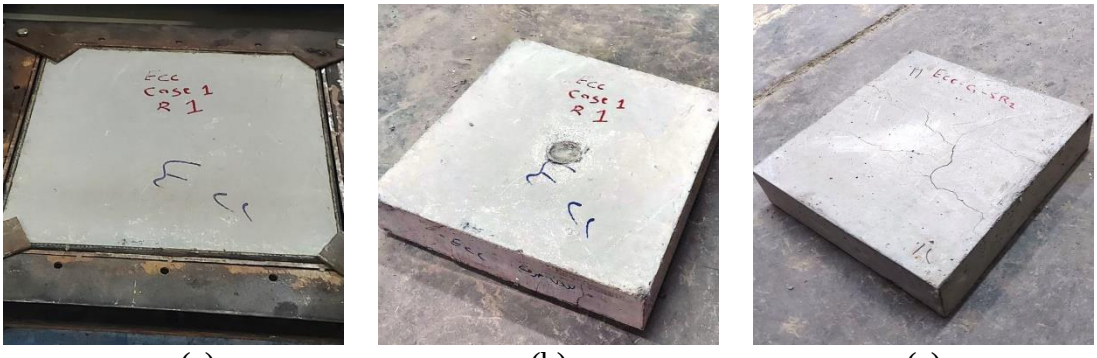

(a) (b) (c)

Figure 5.59. Pictures of ECC clamped unheated reference plate (a) before testing (b) top surface after testing (c) bottom surface after testing.

(a) (b) (c)

Figure 5.60. Pictures of ECC clamped plate heated to 200 °C (a) before testing (b) top surface after testing (c) bottom surface after testing.

(a) (b) (c)

Figure 5.61 Pictures of ECC clamped plate heated to 400 °C (a) before testing (b) top surface after testing (c) bottom surface after testing.

(a) (b) (c)

Figure 5.62. Pictures of ECC clamped plate heated to 600 °C (a) before testing (b) top surface after testing (c) bottom surface after testing.

CHAPTER SIX

STATISTICAL EVALUATION OF TEST RESULTS

6.1 General

Test developers and users can utilize the information provided by statistical analysis of test results to support the general validity argument that establishes a connection between score interpretations and performance observations on language assessments. The statistical studies are conducting on experimental data to determine the effective factor on impact test and also proposed prediction modules as shown in Table 6.1 to Table 6.4.

Table 6.1. The n_{cr} results of the six NC specimen replications with statistical measurements.

Disk No.	R	100	200	300	400	500	600
1	52	28	18	8	4	2	1
2	41	76	25	7	2	2	1
3	78	41	11	6	4	2	1
4	50	90	9	7	3	3	1
5	51	39	9	4	2	1	1
6	58	48	13	7	3	3	1
SD	55.0	53.7	14.2	6.5	3.0	2.2	1.0
n_{cr}	12.5	24.0	6.3	1.4	0.9	0.8	0.0
COV %	22.8	44.8	44.3	21.2	29.8	34.7	0.0

Table 6.2. The n_f results of the six NC specimen replications with statistical measurements.

Disk No.	R	100	200	300	400	500	600
1	53	29	19	9	5	3	2
2	42	78	26	8	3	3	3
3	81	43	12	7	5	3	2
4	53	91	10	8	4	4	2
5	54	41	10	5	3	2	2
6	60	49	14	8	4	3	2
SD	57.2	55.2	15.2	7.5	4.0	3.0	2.2
n_f	13.0	24.0	6.3	1.4	0.9	0.6	0.4
COV %	22.8	43.5	41.4	18.4	22.4	21.1	18.8

Table 6.3. Ncr results of the six ECC specimen replications with statistical measurements.

Disk No.	R	100	200	300	400	500	600
1	26	49	32	31	16	6	12
2	34	74	29	17	14	6	14
3	36	72	69	20	19	9	8
4	40	25	33	35	23	16	3
5	46	41	47	40	15	12	7
6	78	45	39	13	30	13	9
SD	43.3	51.0	41.5	26.0	19.5	10.3	8.8
n_{cr}	18.2	18.9	14.9	10.8	6.1	4.0	3.9
COV %	42.1	37.1	35.9	41.7	31.2	39.0	43.8

Table 6.4. The n_f results of the six ECC specimen replications with statistical measurements.

Disk No.	R	100	200	300	400	500	600
1	232	292	310	51	18	7	13
2	177	477	432	22	14	8	15
3	301	337	229	36	28	10	9
4	185	356	203	48	31	17	4
5	276	233	154	71	20	14	8
6	385	183	212	40	33	14	10
SD	259.3	313.0	256.7	44.7	24.0	11.7	9.8
n_f	78.6	103.0	99.8	16.5	7.7	3.9	3.9
COV %	30.3	32.9	38.9	36.9	32.2	33.7	39.3

6.2 Variation of n_{cr} and n_f records

The coefficient of variation (COV) is a reliable measurement to evaluate the variation of small sample data as in the case of this work, where the averages were considered based on six experimental records for each result.

As disclosed in the previous sections, the ACI 544-2R repeated impact test is known for the high variation of the obtained impact results. Figure 6.1 shows the effect of high-temperature exposure on the variation of the cracking and failure impact numbers of NC disk specimens in terms of the coefficient of variation (COV). It is clear in the figure that the COV was not so high (22.8) at ambient temperature, which is good enough when compared to the typical expected COV values as addressed in the literature.

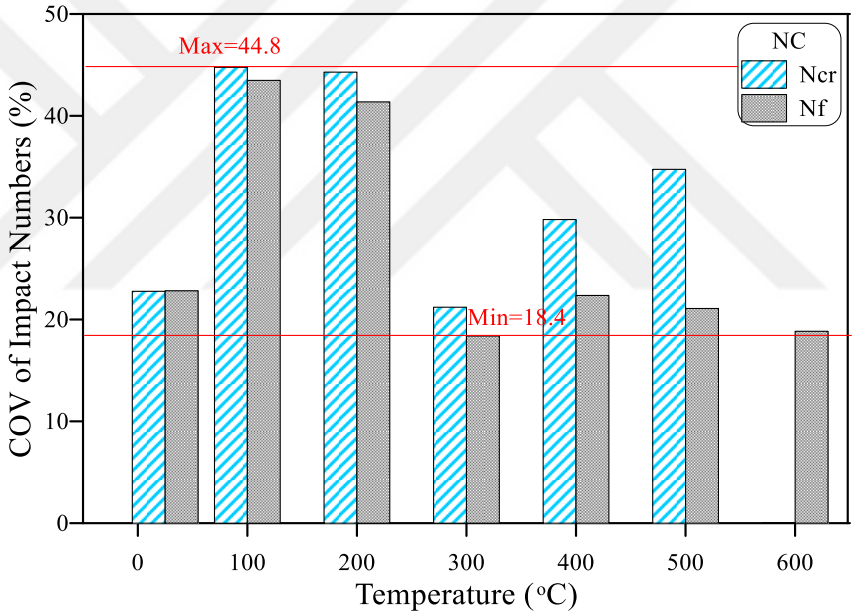

Figure 6.1. COV of cracking and failure impact numbers of NC specimens.

The COV increased at 100 and 200 °C recording values in the range of 41.4 and 44.8% for both the cracking and failure numbers. This increase in the variation of the results can be attributed to the dramatic behaviors at these temperatures. Where at 100 °C, the specimens exhibited an increase and decrease in strength compared to those tested at ambient temperature as listed in Table 6.4. Similarly, the high drop in the impact number records at 200 °C resulted in high percentage variations although of the limited numeral variations. The extremely low records of impact numbers at the higher

temperatures reduced the differences between the tested specimens, which in turn reduced the COV as shown in Figure 6.1.

The differences between the COV of ECC were smaller when compared to those of NC, where as shown in Figure 6.2, the range of the COV of n_{cr} and n_f at all temperatures was 30.3 to 43.8%. However, as in the case of NC, it is also shown in the figure that the lowest COV was recorded for the unheated specimens. On the other hand, the COV was not reduced at the high temperature (above 200 °C) compared to the lower temperatures as in the case of NC, which is also attributed to the same reason. NC retained a very small number of impacts before cracking and failure when exposed to high temperatures, while ECC could withstand longer and carried much higher impact blows compared to NC at these high temperatures as listed in Tables 6.1 through 6.4. As a result, the scattering of results was not noticeably affected by the reduced impact strength as for NC.

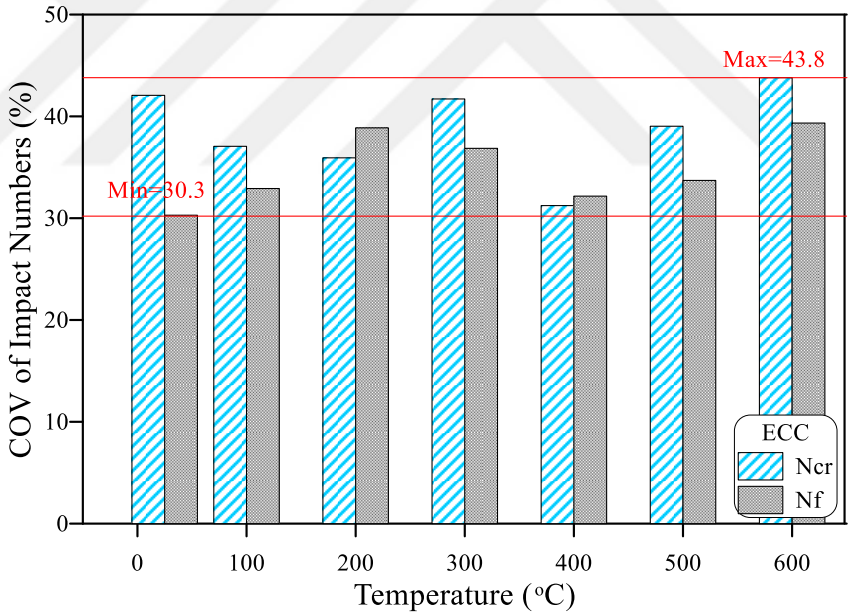

Figure 6.2. COV of cracking and failure impact numbers of ECC specimens.

6.3 Normality Test

The normality test was used here to evaluate the appeal of n_{cr} and n_f results to follow a normal distribution.

6.4 Weibull Distribution

At first, the probabilistic methods were used to provide a rationale for the scattering of fracture strength results with brittleness in nature. This statistical method is most widely used in the statistical variability of impact test results in recent times. Barbero et al. (2000) investigated the mechanical properties of composite materials using the Weibull distribution. The authors recommended that the Weibull distribution is a pragmatic approach for determining 90 and 95% reliability values. The Weibull distribution is accentuated by two parameters, namely shape, and scale, and these parameters can be evaluated by several methods. The scattering of failure impact number of concretes was modeled using a two-parameter Weibull distribution. Lastly, the reliability of concrete in terms of failure impact number was presented in graphical form. The scattering of cracking impact numbers was minor and hence was not modeled using Weibull distribution.

6.4.1 Mean standard deviation method (MSDM)

This method is more useful when mean and standard deviations are known; if this occurs, the shape parameter (α) and scale parameter (β) are determined using the Equations (6.1) and (6.2) as follows (Mohammadi, 2016).

$$\alpha = \left(\frac{\sigma}{\bar{R}}\right)^{-1.086} \qquad (6.1)$$

$$\beta = \frac{\bar{R}\,\alpha^{2.6674}}{0.184+0.816\,\alpha^{2.73855}} \qquad (6.2)$$

Where; $\bar{R}$ is the mean of failure impact number, σ is the standard deviation.

6.4.2 Energy pattern factor method (EPFM)

The EPF is defined by the ratio of the summation of cubes of individual failure impact number to the cube of mean failure impact number. The scale and shape parameters are calculated using Equations (6.3) and (6.4) once the EPF value is known (Akdağ & Dinler, 2009).

$$EPF = \frac{\overline{R^3}}{\bar{R}^3} \qquad (6.3)$$

$$\alpha = 1 + \frac{3.69}{(Epf)^2} \qquad (6.4)$$

The gamma function is defined in Equation (6.5) expressed as follows.

$$\Gamma(x) = \int_0^\infty t^{x-1} \exp(-t)\, dt \qquad (6.5)$$

6.4.3 Method of moments (MOM)

Numerical iteration is involved in this method, and the mean failure impact number and corresponding standard deviation (σ) are used to find shape and scale parameters.

$$\alpha = \left(\frac{0.9874}{\frac{\sigma}{\bar{R}}}\right)^{-1.086} \qquad (6.6)$$

$$\bar{R} = \beta\Gamma\,(1 + 1/\alpha) \qquad (6.7)$$

Table 6.5 demonstrates the results of Weibull parameters of NC obtained from three methods of distribution. It is clear from the table the MSDM and MOM showed approximately the same parameter value. However, EPFM showed a lower value compared to MSDM and MOM. To perform the reliability analysis, the mean value of the three methods was used. The reliability of concrete exposed to various temperatures in terms of failure impact number can be calculated using Equation (6.8).

$$R = \beta(-\ln(R_x)^{(1/\alpha)} \qquad 6.8)$$

Where R_x is the reliability level and R is the failure impact number.

Table 6.5. Results of Weibull parameters for NC.

Temperature (°C)	MSDM		EPFM		MOM		Mean	
	α	β	α	β	α	β	α	β
R	5.00	62.34	3.96	63.15	5.02	62.29	4.66	62.59
100	2.47	62.25	2.80	61.99	2.46	62.24	2.58	62.16
200	2.60	17.12	2.88	17.05	2.59	17.12	2.69	17.10
300	6.19	8.06	4.23	8.25	6.23	8.07	5.55	8.13
400	5.05	4.36	4.01	4.41	5.08	4.35	4.71	4.37
500	5.74	3.24	4.08	3.31	5.78	3.24	5.20	3.26
600	6.37	2.36	4.40	2.41	6.41	2.36	5.73	2.38

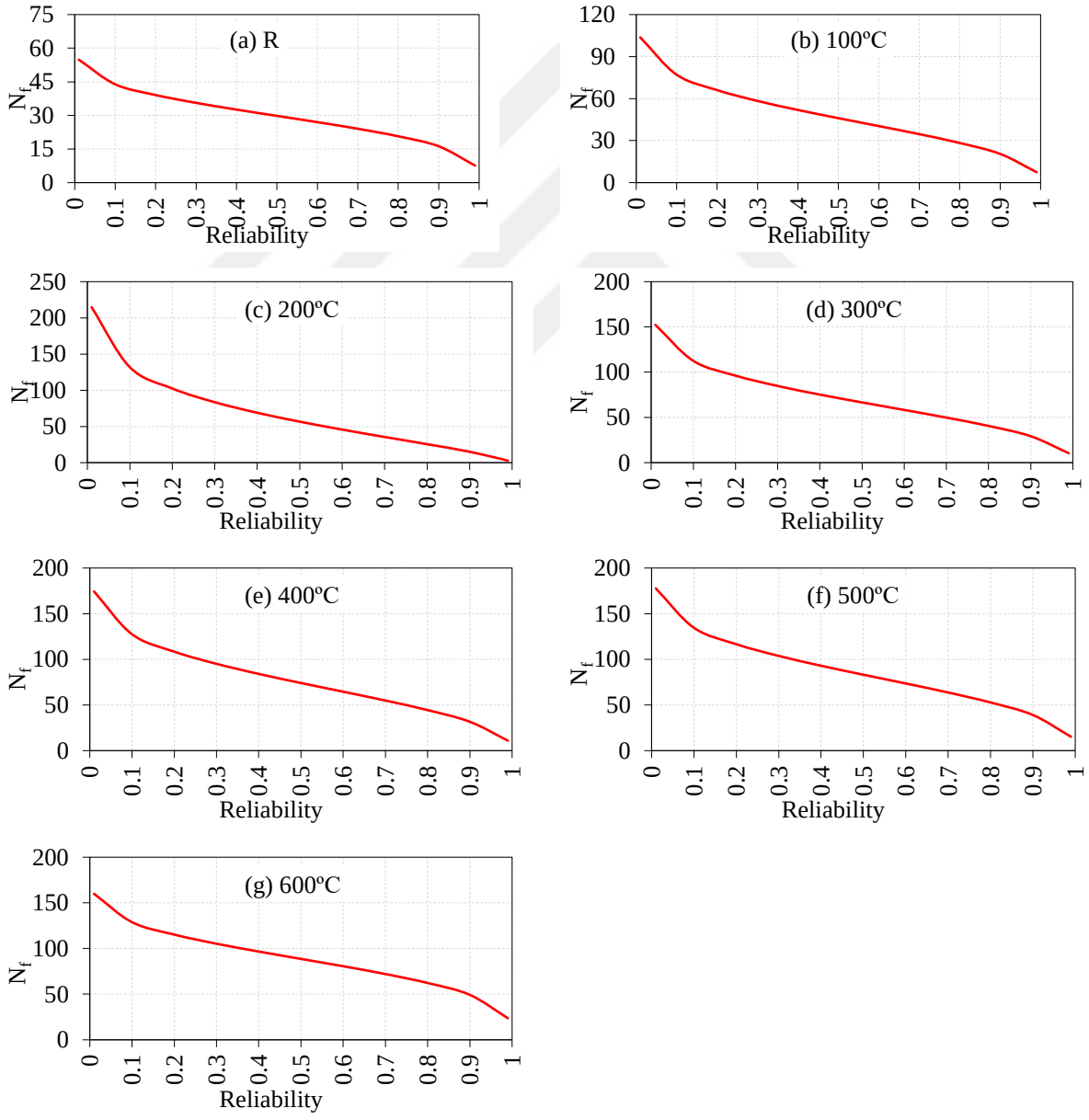

Figure 6.3. Failure impact numbers in terms of reliability of NC.

Using the Weibull parameters, the reliability analysis was performed to estimate the failure impact number. Figure 6.3 illustrates the failure impact number in terms of reliability or survival of probability. By examining 0.99, 0.9, 0.8, 0.7, and 0.6 reliability, the corresponding failure impact number values for the R mixture type concrete were 8, 16, 21, 24, and 27, respectively. When the concrete was exposed to 100 ºC, the failure impact number values were 7, 21, 28, 35, and 40 corresponding to 0.99, 0.9, 0.8, 0.7, and 0.6 reliability, respectively. Likewise, the failure impact number for the concrete exposed to different temperatures can be obtained from Figure 6.3. Using the reliability curves, the design engineer can have the option to choose the required failure impact number at the desired reliability. These values can be used effectively in the design calculations, and the Weibull distribution can be considered a powerful tool to examine an impact strength result scattering.

6.5 Correlations Amongst Impact Numbers, Compressive and Flexural Strengths

In this section, the effect of compressive strength and flexural strength response with temperature on the thermal response of n_{cr} and n_f is evaluated using two approaches. The first is by normalizing n_{cr} and n_f records by compressive strength, while the second is by evaluating the statistically simple correlations between n_{cr} and n_f of NC and ECC with their corresponding Fc and Fr records.

CHAPTER SEVEN

CONCLUSION AND RECOMMENDATIONS

7.1 Conclusions

Within the limits of the investigated parameters, the following concluding remarks can be drawn for the obtained results of the tested plates.

1- Owing to the thermal degradation of stiffness and surface hardness of plates subjected to high temperatures, the major part of the subjected impact energy from the falling weight was dissipated as local deformations, which resulted in shorter-period oscillations of recorded force-time variation compared to reference plates. A small-time lag of less than 3 ms was generally recorded between the times of maximum force and maximum deflection of each tested plate.

2- Owing to its more consistent matrix, the large amount of fine and cementitious materials, and the presence of PP fibers that boost its tensile strength and overall stiffness compared to their corresponding NC plates, reference unheated ECC plates could withstand much higher numbers of impact blows before failure (N_f). ECC plates retained 33 to 34 impact blows, while NC plates recorded a range of 8 to 13 blows. The retained n_f records of ECC plates were 253 to 425% higher than their corresponding NC plates.

3- Regardless of the boundary condition case, the retained N_f decreased as temperature increased for both NC and ECC plates. However, ECC plates exhibited a more severe decay as compared with corresponding NC plates. N_f records of NC plates decreased by approximately 50 to 62%, 50 to 77%, and 75 to 90% after exposure to 200, 400, and 600C^0

The more severe degradation of ECC after exposure to high temperatures compared to NC can be attributed to the denser matrix that restricts the dissipation of water vapor, which results in higher internal pressure. In addition, the melting of PP fibers further weakens the matrix and deteriorates its stiffness and tensile strength.

4- For NC reference plates, n_f increased with the increase of end fixity degree, where it increased from 8 for clamped cases to 10 and 13 for two-end restrained and four-end restrained cases, respectively. On the other hand, no such trend was recorded for reference ECC plates and heated NC and ECC plates.

5- Despite minor record fluctuations, the general trend of impact force reveals a continuous decrease as the number of impact blows increases for NC and ECC plates regardless of boundary case or exposure temperature. Oppositely, the deflection of all specimens exhibited a trend of increase with the increase of impact blows number. The decrease in impact force and increase of deflection is attributed to the gradual degradation of material microstructure under the effects of impact-induced compressive and tensile stresses, which lower the stiffness and lead to less absorbed and more dissipated impact energy after each additional impact blow.

6- Three stages can be recognized from the maximum impact force-temperature relations of NC specimens. Firstly, the maximum force dropped significantly after exposure to 200 °C, then a semi-stabilization stage with a small decrease or increase was recorded from 200 to 400 °C. Finally, a third stage of effective drop of impact force was recorded from 400 to 600 °C, ECC plates showed a similar behavior but with a more recognized slight increase of impact force from 200 to 400 °C ,For ECC the plates exposed to 200, 400, and 600 °C retained residual impact forces of 45.5 to 49.8%, 57.7 to 60.3%, and 6.3 to 7.8%, respectively. The behavior of impact force with temperature is directly attributed to the microstructural hygrothermal effects due to the chemical and physical changes that occur in the cementitious matrix and between this matrix and filler particles after exposure to the three levels of temperature.

7- Due to its better ability to reduce end rotation, the four-ends restriction case revealed the highest impact force records and lowest deflection records for reference NC and ECC plates followed by the two-ends restriction case, while the lowest impact forces and highest deflections were recorded for the clamped case that represents the weakest end restriction case. This behavior was not always recorded for specimens subjected to high temperatures, which might be due to the early fracture of restricted corners of some plate edges owing to thermal-induced material degradation.

7.2 Recommendations

On the basis of the aforementioned conclusions and within the parameters examined in this study, the following titles may be proposed as future research endeavors:

1. Experimental or numerical research on behavior of slab concrete including different types of fiber under cyclic load and impact loading.
2. Experimental or numerical research on behavior of slab concrete uses full - scale specimens.
3. Study the fire performed of slab -columns connection under repeated impact load.
4. Experimental study the durability of impact properties of ECC with low-cost fibers under thermal effect by protection the specimens by fire resistance coating.

REFERENCES

Abbass, A. A., Abid, S. R., Arna'ot, F. H., Al-Ameri, R. A., & Özakça, M. (2020). Flexural response of hollow high strength concrete beams considering different size reductions. Structures, 23, 69–86.

Abbas, A. A., Arna'Ot, F. H., Abid, S. R., & Özakça, M. (2021). Flexural behavior of ECC hollow beams incorporating different synthetic fibers. *Frontiers of Structural and Civil Engineering*, *15*(2), 399–411.

Abid, S. R., Abdul-Hussein, M. L., Ayoob, N. S., Ali, S. H., & Kadhum, A. L. (2020a). Repeated drop-weight impact tests on self-compacting concrete reinforced with micro-steel fiber. *Heliyon*, *6*(1).

Abid, S. R., Hussein, M. L. A., Ali, S. H., & Ala'a, F. K. (2020b). Suggested modified testing techniques to the ACI 544-R repeated drop-weight impact test. *Construction and Building Materials*, 244, 118321.

Abid, S., Ali, S., Goaiz, H., Al-Gasham, T., & Kadhim, A. (2021a). Impact resistance of steel fiber-reinforced self-compacting concrete. *Magazine of Civil Engineering*, 105(5), 10504.

Abid, S. R., Gunasekaran, M., Ali, S. H., Kadhum, A. L., Al-Gasham, T. S., Fediuk, R., Vatin, N., & Karelina, M. (2021b). Impact performance of steel fiber-reinforced self-compacting concrete against repeated drop weight impact. *Crystals*, *11*(2), 91.

Abrams, M. S. (1971). Compressive strength of concrete at temperatures to 1600F. *ACI Symposium Publication,*, *25*, 33–58.

ACI 544.2 R-89, (1999). *Measurement of properties of fiber reinforced concrete*. Reported by ACI Committee, 544.

ACI 544.1 R-96, (2009). *Report on fiber reinforced concrete* (Reapproved 2009). American Concrete Institute

ACI 318-14, (2014). *Building Code Requirements for Structural Concrete* (ACI 318M-14) and Commentary. American Concrete Institute, Farmington Hills, MI

ACI. 544.4-18, (2018). *Guide to Design with Fiber-Reinforced Concrete*. American Concrete Institute: Farmington Hills, MI, USA

AFGC-SETRA (2002) *Ultra High-Performance Fibre-Reinforced Concretes*, Interim recommendations. AFGC Publication, France

Akdağ, S. A., & Dinler, A. (2009). A new method to estimate Weibull parameters for wind energy applications. *Energy conversion and management*, *50*(7), 1761-1766.

Alimrani, N. S., & Balazs, G. L. (2020). Investigations of direct shear of one-year old SFRC after exposed to elevated temperatures. *Construction and Building Materials*, 254, 119308

Al-Ameri, R. A., Abid, S. R., Murali, G., Ali, S. H., & Özakça, M. (2021a). Residual repeated impact strength of concrete exposed to elevated temperatures. *Crystals*, *11*(8), 941.

Al-Ameri, R. A., Abid, S. R., & Özakça, M. (2021b). Mechanical and impact properties of engineered cementitious composites reinforced with PP fibers at elevated temperatures. *Fire*, *5*(1), 3.

Al-Ameri, R. A., Abid, S. R., Murali, G., Ali, S. H., Özakça, M., & Vatin, N. I. (2022). Residual impact performance of ECC subjected to sub-high temperatures. *Materials*, *15*(2), 454.

Albrektsson, J., Flansbjer, M., Lindqvist, J.-E., & Jansson, R. (2011). *Assessment of concrete structures after fire*. SP Report 2011:19, SP Technical Research Institute of Sweden

Alimrani, N. S., & Balazs, G. L. (2020). Investigations of direct shear of one-year old SFRC after exposed to elevated temperatures. *Construction and Building Materials*, *254*, 119308.

Al-Owaisy, S. R. (2006). Post Heat Exposure Properties of Steel Fiber Reinforced Concrete. *Journal of Engineering and Sustainable Development*, *10*(2), 194–207.

Al-Owaisy, S. R. (2007). Effect of high temperatures on shear transfer strength of concrete. *Journal of Engineering and Sustainable Development*, *11*(1), 92–103.

Amin, M. N., & Khan, K. (2020). Mechanical performance of high-strength sustainable concrete under fire incorporating locally available volcanic ash in central Harrat Rahat, Saudi Arabia. *Materials*, *14*(1), 21.

Anto J, Bhuvaneshwari M. A (2022). Comprehensive Summary on the Enhancement of Characteristics of Reinforced Concrete by Employing Polypropylene Materials, available at *Research Square* [https://doi.org/10.21203/rs.3.rs-1498888/v1]

Arna'ot, F. H., Abbass, A. A., Abualtemen, A. A., Abid, S. R., & Özakça, M. (2017a). Residual strength of high strength concentric column-SFRC flat plate exposed to high temperatures. *Construction and Building Materials*, *154*, 204–218.

Arna'ot, F. H., Abid, S. R., Özakça, M., & Tayşi, N. (2017b). Review of concrete flat plate-column assemblies under fire conditions. *Fire Safety Journal*, *93*, 39–52.

Ayoob, N. S., & Abid, S. R. (2020). Analysis of abrasion rates in concrete surfaces of hydraulic structures. *IOP Conference Series: Materials Science and Engineering*, *888*(1), 012052.

Babalola, O. E., Awoyera, P. O., Le, D.-H., & Romero, L. M. B. (2021). A review of residual strength properties of normal and high strength concrete exposed to elevated temperatures: Impact of materials modification on behaviour of concrete composite. *Construction and Building Materials*, *296*, 123448.

Badr, A., & Ashour, A. (2005). Modified ACI Drop-Weight Impact Test for Concrete. *ACI Mater. J.* 102, 249–255

Badr, A., Ashour, A. F., & Platten, A. K. (2006). Statistical variations in impact resistance of polypropylene fibre-reinforced concrete. *International Journal of Impact Engineering*, *32*(11), 1907–1920.

Baer, W., Wossidlo, P., & Abbasi, B. (2022). On the question of how to analyze and apply Charpy pendulum impact test results correctly-shortcomings in corresponding procedures and standards. *Journal of testing and evaluation*, 50(4), 2268-2293

Balaguru, P. N., & Shah, S. P. (1992). *Fiber-reinforced cement composites*. McGraw- Hill Inc, New York.

Bangash, M. Y. H., & Bangash, T. (2005). *Explosion-resistant buildings: design, analysis, and case studies*. Springer Science & Business Media.

Bangash, M. Y. H. (2009). *Shock, impact and explosion: structural analysis and design.* Berlin: Springer

Barbero, E., Fernández-Sáez, J., & Navarro, C. (2000). Statistical analysis of the mechanical properties of composite materials. *Composites Part B: Engineering*, *31*(5), 375–381.

Bažant, Z. P., & Prat, P. C. (1988). Microplane model for brittle-plastic material: I. Theory. *Journal of Engineering Mechanics*, *114*(10), 1672–1688.

Bažant, Z. P. & Kaplan, M. F. (1996). *Concrete at high temperatures: material properties and mathematical models*. Longman.

Bažant, Z. P., & Zhou, Y. (2002). Why did the world trade center collapse?—Simple analysis. *Journal of Engineering Mechanics*, *128*(1), 2–6.

Bažant, Z. P., & Kaplan, M. F. (2018). Concrete at high temperatures: material properties and mathematical models. (No Title).

Behera, M., Bhattacharyya, S. K., Minocha, A. K., Deoliya, R., & Maiti, S. (2014). Recycled aggregate from C&D waste & its use in concrete–A breakthrough towards sustainability in construction sector: A review. *Construction and Building Materials*, *68*, 501–516.

Bhat, P. S., Chang, V., & Li, M. (2014). Effect of elevated temperature on strain-hardening engineered cementitious composites. *Construction and Building Materials*, *69*, 370–380.

Bischoff, P. H., & Perry, S. H. (1991). Compressive behaviour of concrete at high strain rates. *Materials and Structures*, *24*, 425–450.

Bosnjak, J. (2014). *Explosive spalling and permeability of high performance concrete under fire: numerical and experimental investigations*. Ph.D. thesis, Institut für Werkstoffe im Bauwesen der Universität Stuttgart

Brushlinsky, N. N., Ahrens, M., Sokolov, S. V., & Wagner, P. (2018). World fire statistics, Center of Fire Statistics of CTIF. *Int. Assoc. Fire Rescue Serv*, 21(11).

BS EN 12390-3. (2009). Testing hardened concrete. Compressive strength of test specimens. *British Standard Institution*

BS EN 12390-5. (2009). Testing hardened concrete–Part 5: flexural strength of test specimens. *British standards institution and CEN European committee for standardization*

Buchanan, A. H., & Abu, A. K. (2017). *Structural design for fire safety*. John Wiley & Sons

Çavdar, A. (2012). A study on the effects of high temperature on mechanical properties of fiber reinforced cementitious composites. *Composites Part B: Engineering*, *43*(5), 2452–2463.

CEN, EN 14889-2. (2006) *Fibres for concrete—part 2: polymer fibres—definitions, specifications, and conformity*. European Committee for Standardization.

Chen, L., Fang, Q., Jiang, X., Ruan, Z., & Hong, J. (2015). Combined effects of high temperature and high strain rate on normal weight concrete. *International Journal of Impact Engineering*, *86*, 40–56.

Cheng, F.-P., Kodur, V. K. R., & Wang, T.-C. (2004). Stress-strain curves for high strength concrete at elevated temperatures. *Journal of Materials in Civil Engineering*, *16*(1), 84–90.

Chu, H., Jiang, J., Sun, W., & Zhang, M. (2016). Mechanical and physicochemical properties of ferro-siliceous concrete subjected to elevated temperatures. *Construction and Building Materials*, *122*, 743–752.

CNR-DT 204 (2006) *Guidelines for design, construction and production control of fiber reinforced concrete structures*. National Research Council of Italy, Italy

Daudeville, L., & Malécot, Y. (2011). Concrete structures under impact. *European Journal of Environmental and Civil Engineering*, *15*(sup1), 101–140.

Deng, Z. H., Huang, H. Q., Ye, B., Wang, H., & Xiang, P. (2020). Investigation on recycled aggregate concretes exposed to high temperature by biaxial compressive tests. *Construction and Building Materials*, *244*, 118048.

Diederichs, U., & Schneider, U. (1981). Bond strength at high temperatures. *Magazine of Concrete Research*, *33*(115), 75–84.

Ding, Y., Li, D., Zhang, Y., & Azevedo, C. (2017). Experimental investigation on the composite effect of steel rebars and macro fibers on the impact behavior of high performance self-compacting concrete. *Construction and Building Materials*, *136*, 495–505.

Drzymała, T., Jackiewicz-Rek, W., Tomaszewski, M., Kuś, A., Gałaj, J., & Šukys, R. (2017). Effects of high temperature on the properties of high-performance concrete (HPC). *Procedia Engineering*, *172*, 256–263.

Düğenci, O., Haktanir, T., & Altun, F. (2015). Experimental research for the effect of high temperature on the mechanical properties of steel fiber-reinforced concrete. *Construction and Building Materials*, *75*, 82–88.

Eibl, J. (1987). Soft and hard impact. *In Proceedings of the First International Conference on Concrete for Hazard Protection*, Edinburgh, UK.

EN 1991-1-2:2002 (2002) *Eurocode 1: actions on structures: Part 1–2 General actions—structures exposed to fire; 2002*.

Feng, J., Gao, X., Li, J., Dong, H., He, Q., Liang, J., & Sun, W. (2019). Penetration resistance of hybrid-fiber-reinforced high-strength concrete under projectile multi-impact. *Construction and Building Materials*, *202*, 341–352.

für Stahlbeton, D. A. (2007). *Guidelines for steel fiber reinforced concrete*—23th Draft—richtlinie Stahlfaserbeton—DIN 1045 Annex parts 1–4

Gagg, C. R. (2014). Cement and concrete as an engineering material: An historic appraisal and case study analysis. *Engineering Failure Analysis*, *40*, 114–140.

Ghali, Y. A., Sugumar, R., & Musa, H. A. (2015). Impact of fire on steel reinforcement in reinforced concrete structures. *International Journal of Scientific and Research Publications.* 5(10), 790-803.

Goldfein, S. (1965). Fibrous reinforcement for Portland cement. *Modern Plastics*, *42*(8), 156–160.

Guo, Y., Zhang, J., Chen, G., & Xie, Z. (2014). Compressive behaviour of concrete structures incorporating recycled concrete aggregates, rubber crumb and reinforced with steel fibre, subjected to elevated temperatures. *Journal of Cleaner Production*, *72*, 193–203.

Haack, A. (1998). Fire protection in traffic tunnels: general aspects and results of the EUREKA project. *Tunnelling and Underground Space Technology*, 13(4), 377-381.

Hait, P., Karthik, R., Mitra, R., & Haldar, R. (2024). Natural and Artificial Fibre Reinforced Concrete: A State-of-art Review. *International Journal of Engineering*, 37(3), 503-510.

Hao, H., Hao, Y., Li, J., & Chen, W. (2016). Review of the current practices in blast-resistant analysis and design of concrete structures. *Advances in Structural Engineering*, 19(8), 1193-1223.

Haridharan, M. K., Matheswaran, S., Murali, G., Abid, S. R., Fediuk, R., Amran, Y. H. M., & Abdelgader, H. S. (2020). Impact response of two-layered grouted aggregate fibrous concrete composite under falling mass impact. *Construction and Building Materials*, *263*, 120628.

Huo, J. S., He, Y. M., Xiao, L. P., & Chen, B. S. (2013). Experimental study on dynamic behaviours of concrete after exposure to high temperatures up to 700 C. *Materials and Structures*, *46*, 255–265.

Husem, M. (2006). The effects of high temperature on compressive and flexural strengths of ordinary and high-performance concrete. *Fire Safety Journal*, *41*(2), 155–163.

Imbabi, M. S., Carrigan, C., & McKenna, S. (2012). Trends and developments in green cement and concrete technology. *International Journal of Sustainable Built Environment*, *1*(2), 194–216.

Ismail, M. K., & Hassan, A. A. A. (2017). Impact resistance and mechanical properties of self-consolidating rubberized concrete reinforced with steel fibers. *Journal of Materials in Civil Engineering*, *29*(1), 04016193.

Ismail, M. K., Hassan, A. A. A., & Lachemi, M. (2019). Performance of self-consolidating engineered cementitious composite under drop-weight impact loading. *Journal of Materials in Civil Engineering*, *31*(3), 04018400.

ISO 834-1, (1999). *Fire Resistance Tests-Elements of Building Construction, Part 1: General Requirements*

Jabir, H. A., Abid, S. R., Murali, G., Ali, S. H., Klyuev, S., Fediuk, R., Vatin, N., Promakhov, V., & Vasilev, Y. (2020). Experimental tests and reliability analysis of the cracking impact resistance of UHPFRC. *Fibers*, *8*(12), 74.

Jacobs, J. P. (2007). *Comprehensive fire protection and safety with concrete*. British Cement Association, British Ready-mixed Concrete Association, British Precast Concrete Federation and the Cement Admixtures Association.

Jarallah, H., M., S, (2016). *Experimental Study of punching shear resistance of synthetic fiber reinforced concrete interior slabs*. Faculty of the American University of Sharjah College of Engineering. M. Sc. Thesis.

Jin, L., Bai, J., Zhang, R., Li, L., & Du, X. (2021). Effect of elevated temperature on thelow-velocity impact performances of reinforced concrete slabs. *International Journal of Impact Engineering*, *149*, 103797.

Jin, L., Lan, Y., Zhang, R., & Du, X. (2019). Impact performances of RC beams at/after elevated temperature: A meso-scale study. *Engineering Failure Analysis*, *105*, 196–214.

Kakogiannis, D., Pascualena, F., Reymen, B., Pyl, L., Ndambi, J. M., Segers, E., Lecompte, D., Vantomme, J., & Krauthammer, T. (2013). Blast performance of reinforced concrete hollow core slabs in combination with fire: Numerical and experimental assessment. *Fire Safety Journal*, *57*, 69–82.

Kanda, T., & Li, V. C. (1998). *Multiple cracking sequence and saturation in fiber reinforced cementitious composites*.

Kanda, T., & Li, V. C. (1999). New micromechanics design theory for pseudostrain hardening cementitious composite. *Journal of Engineering Mechanics*, *125*(4), 373–381.

Katzer, J. (2006). Steel fibers and steel fiber reinforced concrete in civil engineering. *Pacific Journal of Science and Technology*, *7*(1), 53–58.

Kennedy, R. P. (1976). A review of procedures for the analysis and design of concrete structures to resist missile impact effects. *Nuclear Engineering and Design*, *37*(2), 183–203.

Khan, F. I., & Abbasi, S. A. (1998). Techniques and methodologies for risk analysis in chemical process industries. *Journal of Loss Prevention in the Process Industries*, *11*(4), 261–277.

Khoury, G. A., Grainger, B. N., & Sullivan, P. J. E. (1985). Strain of concrete during first heating to 600 C under load. *Magazine of Concrete Research*, *37*(133), 195–215.

Khoury, G. A. (1999). *Mechanical behaviour of HPC and UHPC at high temperature in compression*. Final HITECO BRITE report.

Khoury, G. A. (2000). Effect of fire on concrete and concrete structures. *Progress in Structural Engineering and Materials*, 2(4), 429–447.

Khoury, G. A. (2006). Strain of heated concrete during two thermal cycles. Part 1: strain over two cycles, during first heating and at subsequent constant temperature. *Magazine of Concrete Research*, 58(6), 367-385.

Kim, G.-Y., Choi, J.-I., Park, S.-E., Kim, H., Lee, Y., & Lee, B. Y. (2018). Response of UHPFRC and HDFRC under static and high-velocity projectile impact loads. *Construction and Building Materials*, *188*, 399–408.

Kodur, V. (2014). Properties of concrete at elevated temperatures. *International Scholarly Research Notices*, *2014*.

Kong, H.-J., Bike, S. G., & Li, V. C. (2003). Development of a self-consolidating engineered cementitious composite employing electrosteric dispersion/stabilization. *Cement and Concrete Composites*, *25*(3), 301–309.

Kunieda, M., & Rokugo, K. (2006). Recent progress on HPFRCC in Japan required performance and applications. *Journal of Advanced Concrete Technology*, *4*(1), 19–33.

Latifi, M. R., Biricik, Ö., & Mardani Aghabaglou, A. (2022). Effect of the addition of polypropylene fiber on concrete properties. *Journal of Adhesion Science and Technology*, 36(4), 345-369.

Li, Q., Gao, X., Xu, S., Peng, Y., & Fu, Y. (2016). Microstructure and mechanical properties of high-toughness fiber-reinforced cementitious composites after exposure to elevated temperatures. *Journal of Materials in Civil Engineering*, *28*(11), 04016132.

Li, Q. M., Reid, S. R., Wen, H. M., & Telford, A. R. (2005). Local impact effects of hard missiles on concrete targets. *International Journal of Impact Engineering*, *32*(1–4), 224–284.

Li, Q.-H., Sun, C.-J., & Xu, S.-L. (2019). Thermal and mechanical properties of ultrahigh toughness cementitious composite with hybrid PVA and steel fibers at elevated temperatures. *Composites Part B: Engineering*, *176*, 107201.

Li, V. C. (1993). From micromechanics to structural engineering the design of cementitious composites for civil engineering applications. *Doboku Gakkai Ronbunshu*, *1993*(471), 1–12.

Li, V. C., Kong, H. J., & Chan, Y.-W. (1998a). *Development of self-compacting engineered cementitious composites*.

Li, V. C. (1998b). Engineered cementitious composites (ECC)-tailored composites through micromechanical modeling. To appear in *Fiber Reinforced Concrete: Present and Future*, Eds: N. Banthia, A. Bentur, and A. Mufti, Canadian Society of Civil the Engineers.

Li, V. C. (2007). Engineering Cementitious Composites (ECC)-Materials, Structural, and Durability Performance. *University of Michigan*.

Li, V. C. (2008). Engineered cementitious composites (ECC) material, structural, and durability performance. Chapter in *Concrete Construction Engineering Handbook*, Ed. E. Nawy, to be published by CRC Press

Li, V. C., (2019). Micromechanics and Engineered Cementitious Composites (ECC) Design Basis. *Engineered Cementitious Composites (ECC) Bendable Concrete for Sustainable and Resilient Infrastructure*, 11-71.

Liu, J.-C., Tan, K. H., & Fan, S. (2018). Residual mechanical properties and spalling resistance of strain-hardening cementitious composite with Class C fly ash. *Construction and Building Materials*, *181*, 253–265.

Maalej, M., Quek, S. T., & Zhang, J. (2005). Behavior of hybrid-fiber engineered cementitious composites subjected to dynamic tensile loading and projectile impact. *Journal of Materials in Civil Engineering*, *17*(2), 143–152.

Mahakavi, P., & Chithra, R. (2019). Impact resistance, microstructures and digital image processing on self-compacting concrete with hooked end and crimped steel fiber. *Construction and Building Materials*, *220*, 651–666.

Mastali, M., & Dalvand, A. (2016). The impact resistance and mechanical properties of self-compacting concrete reinforced with recycled CFRP pieces. *Composites Part B: Engineering*, *92*, 360–376.

McHarg, P. J., Cook, W. D., Mitchell, D., & Yoon, Y.-S. (2000). Benefits of concentrated slab reinforcement and steel fibers on performance of slab-column connections. *Structural Journal*, *97*(2), 225–234.

Mehdipour, S., Nikbin, I. M., Dezhampanah, S., Mohebbi, R., Moghadam, H., Charkhtab, S., & Moradi, A. (2020). Mechanical properties, durability and environmental evaluation of rubberized concrete incorporating steel fiber and metakaolin at elevated temperatures. *Journal of Cleaner Production*, *254*, 120126.

Mirmomeni, M., Heidarpour, A., Zhao, X.-L., & Packer, J. A. (2017). Effect of elevated temperature on the mechanical properties of high-strain-rate-induced partially damaged concrete and CFSTs. *International Journal of Impact Engineering*, *110*, 346–358.

Mohammadi, K., Alavi, O., Mostafaeipour, A., Goudarzi, N., & Jalilvand, M. (2016). Assessing different parameters estimation methods of Weibull distribution to compute wind power density. *Energy Conversion and Management*, 108, 322-335.

Murali, G., Asrani, N. P., Ramkumar, V. R., Siva, A., & Haridharan, M. K. (2019). Impact resistance and strength reliability of novel two-stage fibre-reinforced concrete. *Arabian Journal for Science and Engineering*, 44, 4477–4490.

Murali, G., Abid, S. R., Amran, Y. H. M., Abdelgader, H. S., Fediuk, R., Susrutha, A., & Poonguzhali, K. (2020). Impact performance of novel multi-layered prepacked aggregate fibrous composites under compression and bending. *Structures*, 28, 1502–1515.

Murali, G., Abid, S. R., Abdelgader, H. S., Amran, Y. H. M., Shekarchi, M., & Wilde, K. (2021a). Repeated projectile impact tests on multi-layered fibrous cementitious composites. *International Journal of Civil Engineering*, *19*, 635–651.

Murali, G., Abid, S. R., Amran, M., Fediuk, R., Vatin, N., & Karelina, M. (2021b). Combined effect of multi-walled carbon nanotubes, steel fibre and glass fibre mesh on novel two-stage expanded clay aggregate concrete against impact loading. *Crystals*, *11*(7), 720.

Murali, G., Abid, S. R., Karthikeyan, K., Haridharan, M. K., Amran, M., & Siva, A. (2021c). Low-velocity impact response of novel prepacked expanded clay aggregate fibrous concrete produced with carbon nano tube, glass fiber mesh and steel fiber. *Construction and Building Materials*, *284*, 122749.

Myers, J. J., & Tinsley, M. (2013). Impact Resistance of Blast Mitigation Material Using Modified ACI Drop-Weight Impact Test. *ACI Materials Journal*, *110*(3).

Natta, G., Ercoli, R., Castellano, S., & Barbieri, F. H. (1954). The influence of hydrogen and carbon monoxide partial pressures on the rate of the hydroformylation reaction. *Journal of the American Chemical Society*, 76(15), 4049-4050.

Netinger, I., Kesegic, I., & Guljas, I. (2011). The effect of high temperatures on the mechanical properties of concrete made with different types of aggregates. *Fire Safety Journal*, *46*(7), 425–430.

Nili, M., & Afroughsabet, V. (2010a). Combined effect of silica fume and steel fibers on the impact resistance and mechanical properties of concrete. *International Journal of Impact Engineering*, *37*(8), 879–886.

Nili, M., & Afroughsabet, V. (2010b). The effects of silica fume and polypropylene fibers on the impact resistance and mechanical properties of concrete. *Construction and Building Materials*, *24*(6), 927–933.

Pan, L., Chen, L., Fang, Q., Zhai, C., & Pan, T. (2016). A modified layered-section method for responses of fire-damaged reinforced concrete beams under static and blast loads. *International Journal of Protective Structures*, *7*(4), 495–517.

Phan, L. T., & Carino, N. J. (1998). Review of mechanical properties of HSC at elevated temperature. *Journal of Materials in Civil Engineering*, *10*(1), 58–65.

Phan, L. T., & Carino, N. J. (2003). Code provisions for high strength concrete strength-temperature relationship at elevated temperatures. *Materials and Structures*, *36*, 91–98.

Prasad, N., & Murali, G. (2021). Exploring the impact performance of functionally-graded preplaced aggregate concrete incorporating steel and polypropylene fibres. *Journal of Building Engineering*, *35*, 102077.

Rafiei, P., Shokravi, H., Mohammadyan-Yasouj, S. E., Koloor, S. S. R., & Petrů, M. (2021). Temperature impact on engineered cementitious composite containing basalt fibers. *Applied Sciences*, *11*(15), 6848.

Rahmani, T., Kiani, B., Shekarchi, M., & Safari, A. (2012). Statistical and experimental analysis on the behavior of fiber reinforced concretes subjected to drop weight test. *Construction and Building Materials*, *37*, 360–369.

Ramakrishnan, K., Depak, S. R., Hariharan, K. R., Abid, S. R., Murali, G., Cecchin, D., Fediuk, R., Amran, Y. H. M., Abdelgader, H. S., & Khatib, J. M. (2021). Standard and modified falling mass impact tests on preplaced aggregate fibrous concrete and slurry infiltrated fibrous concrete. *Construction and Building Materials*, *298*, 123857.

Raminugo, K., Kanda, T., Yokota, H., & Sakata, N., (2007). Outline of JSCE recommendation for design and construction of multiple fine cracking type fiber reinforced cementitious composite (HPFRCC). In Proceedings, *5th International Essen Workshop on Transport in Concrete in Nanostructures and Macrostructure - Impact on Durability, Life-Time Prediction and Performance* RILEM Workshop.

Ramkumar, V. R., Murali, G., Asrani, N. P., & Karthikeyan, K. (2019). Development of a novel low carbon cementitious two stage layered fibrous concrete with superior impact strength. *Journal of Building Engineering*, *25*, 100841.

Rao, M. C., Bhattacharyya, S. K., & Barai, S. V. (2011). Behaviour of recycled aggregate concrete under drop weight impact load. *Construction and Building Materials*, *25*(1), 69–80.

Rokugo, K., Kanda, T., Yokota, H., & Sakata, N., (2007). Outline of JSCE recommendation for design and construction of multiple fine cracking type fiber reinforced cementitious composite (HPFRCC). *In Proceedings, 5th International Essen Workshop on Transport in Concrete in Nanostructures and Macrostructure - Impact on Durability, Life-Time Prediction and Performance* RILEM Workshop

Romualdi, J. P., & Batson, G. B. (1963). Mechanics of crack arrest in concrete. *Journal of the Engineering Mechanics Division*, 89(3), 147-168.

Romualdi, J. P., & Mandel, J. A. (1964). Tensile strength of concrete affected by uniformly distributed and closely spaced short lengths of wire reinforcement. In *Journal Proceedings* (Vol. 61, No. 6, pp. 657-672).

Roufael, G., Beaucour, A.-L., Eslami, J., Hoxha, D., & Noumowé, A. (2021). Influence of lightweight aggregates on the physical and mechanical residual properties of concrete subjected to high temperatures. *Construction and Building Materials*, *268*, 121221.

Sahmaran, M., Lachemi, M., & Li, V. C. (2010). Assessing Mechanical Properties and Microstructure of Fire-Damaged Engineered Cementitious Composites. *ACI Materials Journal*, *107*(3).

Şahmaran, M., Özbay, E., Yücel, H. E., Lachemi, M., & Li, V. C. (2011a). Effect of fly ash and PVA fiber on microstructural damage and residual properties of engineered cementitious composites exposed to high temperatures. *Journal of Materials in Civil Engineering*, *23*(12), 1735–1745.

Salaimanimagudam, M. P., Suribabu, C. R., Murali, G., & Abid, S. R. (2020). Impact response of hammerhead pier fibrous concrete beams designed with topology optimization. *Periodica Polytechnica Civil Engineering*, *64*(4), 1244–1258.

Schneider, U., Diederichs, U., & Ehm, C. (1982). Effect of temperature on steel and concrete for PCRV's. *Nuclear Engineering and Design*, *67*(2), 245–258.

Shallal, M. A., & Al-Owaisy, S. R. (2007). Strength and elasticity of steel fiber reinforced concrete at high temperatures. *Journal of Engineering and Sustainable Development*, *11*(2), 125–133.

Shang, X., & Lu, Z. (2014). Impact of high temperature on the compressive strength of ECC. *Advances in Materials Science and Engineering*, *2014*.

Sharma, N. K., Kumar, P., Kumar, S., Thomas, B. S., & Gupta, R. C. (2017). Properties of concrete containing polished granite waste as partial substitution of coarse aggregate. *Construction and Building Materials*, *151*, 158–163.

Singh, H. (2016). *Steel fiber reinforced concrete: behavior, modelling and design*. Springer.

Standard, B. (2009). Testing hardened concrete. *Compressive Strength of Test Specimens*, *BS EN*, 12390–12393.

Sultan, H. K., & Alyaseri, I. (2020). Effects of elevated temperatures on mechanical properties of reactive powder concrete elements. *Construction and Building Materials*, *261*, 120555.

Swamy, R. N., Al-Taan, S., & Ali, S. A. R. (1979). Steel fibers for controlling cracking and deflection. *Concrete International*, *1*(8), 41–49.

Thomas, R. J., & Sorensen, A. D. (2018). Charpy impact test methods for cementitious composites: Review and commentary. *Journal of Testing and Evaluation*, 46(6), 2422-2430.

Torić, N., Boko, I., & Peroš, B. (2013). Reduction of postfire properties of high-strength concrete. *Advances in Materials Science and Engineering*, *2013*.

Tufail, M., Shahzada, K., Gencturk, B., & Wei, J. (2017). Effect of elevated temperature on mechanical properties of limestone, quartzite and granite concrete. *International Journal of Concrete Structures and Materials*, *11*, 17–28.

Varona, F. B., Baeza-Brotons, F., Tenza-Abril, A. J., Baeza, F. J., & Bañón, L. (2020). Residual compressive strength of recycled aggregate concretes after high temperature exposure. *Materials*, *13*(8), 1981.

Wald, F., Chlouba, J., Uhlíř, A., Kallerová, P., & Štujberová, M. (2009). Temperatures during fire tests on structure and its prediction according to Eurocodes. *Fire Safety Journal*, 44(1), 135-146

Wang, W., & Chouw, N. (2017). The behaviour of coconut fibre reinforced concrete (CFRC) under impact loading. *Construction and Building Materials*, *134*, 452–461.

Wardhana, K., & Hadipriono, F. C. (2003). Analysis of recent bridge failures in the United States. *Journal of Performance of Constructed Facilities*, *17*(3), 144–150.

Yang, Z. H., Diederich, D., Schneider, K., Siebenmann, R., Stulz, P., Von Segesser, L., Turina, M., Bühler, F. R., & Lüscher, T. F. (1989). Endothelium-derived relaxing factor and protection against contractions induced by histamine and serotonin in the human internal mammary artery and in the saphenous vein. *Circulation*, *80*(4), 1041–1048.

Yu, X., Chen, L., Fang, Q., Ruan, Z., Hong, J., & Xiang, H. (2017). A concrete constitutive model considering coupled effects of high temperature and high strain rate. *International Journal of Impact Engineering*, *101*, 66–77.

Zhai, C., Chen, L., Fang, Q., Chen, W., & Jiang, X. (2017). Experimental study of strain rate effects on normal weight concrete after exposure to elevated temperature. *Materials and Structures*, *50*, 1–11.

Zhai, C., Chen, L., Xiang, H., & Fang, Q. (2016). Experimental and numerical investigation into RC beams subjected to blast after exposure to fire. *International Journal of Impact Engineering*, *97*, 29–45.

Zhang, J., Maalej, M., & Quek, S. T. (2004). Hybrid fiber Engineered Cementitious Composites (ECC) for impact and blast-resistant structures. *Proceedings of the First International Conference on Innovative Materials and Technologies for Construction and Restoration–IMTCR04*, *1*, 136–149.

Zhihui, Y. U., Zhen, Y., Chaofan, X. I. A., & Zhang, C. (2020). High temperature flexural deformation properties of engineered cementitious composites (ECC) with hybrid fiber reinforcement. *Research and Application of Materials Science*, *2*(2).

Zhu, D., Gencoglu, M., & Mobasher, B. (2009). Low velocity flexural impact behavior of AR glass fabric reinforced cement composites. *Cement and Concrete Composites*, *31*(6), 379–387.

CURRICULUM VITAE

Personal Information:

Name: RAAD A.Naser

Surname: ALAMERI

Education:

- Ph.D. Civil Engineering, University of Gaziantep College of Engineering, Civil Engineering Department, Gaziantep / Turkey.
- M.Sc. Civil Engineering, University of Gaziantep College of Engineering, Civil Engineering Department, Gaziantep / Turkey.
- BSc. Civil Engineering, Al–Mustansiriya University, College of Engineering, Civil Engineering Department, Baghdad / Iraq.

Publications in PhD journey:

1. Flexural response of hollow high strength concrete beams considering different size reductions, Structures journal, 2020.
2. Residual Impact Performance of ECC Subjected to Sub-High Temperatures, Materials, 2021.
3. Residual Repeated Impact Strength of Concrete Exposed to Elevated Temperatures, Crystals, 2021.
4. Mechanical and Impact Properties of Engineered Cementitious Composites Reinforced with PP Fibers at Elevated Temperatures, Fire, 2021.
5. Recent Literature on Steel Fiber Role in Resistance Improvement of Fibrous Concrete to Repeated Impacts, Wasit Journal of Engineering Sciences, 2023.